MODELING NUTRIENT LOADING TO WATERSHEDS IN THE GREAT LAKES BASIN: A DETAILED SOURCE MODEL AT THE REGIONAL SCALE

By

Emily Catherine Luscz

A THESIS

Submitted to
Michigan State University
in partial fulfillment of the requirements
for the degree of

Environmental Geosciences – Master of Science

2013

ABSTRACT

MODELING NUTRIENT LOADING TO WATERSHEDS IN THE GREAT LAKES BASIN: A DETAILED SOURCE MODEL AT THE REGIONAL SCALE

by

Emily Catherine Luscz

Nutrient loading has been linked to many issues including eutrophication, harmful algal blooms, and decreases in aquatic species diversity. In the Great Lakes, algal blooms continue to plague Lake Erie and Saginaw Bay despite reduction in point source loading to the lakes. Though many watershed nutrient models exist in the literature, there is generally a tradeoff between the scale of the model and the level of detail regarding the individual sources of nutrients and basin characteristics. To examine the link between watershed nutrient sources, landscape processes, and in-stream loads in the Lower Peninsula of Michigan a spatially explicit nutrient loading model was developed. The model is composed of two parts: GIS models that predict nutrient sources and a statistical model that predicts nutrient loads from the source models and basin characteristics. Observations collected during baseflow, melt, and rain conditions from 2010-2012 were used to calibrate and validate the model. The model predicts nutrient loads and provides information on the sources of nutrients within each watershed and the relative contribution of different sources to the overall nutrient load.

The model results indicated that there is a high degree of variability in nutrient export rates, even within the same land use class, and export rates can be as much as 15 times greater for nitrogen and as much as 9 times greater for phosphorus depending on the season. The model performed as well as other regional scale nutrient models and showed less bias due to land use. In addition, nitrate isotope data agreed with the model's predictions of the relative source of nutrients. This work has the potential to provide valuable information to environmental managers regarding how and where to target efforts to reduce nutrient loads in surface water.

ACKNOWLEDGEMENTS

I would first like to thank my advisor, David Hyndman for his encouragement and support throughout this process and particularly when I decided to finish my thesis while starting a new job, half way across the country. I'm hugely indebted to Anthony Kendall for his guidance, collaboration, and inspiration. From Python to Euchre, Anthony patiently taught me so many things required to complete this work. Most importantly, he regularly challenged me to be my best.

This work would not have been possible without the help of Briana Jasinski, Blaze Budd, and Ryan Nagelkirk who worked 12+ hour days, collectively logging over a month in the field with me. Their smiles and positive attitudes were invaluable, especially when field days started before sunrise and ended after sunset. Anthony Kendall, Sherry Martin, Lon Cooper, Bobby Chrisman, Erin Haacker, Brian Eustice, and Ryan Vannier also logged many hours in the field for which I'm extremely grateful.

I would also like to acknowledge my friends and officemates, Brian Eustice, Sherry Martin, Erin Haacker, Yuteng Ma, and Alex Kuhl for their moral support and for putting up with all my whining. I hope that I'm lucky enough to have coworkers who are half as wonderful as they are in my future.

TABLE OF CONTENTS

LIST OF TABLES

LIST OF FIGURES

CHAPTER 1

HIGH-RESOLUTION SPATIALLY EXPLICIT NUTRIENT SOURCE MODELS FOR THE LOWER PENINSULA OF MICHIGAN

1.1 Introduction

Elevated concentrations of nitrogen and phosphorus in lakes, rivers, groundwater and streams have become a major concern for environmental managers. Nutrients have been identified as one of the leading causes of river and lake impairment in the United States and have been an ongoing issue in the Great Lakes, specifically Lake Erie (*USEPA*, 2009, 2002b). Blooms of the cyanobacteria Microsystis can potentially produce the toxin Microsytin which is hazardous to human and aquatic animal health (*Davidson et al.*, 2012; *Correll*, 1998). Growth of clydophera, an algae scum that grows on solid substrates, is not only odorous and unsightly but can clog water intake pipes. Excessive growth of algae and cyanobacteria lead to oxygen depletion which impacts benthic organisms and can cause fish kills (*Auer et al.*, 2010; *Anderson et al.*, 2002). Issues associated with nutrient loading to the Great Lakes include eutrophication, harmful algal blooms, hypoxia, and decreases in biologic diversity making water unsuitable for recreational, industrial, and municipal uses. Seasonal algal blooms are common in the western basin of Lake Erie and Saginaw Bay (*Hinderer and Murray*, 2011; *Dolan and Chapra*, 2012).

Since the late 1960's cooperative efforts by the governments of the United States and Canada resulted in extensive monitoring, reporting, and legislation in the Great Lakes Basin with the goal of improving water quality in the Great Lakes. Legislation was passed to limit phosphorus point source effluents and establish limits on phosphorus loads to the lakes (*Nicholls et al.*, 2001; *Dolan et al.*, 1981; *Dolan*, 1993). Initial improvements were realized through point source load reduction, but since 1991 total phosphorus loading to Lake Erie has been more variable and even shows signs of increasing. This has been attributed to increases

in non-point sources of phosphorus (*Dolan and McGunagle*, 2005; *Moon and Carrick*, 2007). Increases in nitrate delivery to the Great Lakes, particularly from agricultural watersheds, have also been observed (*Smith et al.*, 1987).

Addressing the impact of non-point sources on in-stream nutrient loads requires an understanding of the location and rates of nutrient application. However, non-point sources of nitrogen and phosphorus are difficult to quantify, because they can not be directly measured, and how and where they are applied affect the delivery of nutrients to surface water (*Carpenter et al.*, 1998; *Nikolaidis et al.*, 1998). Data reporting related to sources of nutrients varies from state to state; often data is only available on a county or state level or may not be directly available.

One approach used to predict nutrient sources across large spatial scales is to use other variables such as land use and population to estimate non-point sources of nutrients. This type of approach (ie., *Johnes* (1996)) assumes that changes in land use or land management will lead to proportional responses in nutrient sources which may lead to problems when there is a large degree of variability in sources within a particular land use. Reliable estimates of non-point sources are necessary to develop strategies to manage non-point sources and predict how they will change with future climate and land use.

In this study, GIS models were developed to generate a spatially explicit description of nutrient sources. Estimates of nutrient sources are compared to sampled surface water nitrogen and phosphorus concentrations in order to better understand the retention of nutrients within watersheds and the contribution of nutrient sources to surface water loading across various land uses. The resulting descriptions provide a basis to quantify the impacts of non-point sources and serve as inputs for watershed nutrient loading models.

1.2 Methods

1.2.1 Model Descriptions

GIS models were developed to estimate nitrogen and phosphorus inputs from atmospheric deposition (*Atm*), chemical agricultural fertilizer application (*ChemAg*), non-agricultural fertilizer application (*NonAg*), manure production/application (*Manure*), septic tanks (*Septic*), and point sources (*Point*). Nutrient loading rates for each source were estimated for 30 meter cells across the Lower Peninsula. The method used to estimate each source is described in the following sections. Each section is accompanied by a flow chart illustrating the steps taken to generate estimates of nutrient sources.

1.2.2 Description of Study Area

Source models were constructed for the Lower Peninsula of Michigan which has watersheds that drain to 3 of the 5 Great Lakes: Lakes Michigan, Huron and Erie. Watersheds in the southern portion of the study area are dominated by agriculture, specifically row crops, and include significant urban centers including Grand Rapids and Detroit. The primary land cover in the northern portion of the study area is forest with small pockets of agriculture.

1.2.3 GIS Source Models

1.2.3.1 Point Sources

Relative to non-point sources, point sources can be easily identified, quantified, and monitored, and were thus early targets of management efforts to improve the nation's water quality (*Dolan*, 1993). The National Pollutant Discharge Elimination System (NPDES) monitors and regulates effluent information for facilities that discharge to surface water in the United States. Flows and concentrations of various parameters are measured and reported according to a facility's permit. The parameters sampled and the reporting frequency

vary between facilities, making assessment of an average load challenging (*Maupin and Ivahnenko*, 2011; *McMahon et al.*, 2007). Due to issues with data entry, data from NPDES permits (as reported to the Permit Compliance System-PCS and Integrated Compliance Information System-ICIS for the National Pollutant Discharge Elimination System-NPDES) required review and considerable quality control before it could be used. There are also issues with the completeness of the data reported to the PCS and ICIS-NPDES databases (*Maupin and Ivahnenko*, 2011). State agencies are required to report data from major dischargers but are not required to report data from minor facilities. In Michigan around 50-60% of facilities have reported data for years 2007-2011. For major facilities, the percent is higher, almost 100% for 2009-2011 and 73% and 86% for 2008 and 2009, respectively (*McMahon et al.*, 2007; *Maupin and Ivahnenko*, 2011).

Loading estimates from the Discharge Monitoring Report (DMR) Pollutant Loading Tool, which was developed by the EPA were used in the model. Loading is estimated by the tool from data available through the PCS-ICIS. The tool identifies outliers and estimates loads for locations where data is not reported. The tool also estimates concentrations for facilities that are likely to discharge nutrients based on their Standard Industrial Classification (SIC). Average loading rates for each SIC are estimated regionally by the tool and used to estimate loads for facilities where data is missing or not reported.

Loading estimates of total phosphorus and total nitrogen were downloaded from the DMR website. Facility discharge locations were mapped to the nearest model river cell based on the coordinates provided with the data. Facility receiving waters were verified through permit data available from the EPA's web page Enforcement and Compliance History Online (ECHO). These steps are summarized in Figure 1.1.

1.2.3.2 Atmospheric Loading

Atmospheric data was available from three networks that monitor atmospheric deposition of various compounds: the National Atmospheric Deposition Program (NADP) (*NADP*, 2007),

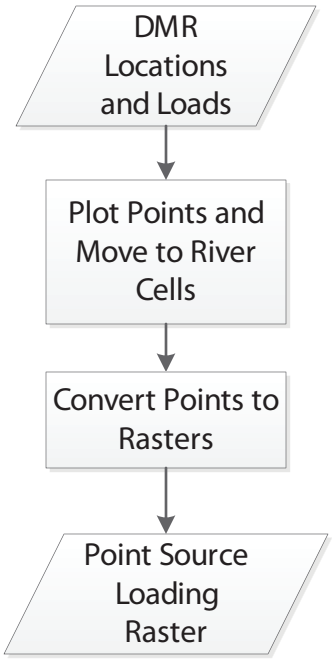

Figure 1.1: Flow chart summarizing process for estimating point sources.

a wet deposition monitoring program in the United States, the Great Lakes Precipitation Network (GLPN) (*Lisa Bradley, personal communication*, 2011) a joint project between the United States and Canada established to monitor wet deposition to each of the Great Lakes, and the U.S. Environmental Protection Agency's dry deposition monitoring network called Clean Air Status and Trends Network (CASTNET).

Weekly data was downloaded from CASTNET which reports fluxes of nitrate, ammonium, and nitric acid by dry deposition (particle velocity is estimated along with the data). Wet deposition from the Great Lakes Precipitation Network was obtained from the Canada Centre for Inland Waters which collects samples monthly and measures Total Kjeldahl Nitrogen (TKN) and nitrate/nitrite. TKN includes both organic and ammonia nitrogen, so TKN and nitrate/nitrite were summed to obtain total nitrogen. National Atmospheric Deposition Program data was downloaded as monthly averages of weekly samples (to be consistent with GLPN data). NADP reports only nitrate and ammonia.

Once concentrations were determined, measured precipitation volume and sampler area

were used to calculate total nitrogen deposition ($kg/m^2/year$). For wet deposition, loading was calculated by multiplying the concentrations by precipitation values for each month of available data. Monthly readings were classified as Winter-Spring (December-May) and Summer-Fall (June-November), and an average was calculated for each summary period for data after 2005. Averages were then interpolated to the model grid using Simple Kriging.

The same approach was used for dry deposition which is reported weekly. Loads for each summary period were averaged for data after 2005. Because a limited number of data points were available for dry deposition of nitrogen and wet deposition of phosphorus, inverse distance weighting was used to develop loading prediction estimates for those species.

Several studies have shown that organic nitrogen can contribute about a third (median of 30%) of the total nitrogen atmospheric deposition (*Neff et al.*, 2002). NADP sites only measure inorganic nitrogen species while the GLPN data includes both organic and inorganic nitrogen. Data from the Sibley GLPN site was compared to data from the nearby Isle Royale NADP site to assess contribution of organic nitrogen to total atmospheric nitrogen deposition in the Great Lakes. The Sibley site is in the Sleeping Giant Provincial Park on the Sibley Peninsula, Ontario, while the Isle Royale site is on the western side of Isle Royale National Park (Figure 1.2). Both sites are within 50 kilometers of each other, located near the Lake Superior shoreline. Concentration data from overlapping months were compared. On average, the concentration at the Sibley site was 24% greater than at the Isle Royale site. Annually, the percent difference ranged from 14.5 % to 44.5%. This agrees well with studies of the contribution of organic nitrogen to total atmospheric nitrogen deposition. *Neff et al.* (2002) compared data from several atmospheric deposition studies and found that 60% of reported measurements had a range of 10% to 40% dissolved organic nitrogen with an average of 33%. *Nicholls et al.* (2001) measured atmospheric nitrogen deposition in Harp Lake, in southern Ontario, and estimated a dissolved organic contribution of approximately 27% to total annual nitrogen loading. To account for the organic nitrogen contribution, the average annual percent difference between the concentration at the Sibley and Isle Royale sites

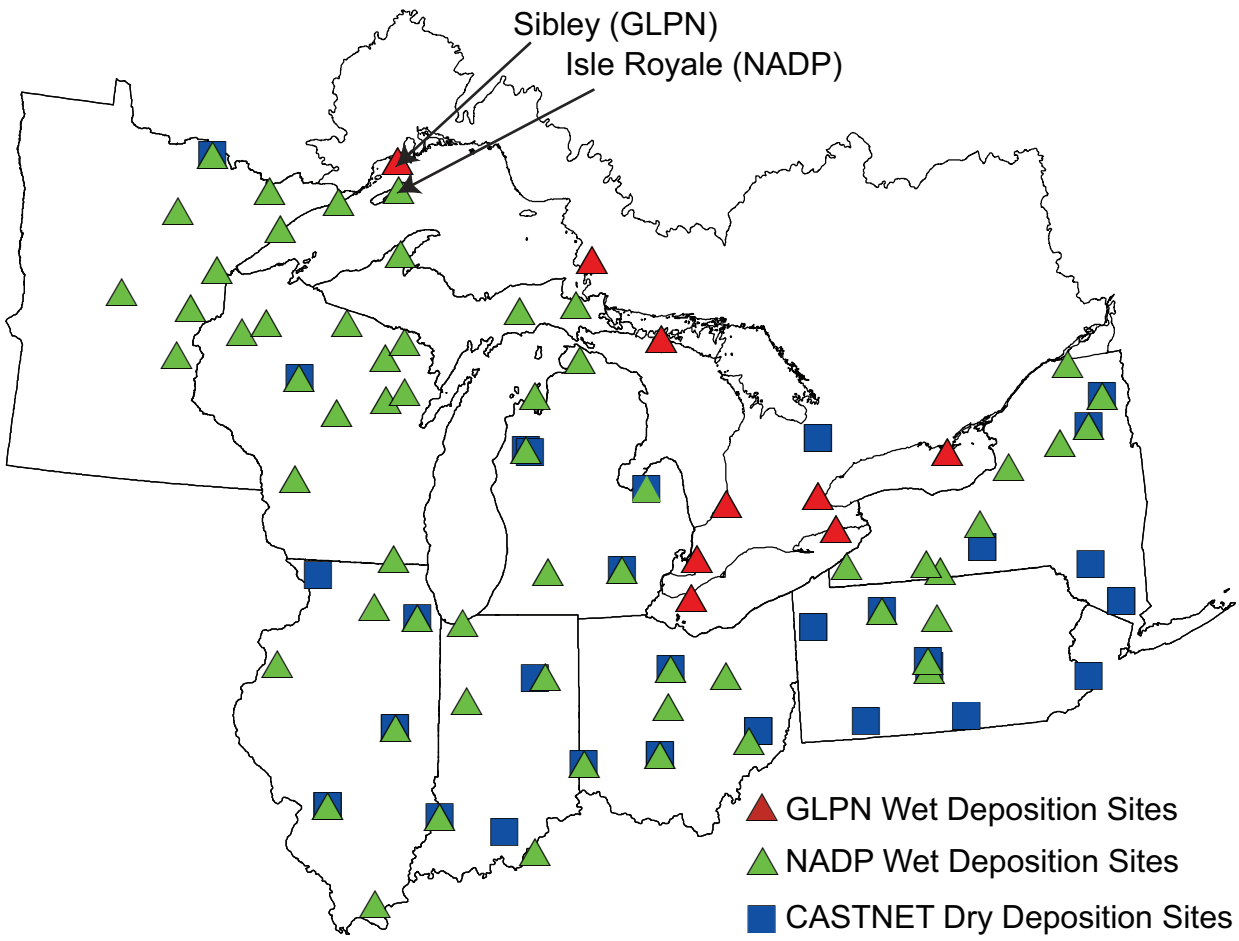

Figure 1.2: Location of atmospheric deposition monitoring networks. The Sibley and Isle Royale sites were compared to determine the contribution of organic nitrogen to the total wet deposition load. For interpretation of the references to color in this and all other figures, the reader is referred to the electronic version of this thesis.

was assumed to represent the regional proportion of total nitrogen deposition contributed by organic nitrogen. Concentrations of all NADP sites were adjusted to account for this calculated percent difference. This process is illustrated in Figure 1.3.

1.2.3.3 Septic Tank Loading

No statewide database of septic tank locations or treatment plant service areas currently exists in Michigan. The location of septic tanks was estimated using existing information on treatment plants and water wells. An inventory of operating waste water treatment plants

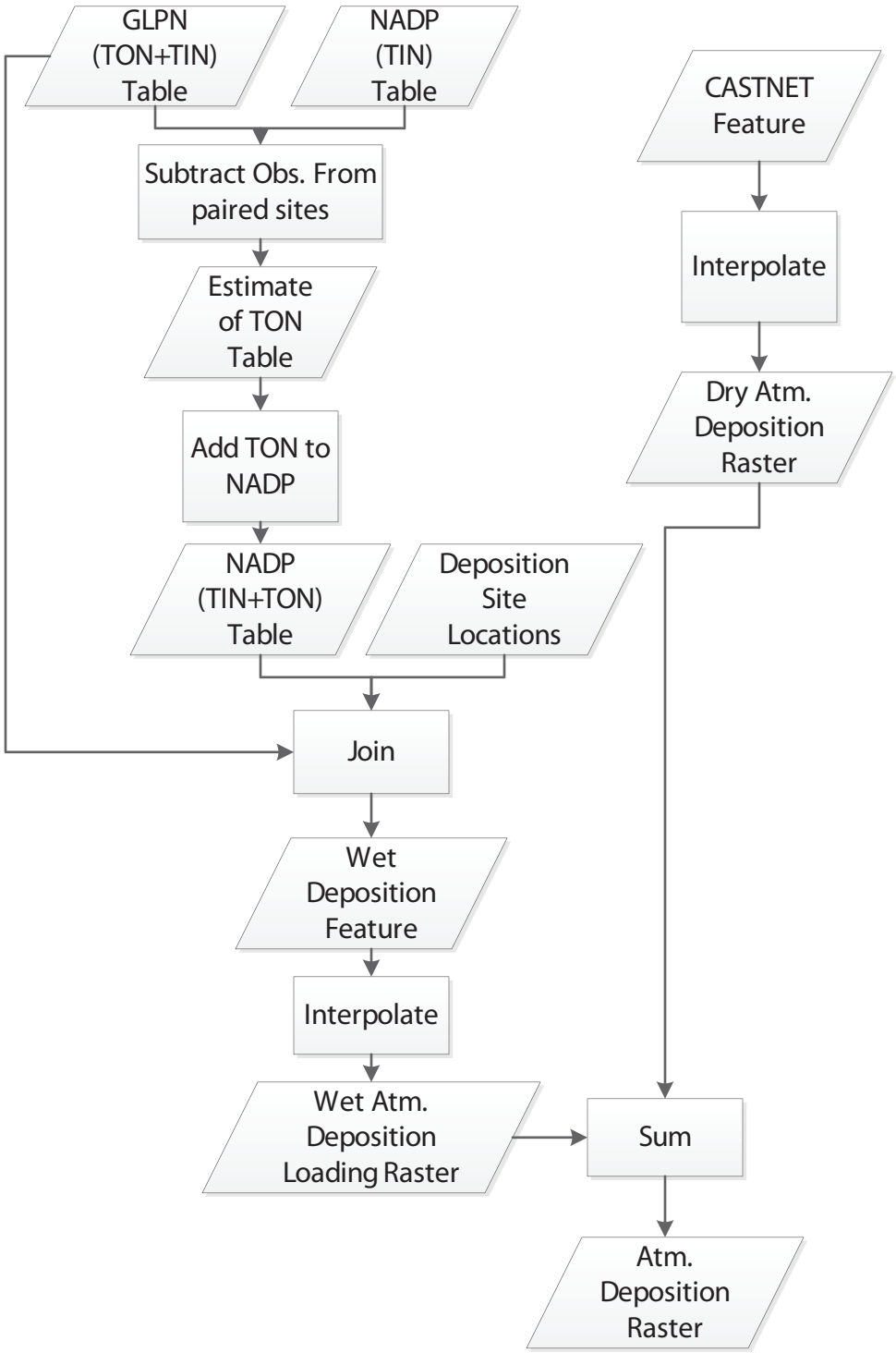

Figure 1.3: Flow chart summarizing process for estimating atmospheric deposition.

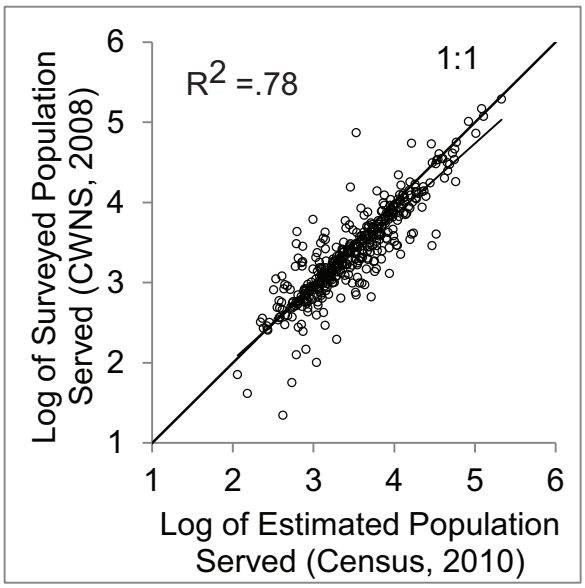

Figure 1.4: Comparison between the population served by treatment plants based on EPA's CWNS survey and the population served based on the estimated treatment plant service areas and the 2010 Census.

and collection systems was obtained from current NPDES permits, the Clean Watershed Needs Survey (CWNS-a national survey of watershed needs conducted by the EPA), and the Southeast Michigan Council of Governments (SEMCOG). For plants and collection systems without plant service area data, an area around each plant/collection system was designated to represent where residents receive sewage collection. This service area was estimated from the location of the treatment plant and the incorporated area of the town served by the treatment plant (from Census 2010). The density of residential wells in the area was also considered; an area with a high density of residential wells was assumed to be outside of a treatment plant service area even if it was inside an incorporated area.

The population served by each facility was estimated by intersecting the estimated service areas and the 2010 Census blocks. This was compared to CWNS which provides an estimate of the population receiving collection from each facility. A comparison of population served reported in the CWNS and the population served estimated using the method described above is shown in Figure 1.4.

It was assumed that all households outside the designated waste treatment service areas

have a septic system or some other form of on site waste water disposal. The number of septic tanks in a given area was determined from the number of households reported in the 2010 Census blocks. Initially, septic tanks were placed in census blocks where residential wells existed according to the Michigan Wells Summary Database (*MDEQ*, 2005). However, the number of residential wells in the Michigan Well Database is only a fraction of the total number of septics that exist in the state. The 2006 National Land Cover Database (*Fry et al.*, 2011) was used in conjunction with a roads layer from the 2010 Census to determine potential areas where the remaining septic tanks estimated for the census block were most likely to be located. The remaining septic tanks (the difference between the number estimated and the number distributed to well locations) were randomly distributed to NLCD urban cells within each census block that were between 10 and 60 meters from the center-line of roads and at least 15 meters from surface water using the Geospatial Modeling Environment (GME) (*Beyer*, 2012). This was done because residences are generally located adjacent to roads, and most Michigan county health departments require a buffer between surface water and septic tanks. If there were no urban cells in a census block, septic tanks were placed randomly in other land cover types excluding water and wetlands.

Once septic systems were located, they were assigned an estimated nutrient load based on the average household size and a yearly estimate of per person nutrient loading rates to septic systems (*USEPA*, 2002a). A factor was applied to vacant and seasonal households (0 for vacant and 0.25 for seasonal) to account for the fact that these systems do not receive loading during the entire year. Figure 1.5 is a flow chart illustrating this process.

1.2.3.4 Non-agricultural Fertilizer

Two forms of non-agricultural fertilizer use were considered in the model: the amount applied to golf courses and the amount applied to residential and commercial lawns. While county level inventories of agricultural fertilizer purchases are readily available for states through the agricultural census, data for non-agricultural fertilizer use is limited. This issue

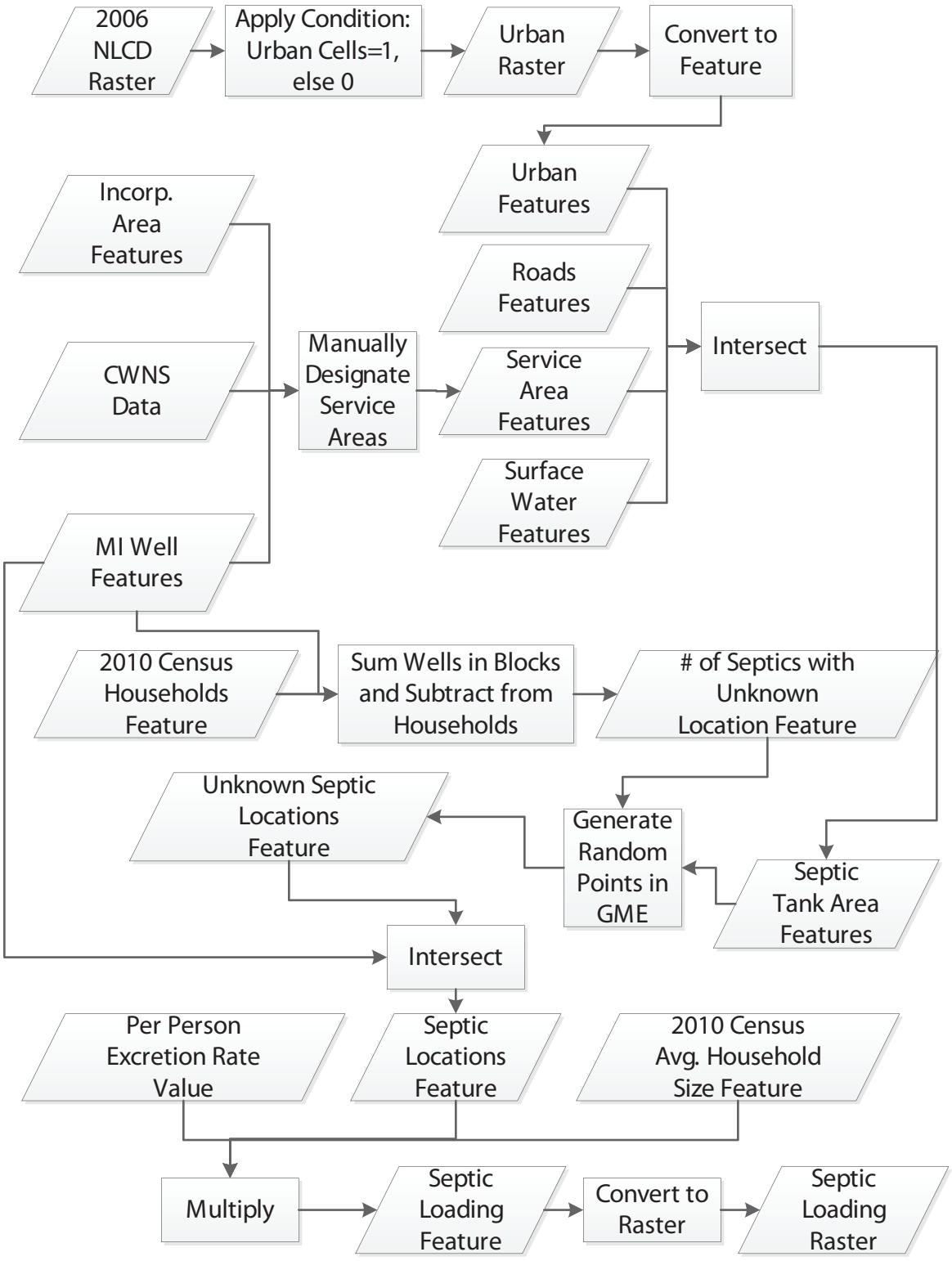

Figure 1.5: Flow chart summarizing process used to estimate loading from septic tanks.

was confronted by *Ruddy et al.* (2006) in their county level inventory of nutrients. They estimated both the portion of fertilizer sales resulting from non-agricultural fertilizer use and the portion of the state level non-agricultural fertilizer used in each county. State and county non-agricultural fertilizer use in pounds of nitrogen and phosphorus were estimated from 1987 to 2001.

In addition to estimating non-agricultural fertilizer use for the state, *Ruddy et al.* (2006) developed a model to distribute statewide fertilizer sales data to each county based on population density. By plotting the available county level data and population density, they concluded that non-agricultural fertilizer use increased with population density until a threshold of about 700 people/km^2, above which fertilizer use did not increase. Their estimates suggest that for Michigan, the total non-agricultural fertilizer use has not changed significantly since 1996, therefore, the 2001 estimate of total non-agricultural phosphorus and nitrogen for Michigan was assumed to be reasonable for years 2005-2012. This estimate was redistributed to counties based on the relationship described above and the 2010 Census population data to obtain a county level estimate of non-agricultural fertilizer use for the study period.

Once county level estimates were obtained, golf course areas were established using a directory of golf courses from the Michigan Golf Association and manual digitization of boundaries using aerial imagery. Addresses were geocoded and polygons were manually digitized around each course using satellite images. The golf course polygons inevitably included areas that are not fertilized including cart paths, sand traps, and forested landscapes. From the most compact courses (those with the largest ratio of greens to golf course area, ˜10% of the total) an average area per hole was estimated. The proportion of fertilizable area for each golf course polygon was then estimated based on number of holes. An average course fertilization rate was obtained from locally (Midwest) observed rates of course application from a survey conducted by the Environmental Institute for Golf of the Golf Course Superintendents Association of America (*Throssell et al.*, 2009). It was visually estimated that

even for the most compact courses (those lacking tree parks and lakes) only about 85% of the total course area is fertilizable. Fertilizer was randomly distributed to 85% of the area within the manually designated golf course areas at the surveyed rate.

The estimated fertilizer contribution for golf courses was removed from the non-agricultural fertilizer estimated for each county by *Ruddy et al.* (2006). This adjusted amount was then distributed to census tracts following the population density model outlined by *Ruddy et al.* (2006). After per tract fertilizer use was estimated, potential fertilizable area within each census tract was established using the 2006 NLCD Land Cover and Impervious Area data layers, Michigan roads, and the manually generated layer of golf course areas. It was assumed that commercial and residential fertilizer is predominantly applied in urban, pervious areas that are close to roads. It was also assumed that most home and business owners only apply fertilizer to parts of their property that are adjacent to roads. Areas available to receive residential or commercial fertilizer were established by selecting all NLCD 2006 medium to high density urban cells and creating an inclusion buffer of 30 meters from road polylines but excluding the portion of the buffer occupied by the right of way and the road itself (20 meters from any polyline). Additionally golf course areas were removed from the selected cells since application to golf courses was already considered (as described above). The cell areas were multiplied by the NLCD pervious area product to establish what proportion of the cell was occupied by fertilizable land.

Literature values (*Zhou et al.*, 2008; *Law et al.*, 2004) were used to establish commercial and residential application rates of nitrogen and phosphorus. Recommended rates over the lifetime of a lawn and for various residual phosphorus levels were averaged. While all the selected cells could potentially be fertilized, applying fertilizer to all cells grossly overestimates fertilizer application. This was determined by comparing county level totals for non-agricultural fertilizer from *Ruddy et al.* (2006) and county levels estimated by applying fertilizer at the recommended rate to all potentially fertilizable cells. In order to maintain locally reasonable application rates while honoring the observed totals, fertilizer was

randomly applied to cells, at the recommended rate, until the total application matched observed county totals. This process is summarized in Figure 1.6.

1.2.3.5 Animal Manure

In recent decades there have been significant changes in agricultural management practices. Animal production has shifted from small farms where animals are primarily raised on pasture land to concentrated animal feeding operations (CAFOs) where large numbers of animals are raised in confinement (*Cheng*, 2003; *Kellogg et al.*, 2000). Waste produced by confined operations is collected and distributed to surrounding cropland. As CAFO size increases, an ever increasing area of cropland is needed to assimilate waste, and facilities are required to transport waste to neighboring farms (*Kellogg et al.*, 2000). In order to accurately describe waste management of large operations as well as small farms, two approaches were used to distribute animal manure to model cells.

The Michigan Department of Environmental Quality (MDEQ) has data on the location and inventory for approximately 200 of the largest confined feeding operations in the state. This information, was combined with the 2007 Agricultural Census data to determine the approximate location and extent of large confined animal feeding operations. Facilities and animal inventories for operations described by the MDEQ were removed on a county basis from the 2007 Agricultural Census data in order to determine the inventory of the remaining unknown farms. After those facilities were removed, the average herd/flock size of a particular animal type and inventory level was re-calculated for each county based on the remaining number of farms and animal inventories.

Once the average county inventory was established, farms in each county were classified as confined operations and pasture operations based on a threshold inventory level. If the inventory was above a certain level, it was assumed that the farms likely confine their animals for the majority of the time. The thresholds, taken from *Kellogg et al.* (2000), were varied based on animal group. For instance, dairy farms have no threshold since dairy farming

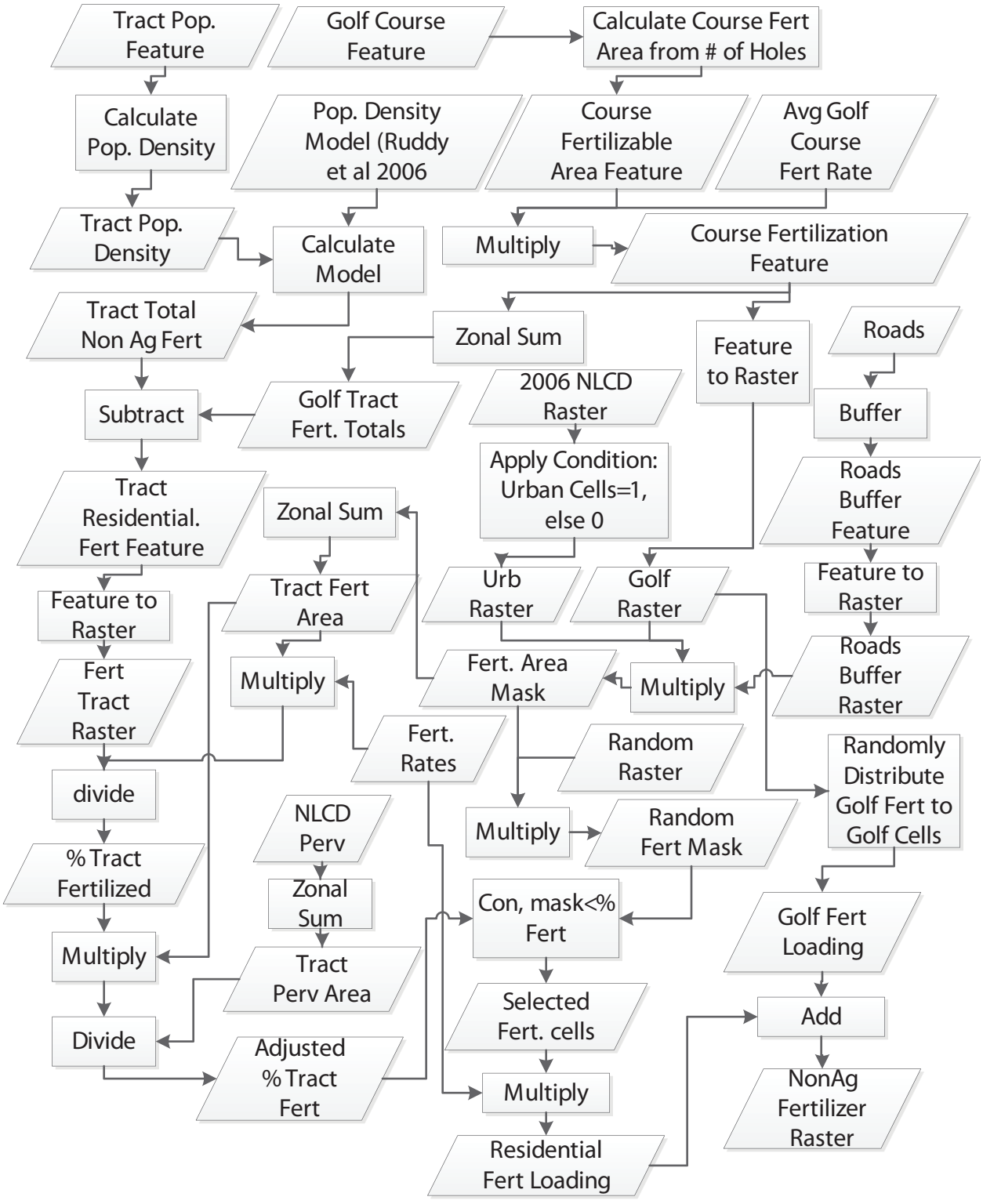

Figure 1.6: Flow chart summarizing process used to estimate non-agricultural fertilizer.

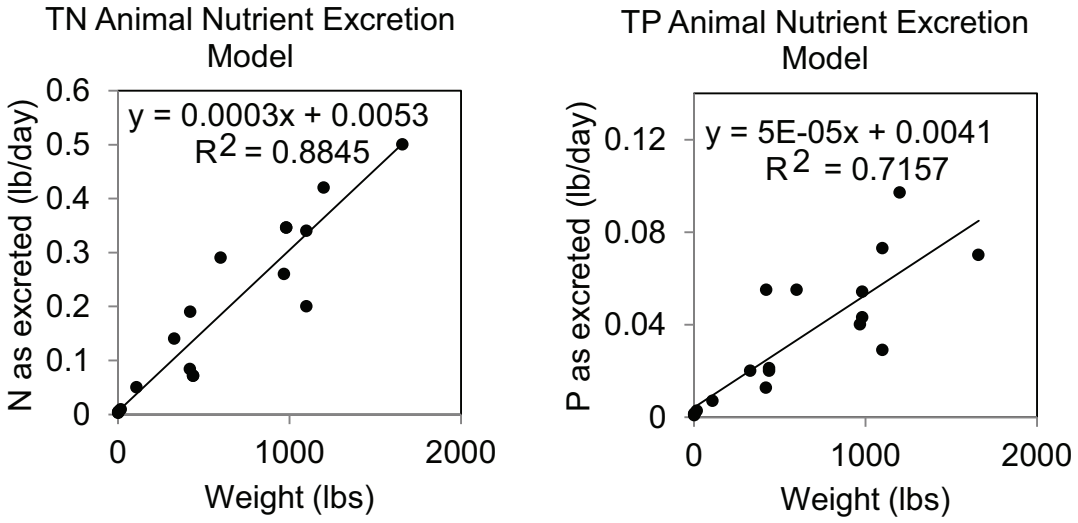

Figure 1.7: Linear regressions of animal weight and nutrient excretion rates. These linear models were used to predict animal excretion rates for animals not discussed in the NRCS Waste Management Handbook (*NRCS*, 2008) including bison, elk, emus, pheasant and others.

requires partial to complete confinement of animals.

Nutrient loads were calculated for each herd/flock type, in each county based on estimated nutrient excretion rates for each animal type (*NRCS* (2008) estimates excretion rates for common animal groups). From available excretion data and average animal weight (excluding lactating cows), a linear model was developed to estimate excretion rates based on animal size (Figure 1.7). This was used for animal groups in the agricultural census that did not have a nutrient excretion rate provided by the NRCS Waste Management Handbook. Using excretion rates and farm inventory, a total farm load was calculated.

Inevitably, during collection, transport and storage, a portion of the load is lost before it reaches the fields. An estimate of this efficiency (*Kellogg et al.*, 2000) was used to calculate the spreadable manure load. Spreadable acreage for each farm was calculated from the proportion of the total county animal waste produced by the farm and the total amount of acreage receiving manure in the county (reported in the 2007 Agricultural Census).

While some location data was available for confined operations from MDEQ, the location

of the remaining confined operations was unknown. Due to fuel and labor costs, there is a limit to the distance a farmer is willing to transport waste (*Kellogg et al.*, 2000). This distance was estimated to be about three miles. To determine the most probable location of operations not included in the MDEQ data, model cells were selected based on available cropland within 3 miles of the cell and compared to the spreadable acreage calculated for each farm. If enough land was available, the cell was selected as a possible location for a particular farm. Farms were then randomly distributed to selected cells using GME.

After farm locations were selected, buffers were created around each farm designating the land receiving manure. Initially, buffer radius was estimated from the farm's proportion of manure acreage in the county. However, some of the land in each buffer was occupied by roads or non-agricultural land reducing the land available for manure application. Therefore, the radius of the buffer was iteratively increased until the buffer incorporated enough fertilizable land to meet the actual spreadable land estimated for each farm. This ensured that the total observed acreage fertilized by manure in a county was honored, but roads and non-agricultural cells did not receive fertilizer. Buffers were adjusted until at least 98% of the farms met their estimated manure acreage. As buffers increased, neighboring farm manure acreage overlapped, and thus it was necessary to sum overlapping buffers, to avoid cells receiving multiple fertilizer contributions.

The five year crop rotation from the Cropland Data Layer (CDL), a remotely sensed product from the National Agricultural Statistics Service (*USDA*, 2011), was used to estimate the rate at which manure was applied in each cell within a farm's buffer. The CDL is available for Michigan for 2007-2011. Recommended fertilizer rates from extension literature (*Warncke et al.*, 2004) were calculated for each crop type in the CDL; the recommended rate was averaged over the five year period to calculate the average rate of application over the 5 year rotation period. Within each farm's buffer, a proportion of the total manure generated by the farm was applied to each cell based on the fertilization rate estimated from the 5 year rotation. This allowed manure to be over-applied relative to the recommended rate based on

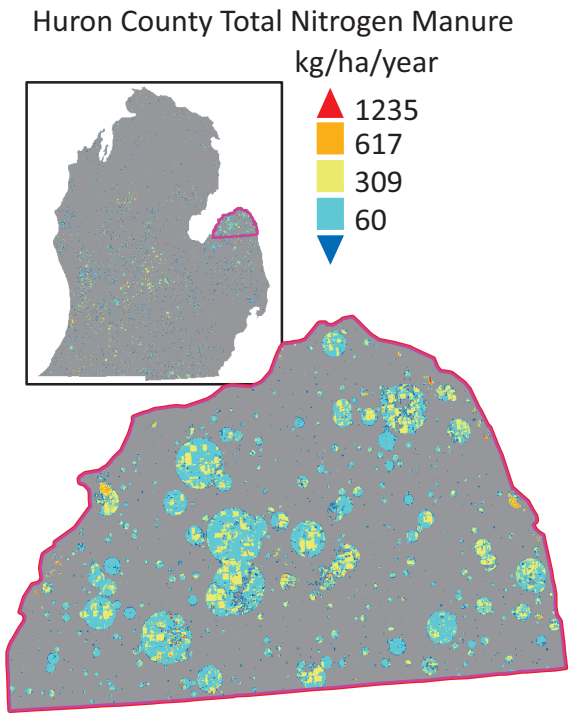

Figure 1.8: Applied manure predicted by the model for Huron County, MI.

the farm's available manure. Other studies (*Kellogg et al.*, 2000) have calculated that manure generation in several counties exceeds the nutrient demands of available cropland; therefore, it is likely that many farms apply manure above the average recommended rate. The non-spreadable portion of the manure load (the portion lost during transport and storage) was applied within the cell at the farm, assuming that this portion becomes part of the farm runoff, generating locally concentrated sources of nutrients (see Figure 1.8).

For farms designated as unconfined, waste was only applied to NLCD pasture land. Pasture land application rates were determined within each county based on the total waste produced and the total pasture area within a county. The processes used to estimate manure application are shown in Figures 1.9 and 1.10.

1.2.3.6 Commercial Fertilizer

It was assumed that cultivated land that did not receive animal manure application, received chemical fertilizer. A linear regression was fit to 2001 nutrient application estimates of

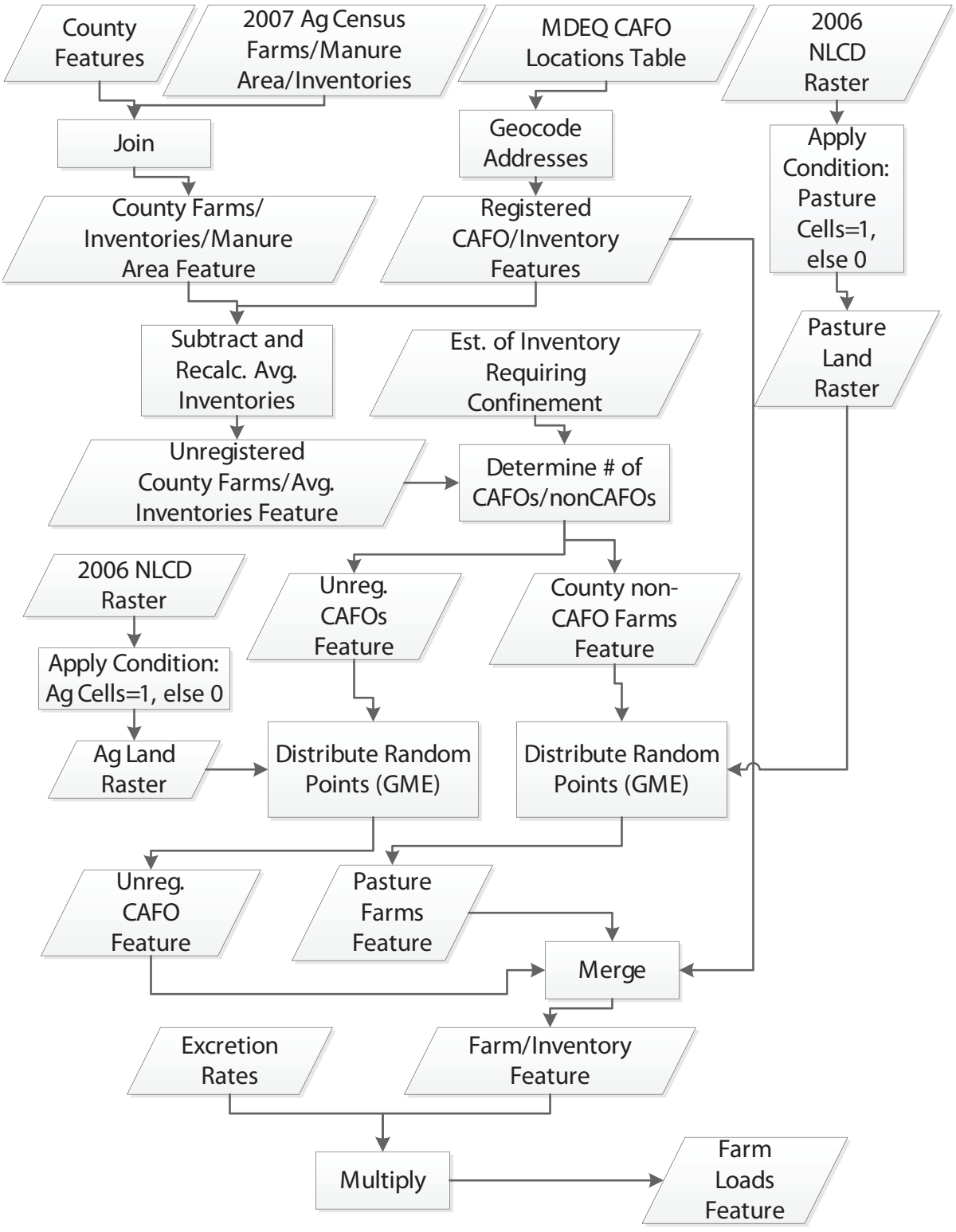

Figure 1.9: Manure Application Part I: Flow chart summarizing the process used to estimate the location and inventories of farms that produce manure.

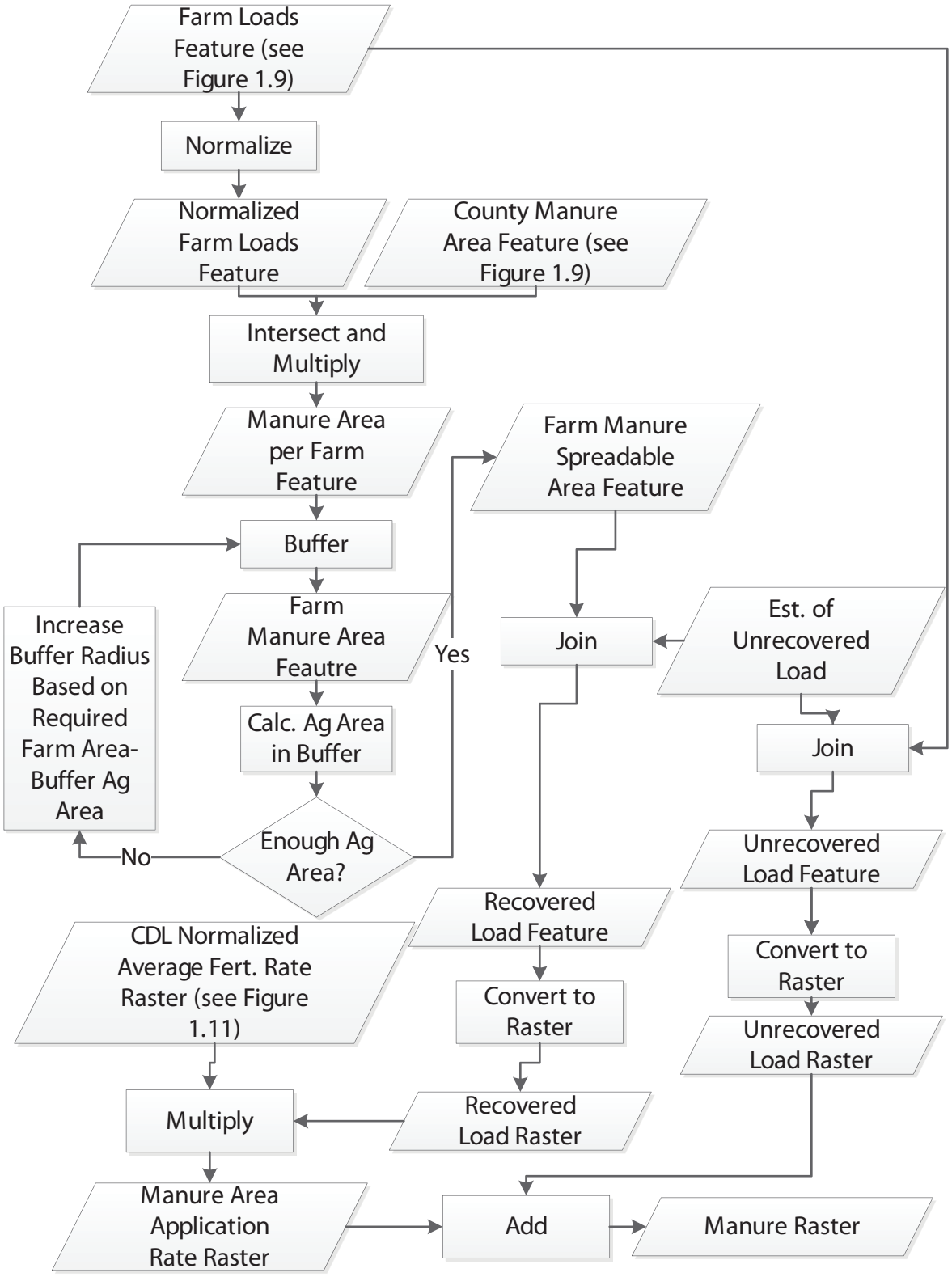

Figure 1.10: Manure Application Part II: Flow chart summarizing the process used to estimate the rate and extent of manure application.

chemical fertilizer for Michigan counties (*Ruddy et al.*, 2006) and NLCD cultivated area for 2001. This relationship was used to estimate county nutrients from agricultural chemical fertilizer for 2005-2012 using the 2006 NLCD land cover. The county level estimates of chemical fertilizer were then distributed to available cropland area within the county that did not receive manure.

Similar to manure, application rates of chemical fertilizer were estimated from the total observed chemical fertilizer in the county and the relative recommended application rate based on a cell's 5 year crop rotation. Due to variable environmental factors (climate, soil types) and local social practices, it is likely that fertilization rates for a single crop type are variable across the state. While this can create an artificial gradient at the county border, the estimate honors observed fertilizer consumption for the state. This process is shown in Figure 1.11.

1.2.4 Sample Collection

Flow measurements and nutrient samples were collected from the fall of 2011 to the spring of 2012 in two field campaigns intended to capture synoptic conditions during baseflow and melt. Sampling focused on 4 major watersheds in the Lower Peninsula of Michigan: Grand River in south central Michigan, Saginaw Bay in eastern Michigan, Muskegon River in north central Michigan, and Boardman-Charlevoix in northwest Michigan. Between 15 and 30 sites were sampled within each watershed for a total of 90 sites. Sample locations were chosen in an effort to evenly distribute samples throughout the watershed. This was accomplished by selecting points so that the area upstream of each sample point would have, approximately, the same incremental watershed area. The watersheds for the combined sampling covers over 40% of the land area of the Lower Peninsula.

A Sontek RiverSurveyor S5 Acoustic Doppler Profiler (ADCP) was generally used to measure flow in all but low flow streams, which were measured using a Marsh-McBirney Flo-Mate. Samples were also collected near USGS stream gauges, and data from gauges was

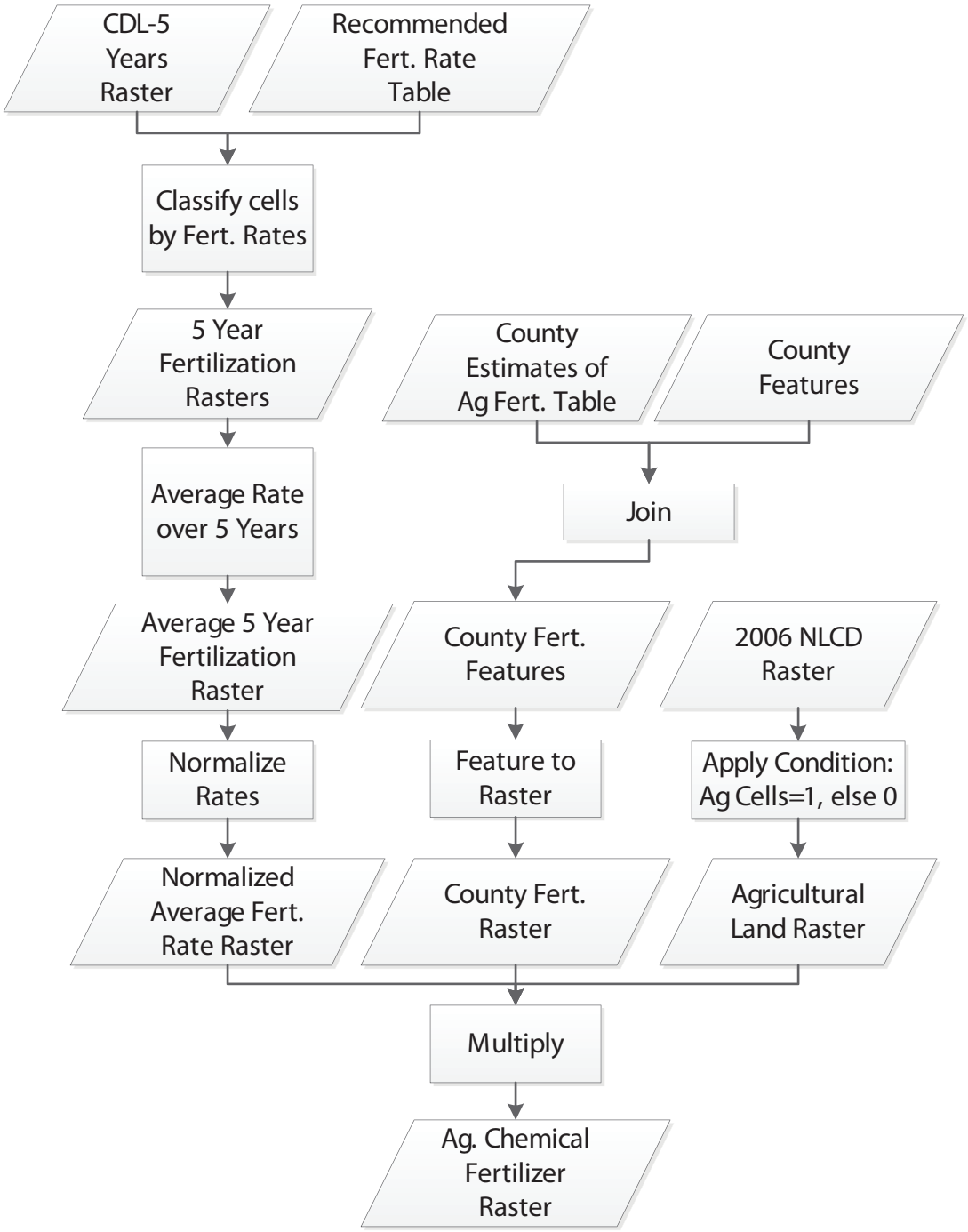

Figure 1.11: Flow chart summarizing processes used to estimate loading from commercial agricultural fertilizer.

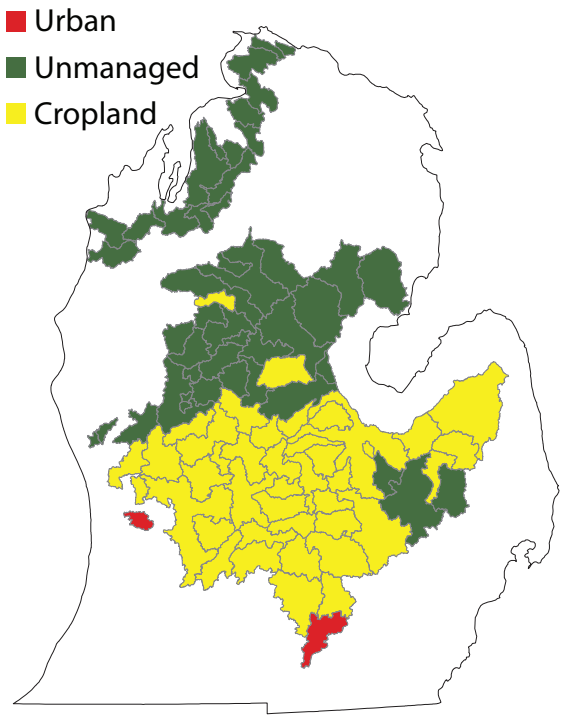

Figure 1.12: Sampled watersheds with dominant land use indicated.

downloaded to coincide with the time of the sample collection. Samples for total nitrogen and total phosphorus were collected at the time of flow measurement.

Samples were collected in-stream or from bridge crossings and then frozen on dry ice. The samples were analyzed by the Michigan State University Algae Lab using second derivative spectroscopy (TN) (*Crumpton et al.*, 1992) and ascorbic acid methods (TP) following persulfate digestion (Standard Methods 4500-P.E. and 4500-N.C). Figure 1.12 shows the incremental watersheds for each sample point with the dominant land use indicated for each watershed. Flow and sample data are provided in Appendix A.

1.3 Results

1.3.1 Sources

The results from each source model are shown in Figures 1.13 and 1.14. Total nitrogen loading to the Lower Peninsula is estimated to be an average of 23 kg/ha/year; total phosphorus loading is estimated to be an average of 3 kg/ha/year.

The proportion of the total load contributed by each land use is shown in Figure 1.15. Chemical agricultural fertilizer contributes 39% of nitrogen and ranges from nearly 62% of the total nitrogen source in cropland to 0% in unmanaged land. The largest overall source of phosphorus is also commercial fertilizer. The highest rate of phosphorus and nitrogen loading is estimated to be a result of confined animal feeding operations. This situation arises due to a lack of available land to distribute animal waste and the unrecovered portion of waste generated during confined animal feeding operations that becomes part of farm runoff. *Beaulac and Reckhow* (1982) estimate that nutrient export from confined animal feed lots may be 2-3 times greater than runoff from other agricultural land and may even be the same order of magnitude as municipal treatment plant loads.

Figure 1.16 shows total loading of phosphorus and nitrogen as well as the ratio of total phosphorus to total nitrogen. Total phosphorus loading by atmospheric deposition is low relative to nitrogen. In the north, where atmospheric deposition is the main source of nitrogen, the ratio of phosphorus to nitrogen is very low; total nitrogen loading rates are as much as 20 times greater than phosphorus loading rates from atmospheric deposition. However, in agricultural areas, the estimated ratio of total phosphorus to nitrogen is much higher, particularly in areas around confined animal feeding operations.

1.3.2 Rates by Land use

Loading rates varied significantly between land uses. The average loading rate by land use is shown in Table 1.1. The largest loading rates were estimated for cropland, which had

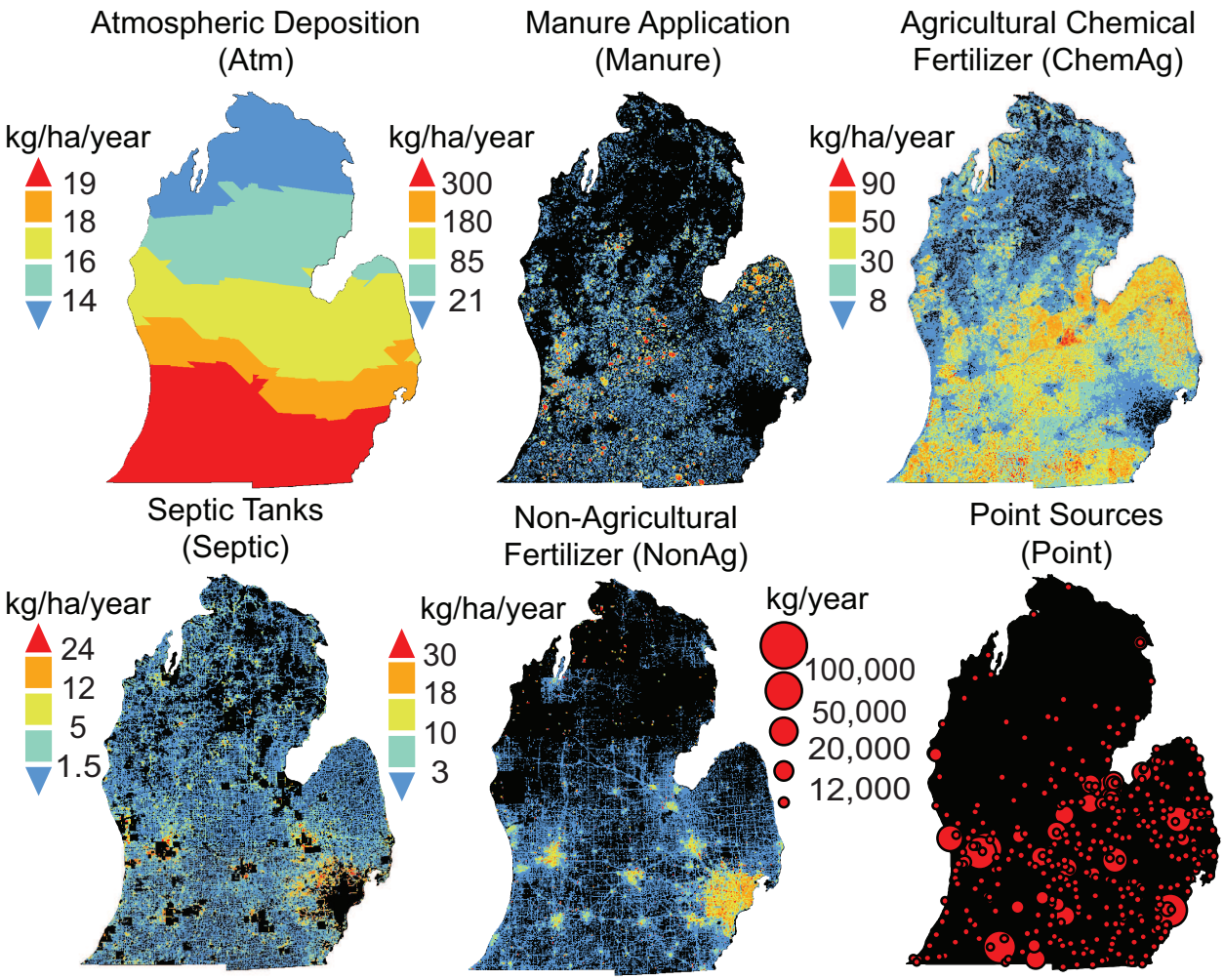

Figure 1.13: Total nitrogen application rates for each modeled source.

an average nitrogen loading rate of over 100 kg/ha/year, 2 times greater than pasture land and 3 times greater than urban land. Phosphorus loading rates estimated for cropland are 6 times greater than pasture land and 15 greater than urban land. The dominant nutrient source in unmanaged land is atmospheric deposition which is approximately 16 kg/ha/year for nitrogen and 0.2 kg/ha/year for phosphorus.

There is a high degree of variability in loading rates within land use classes. Box plots showing the range in average loading rates within sampled watersheds are shown in Figures 1.17 and 1.18. The results show that loading of chemical fertilizer within agricultural land can range from less than 0.01 kg/ha/day (3.65 kg/ha/year) to nearly 0.50 kg/ha/day

Land Use	TN	TP
	kg/ha/year	
Ag	127	19
Pasture	52	2.8
Urban	39	1.2
Unmanaged	16	0.2

Table 1.1: Nutrient loading rates by land use.

(182.5 kg/ha/year) amongst sampled watersheds for nitrogen (as a reference, the agricultural census estimated an average rate of 130 kg/ha/year of nitrogen application for corn). This illustrates the potential bias introduced to source estimates derived from land use alone, particularly across areas with diverse crop types. In Michigan, cropland in the southern areas are dominated by corn and soy while in the north, orchards, which have lower fertilization rates, are more prevalent.

1.3.3 Loading Rates and In-stream Concentration

In order to assess the relationship between loading and in-stream water quality, a linear model was fit to average loading rates within watersheds and total nitrogen and total phosphorus concentrations under baseflow and melt conditions. The form of the linear model is

$$C_i = \alpha_1 Point_i + \alpha_2 ChemAg_i + \alpha_3 Manure_i + \alpha_4 NonAgFert_i + \alpha_5 Septic_i + \alpha_6 Atm_i + B \quad (1.1)$$

where C_i is the concentration (μg/L) of total phosphorus or total nitrogen measured for watershed i, each alpha is a model coefficient, each source term is the average loading rate (kg/ha/day) in watershed i, and B is the model intercept. The results of each linear model are shown in Table 1.2.

The R^2 was 0.50 for the nitrogen melt model and 0.29 for the nitrogen baseflow model. The phosphorus melt model had an R^2 of 0.06 and the baseflow model R^2 was 0.24. The results of the models are plotted with observed values in Figure 1.19.

Source	TN Melt		TN Base	
	α	p-value	α	p-value
Atm	1.66E+06	0.95	1.12E+07	0.23
ChemAg	2.00E+07	**8.34E-05**	-3.12E+05	0.84
Manure	3.25E+06	0.37	3.21E+06	**7.17E-03**
NonAg	7.64E+07	0.49	9.12E+07	**1.19E-02**
Septic	-2.50E+08	0.13	3.21E+07	0.16
Point	3.44E+08	0.22	-7.52E+07	0.72
Intercept (B)	7.17E+02	0.55	-1.10E+02	0.78
	TP Melt		TP Base	
Atm	4.07E+08	0.51	1.64E+09	**7.93E-04**
ChemAg	2.69E+05	0.88	-4.32E+05	0.75
Manure	2.85E+05	0.82	8.83E+05	0.35
NonAg	4.15E+07	0.54	6.46E+07	0.22
Septic	-4.32E+06	0.94	-5.41E+07	0.20
Point	1.98E+07	0.63	-1.07E+07	0.74
Intercept (B)	2.98E+01	0.82	-2.90E+02	**3.95E-03**

Table 1.2: Results of linear regression models of source loading and observed in-stream concentration. The α value represents the fitted coefficient. Bold values indicated parameters with a p-value $\leq$0.05

The p-values which indicate the significance of each model parameter show that commercial fertilizer is the only significant predictor of nitrogen concentration in watersheds. None of the sources were significant in the phosphorus model. When observations with concentrations above 200 (μg/L) are removed from the total phosphorus baseflow observations, the R^2 improves to 0.46 and manure, atmospheric deposition, and non-agricultural fertilizer have significant coefficients.

The source inputs for this linear model include source loading throughout the entire watersheds. In larger watersheds, sources applied at large distances from surface water may never be delivered to the stream due to attenuation of nutrients within the watershed. A second linear model was constructed using source inputs applied within a 1 km flow distance from surface water. Flow distance was calculated using the ArcGIS Hydro Toolbox and the National Elevation Dataset (NED) (*Roth and Dewald*, 1999). The results are shown in Table 1.3 and Figure 1.20. This approach slightly improved the R^2 value for the melt models but

Source (within 1 km of surface water)	TN Melt		TN Base	
	α	p-value	α	p-value
Atm	2.71E+07	0.59	8.76E+06	0.61
ChemAg	**3.90E+07**	**1.78E-04**	4.53E+05	0.89
Manure	1.05E+07	0.17	**7.86E+06**	**3.56E-03**
NonAg	6.87E+07	0.74	1.34E+08	0.06
Septic	-5.47E+08	0.10	-9.05E+07	0.42
Point	3.93E+08	0.15	1.03E+07	0.91
Intercept (B)	4.74E+02	0.61	2.14E+02	0.49
	TP Melt		TP Base	
Atm	1.23E+09	0.20	**1.64E+09**	**7.93E-04**
ChemAg	-2.27E+06	0.56	-4.32E+05	0.75
Manure	1.01E+06	0.73	8.83E+05	0.35
NonAg	5.61E+07	0.65	6.46E+07	0.22
Septic	9.51E+06	0.93	-5.41E+07	0.20
Point	2.60E+07	0.53	-1.07E+07	0.74

Table 1.3: Results of linear regression models of source loading within 1 km of surface water and observed in-stream concentration. The α value represents the fitted coefficient. Bold values indicated parameters with a p-value $\leq$0.05

decreased the R^2 for the baseflow models.

1.4 Discussion

An understanding of the relationship between nutrient source loading and in-stream water quality is not only necessary to effectively manage surface water quality but is also fundamental to predicting how water quality will change with alterations of land use and land management. Average loading rates of nutrients to watersheds in the Lower Peninsula are highly variable ranging from 0 kg/ha/year to over 200 kg/ha/year of nitrogen and over 40 kg/ha/year of phosphorus. These high rates of loading are estimated to result from confined animal feeding operations. Manure is the second largest source of nitrogen and third largest source of phosphorus. As animal production shifts to increasingly consolidated operations, nutrients from manure have the potential to become a major concentrated source of nutrients in agricultural watersheds (*Chang et al.*, 2003; *Kellogg et al.*, 2000). Within all

land use types, except unmanaged land where the major source is atmospheric deposition, loading rates for major sources exhibited at least 1 order of magnitude of variability. This illustrates the difficulty in assigning loading rates of nutrients based on land use alone in diverse watersheds.

While these estimates provide an indication of the source of nutrients to the landscape, estimating in-stream concentrations from total sources of nutrients is more complicated. Attenuation processes occurring within watersheds alter nutrient loads as they travel within the basin to surface water. The results of the linear model suggest that with source estimates alone, less than 50% of the variability in concentrations can be explained (the nitrogen melt model had the highest R^2 of 0.50). The results indicate that phosphorus sources are a poor predictor of melt phosphorus (R^2 was only 0.06). In addition, during baseflow, concentrations increase linearly with increasing sources for watersheds with concentrations less than 200 μg/L but watersheds with concentrations above 200 μg/L are not characterized by greater rates of source application. These results suggests that other factors are important to estimate watershed phosphorus concentrations, including biological processes, processes that occur in-stream, as well as legacy and natural sources of phosphorus. In all but the nitrogen baseflow model, the coefficient for septic was negative and in both baseflow models, the coefficient for point sources was negative. While this may seem counter intuitive, it may be the result of dilution by these sources since they are associated with large amounts of waste water.

Both phosphorus and nitrogen melt models improved when only sources within 1 km of surface water were considered. However, sources within 1 km of surface water provided poorer predictions of in-stream concentrations during baseflow. There are several explanations for this effect including legacy sources of nutrients and the influence of nutrients in groundwater during baseflow. It is important to note, however, that the differences between models was only slight, and it appears that additional factors other than source distance control source delivery. The relationship between nutrient sources, basin attenuation, and observed nutrient

loads is explored further in CHAPTER 2 of this thesis.

This methodology provides a means to investigate locally important concentrated sources of nutrients such as golf courses and septics. Source estimates not only provide the potential to investigate the relationship between nutrients and concentration but can be used to examine relationships between water quality and the sources of other pollutants, particularly those associated with waste. For instance, *Verhougstraete* (2012) compared estimates of septic loads developed using these methods to the occurrence of B. thetaiotaomicron (B. theta) a human marker for fecal contamination, in surface water samples from the Lower Peninsula.

Since data related to sources of nutrient loads is limited at the spatial scale used in this research, it is difficult to determine the error associated with some of these estimates. The accuracy of the estimates is in large part based on the the accuracy of the remotely sensed products used to distribute many of the sources including the 2006 NLCD and the 2007-2011 Cropland Data Layers. Additionally, random distributions of points were used to estimate the locations of unknown septics and confined animal feeding operations and to distribute loads within receiving areas. Since manure is the second largest source of phosphorus and the third largest source of nitrogen, this is a potentially important source of error. Additional validation of the septic and CAFO locations will improve the confidence of these source estimates.

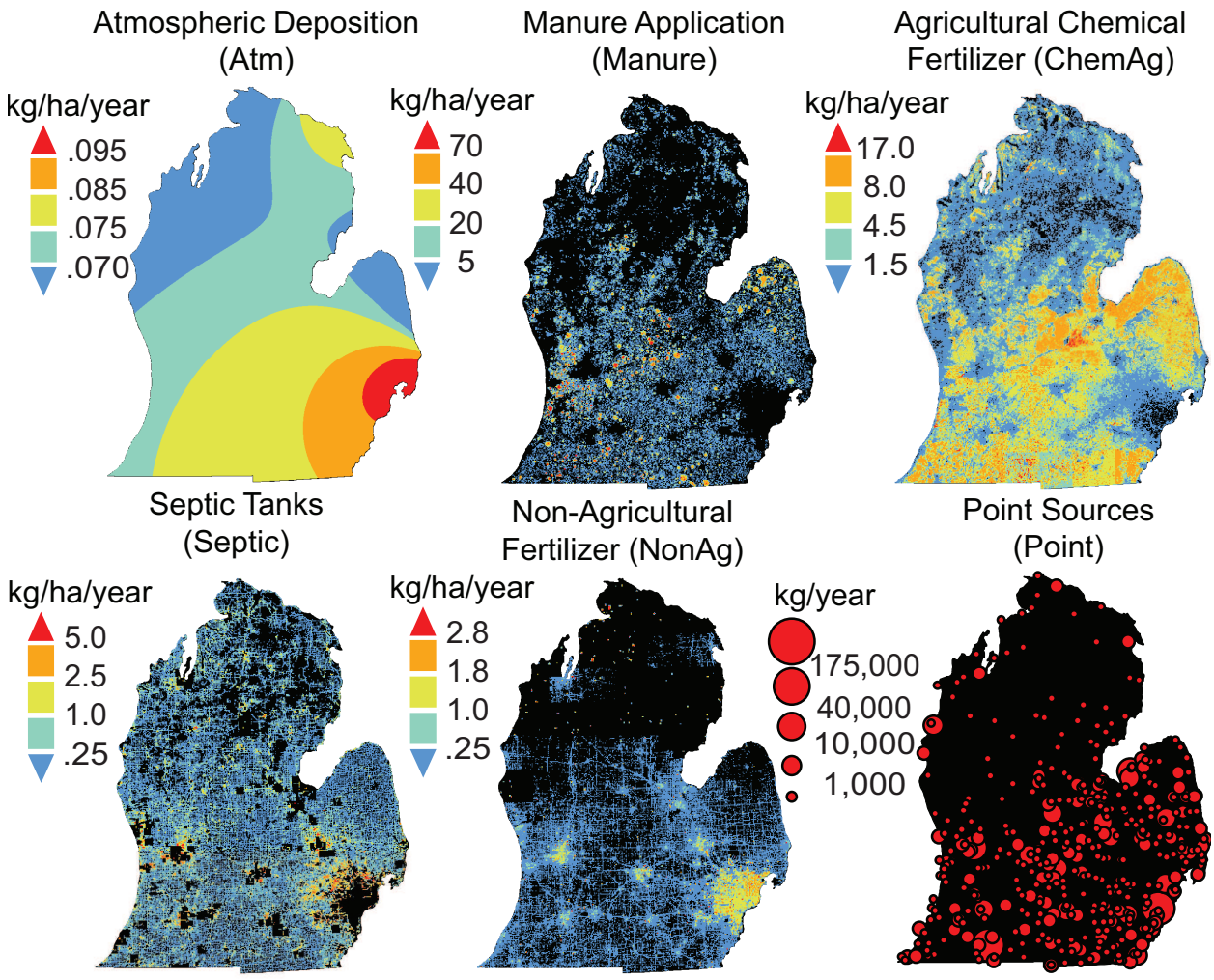

Figure 1.14: Total phosphorus application rates for each modeled source.

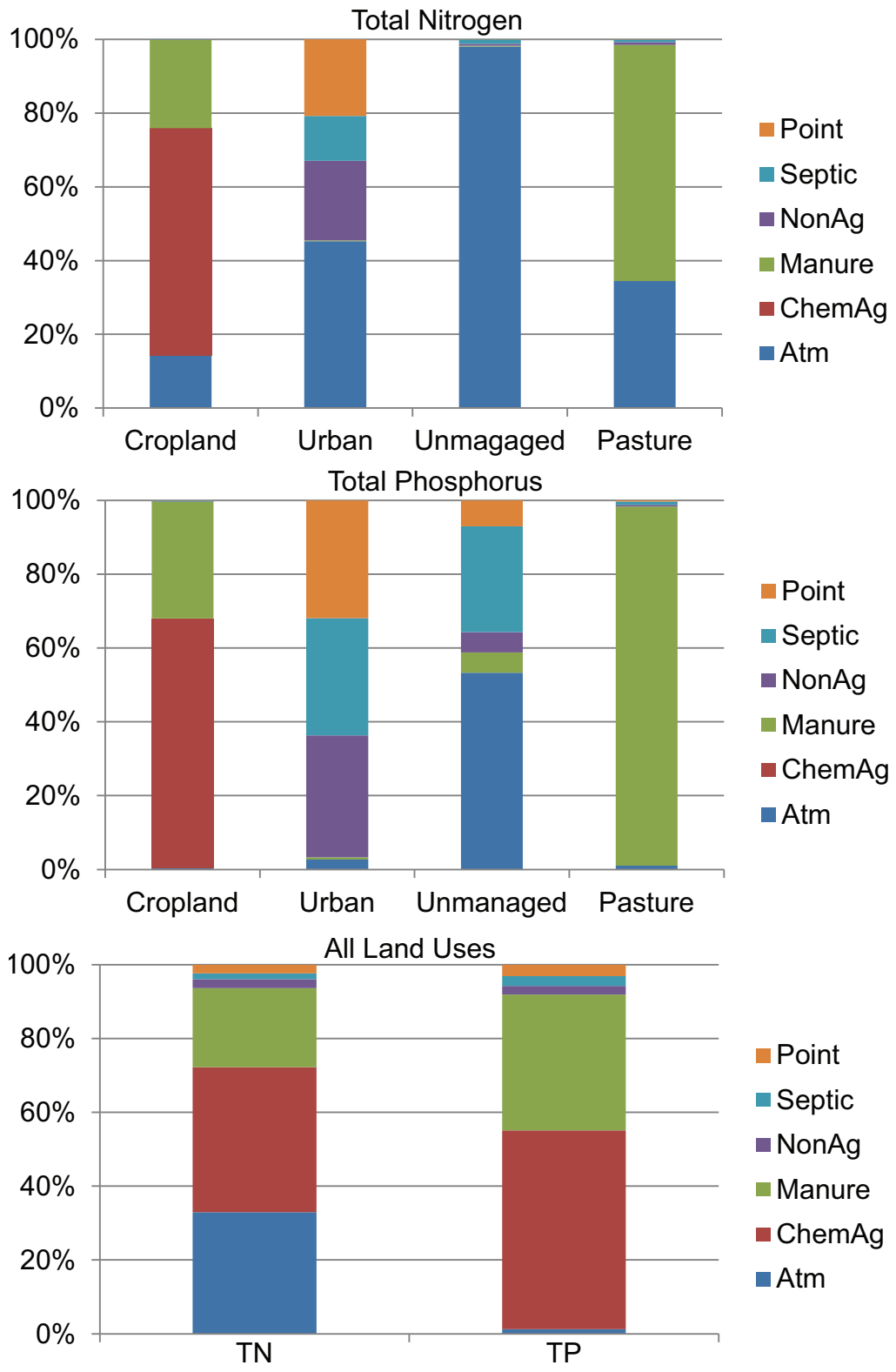

Figure 1.15: Proportion of the total nutrient load contributed by each source for the entire Lower Peninsula and within different land uses.

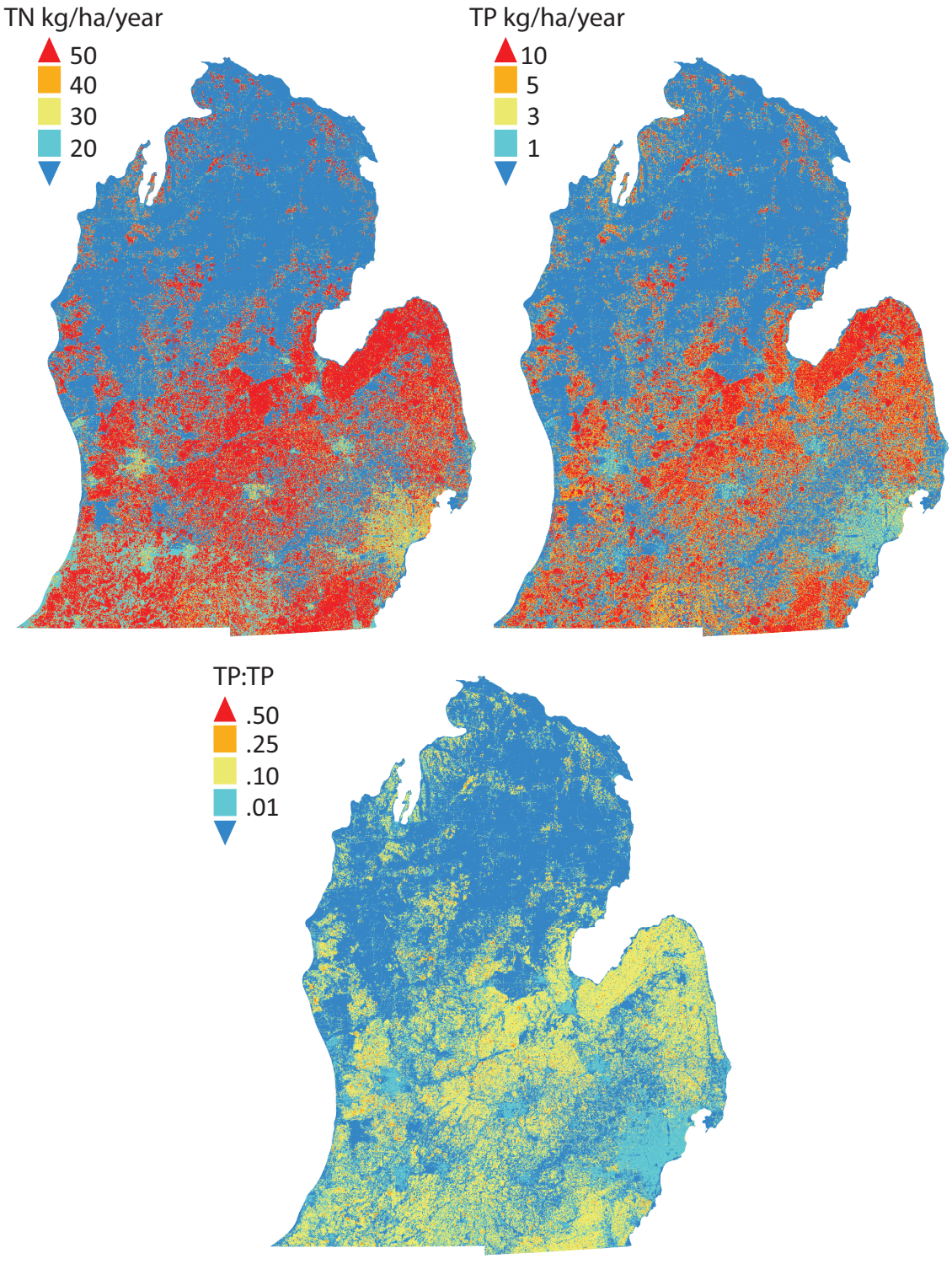

Figure 1.16: Total nitrogen and phosphorus loading in the Lower Peninsula. The ratio of total phosphorus to total nitrogen is shown in the bottom panel.

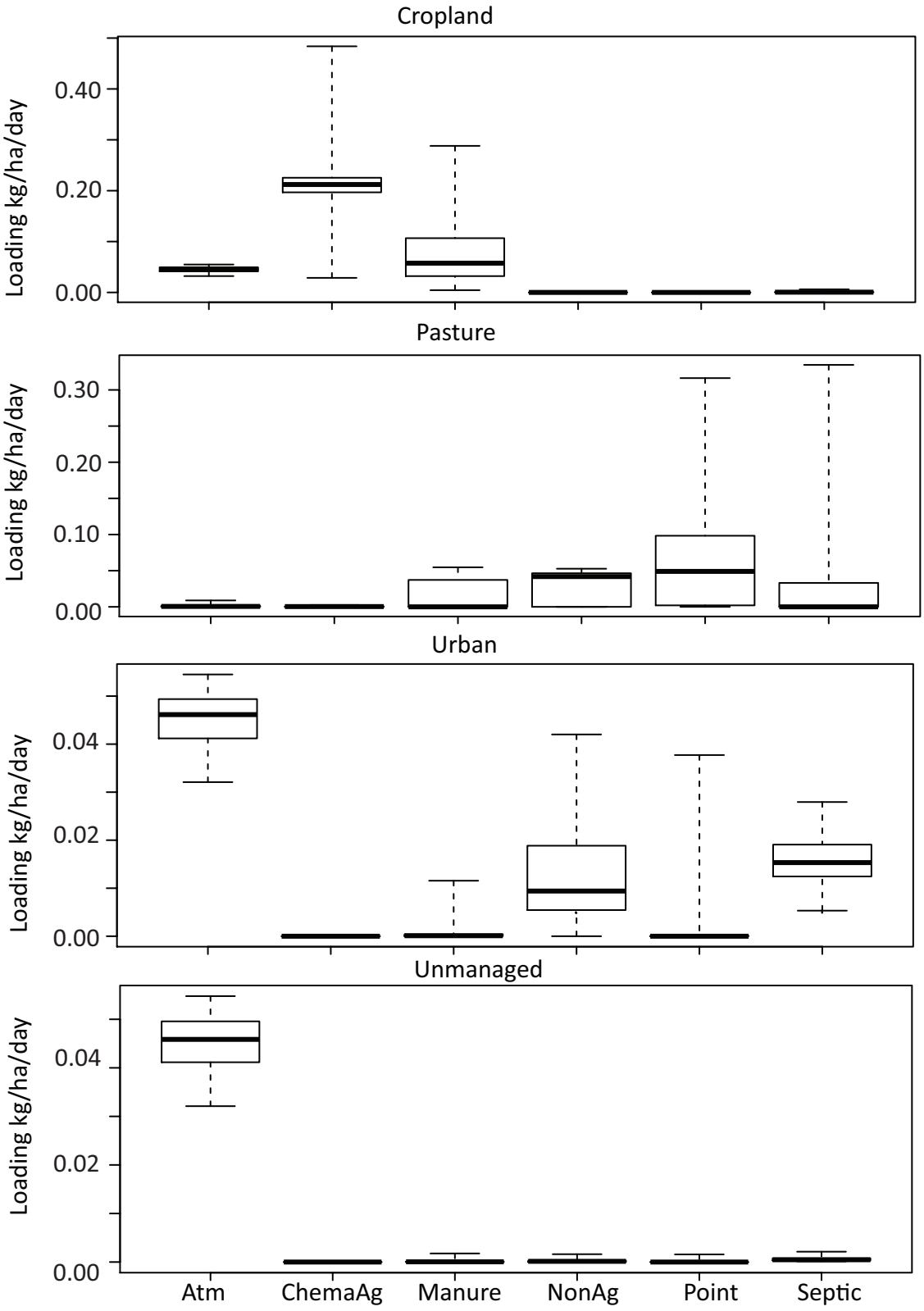

Figure 1.17: Box plots of total nitrogen loading rate variability in sampled watersheds. Loading rates are subset by land use.

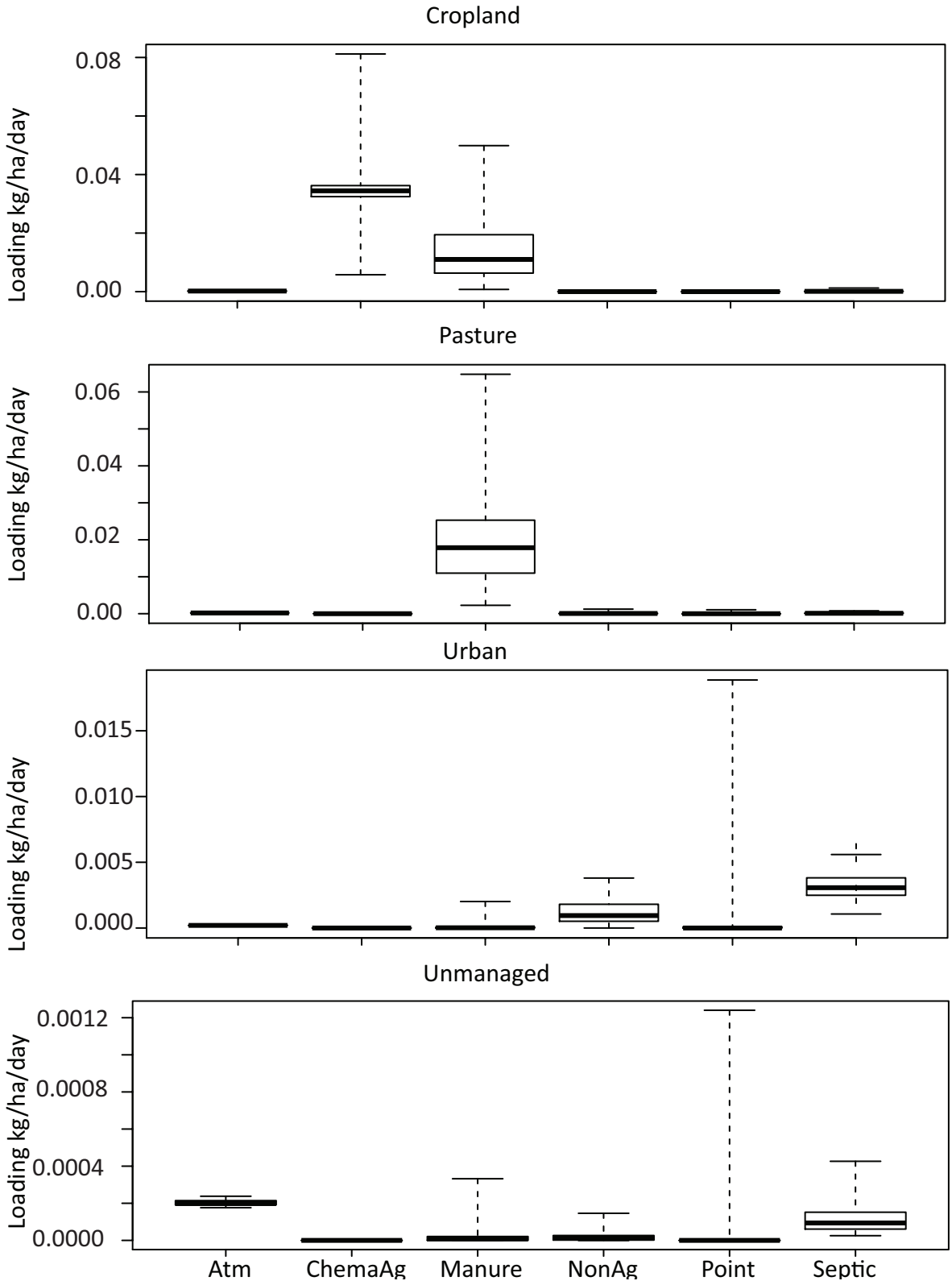

Figure 1.18: Box plots of total phosphorus loading rate variability in sampled watersheds. Loading rates are subset by land use.

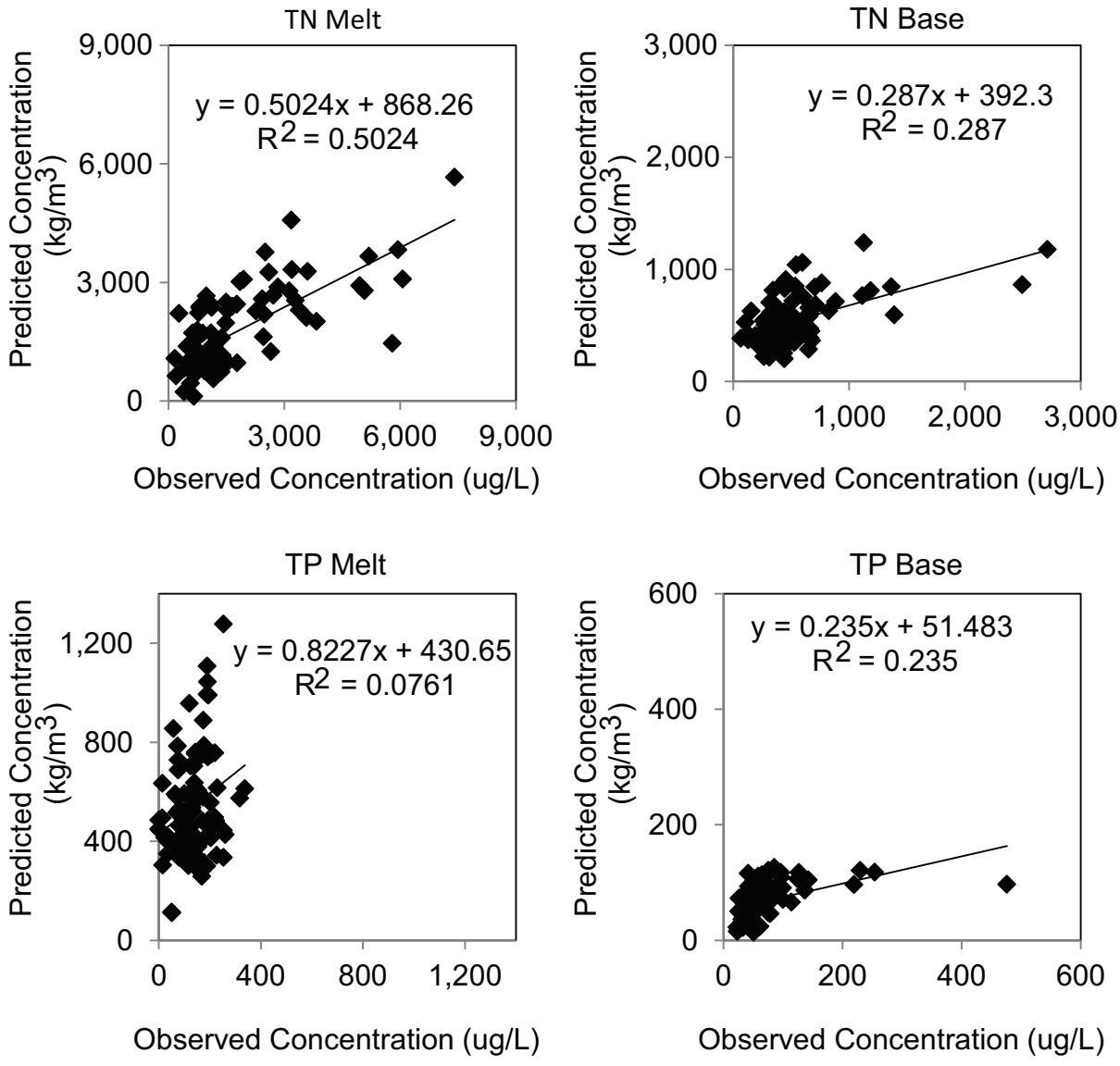

Figure 1.19: Graphs showing linear regression model predictions compared to observed concentrations.

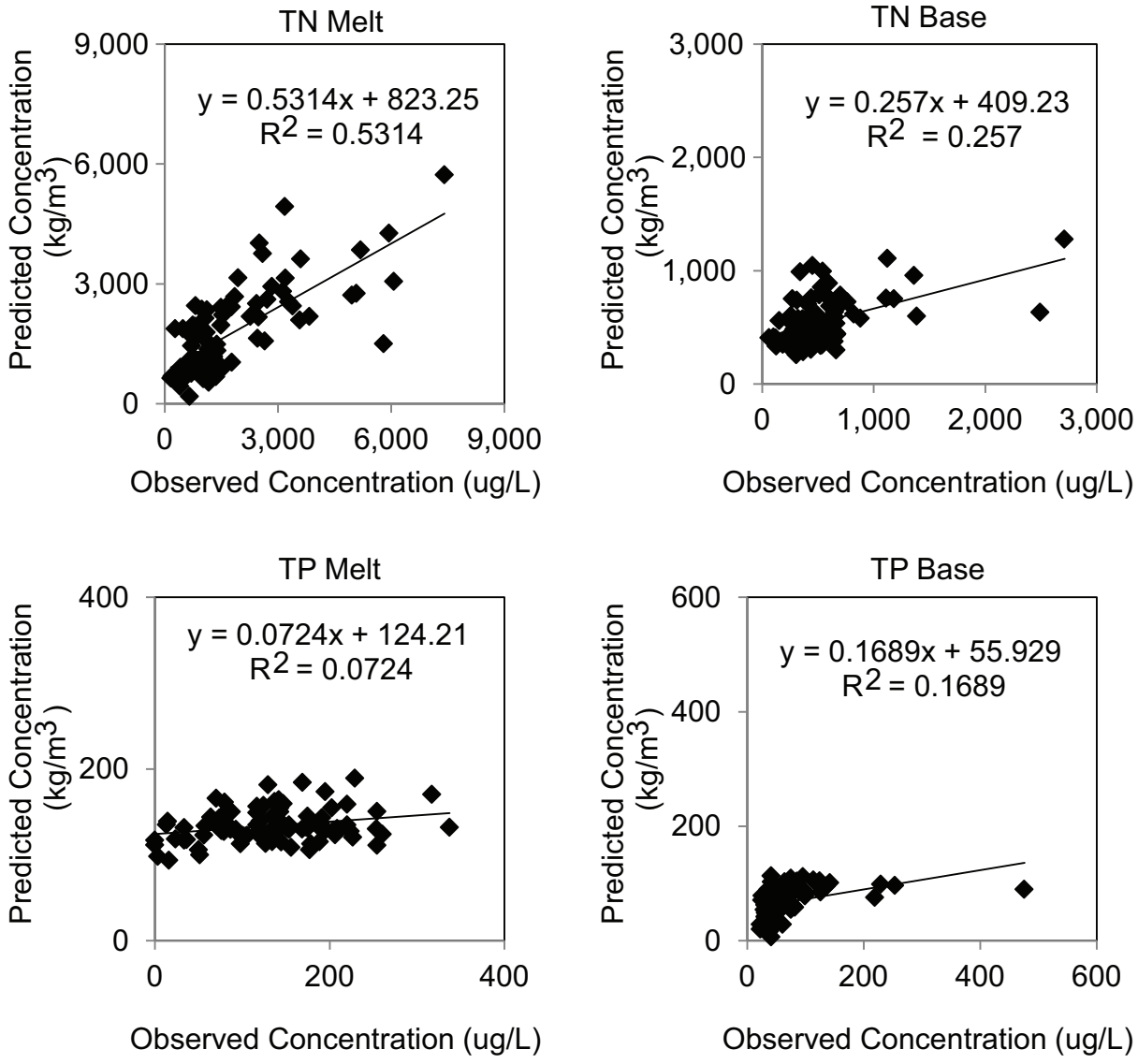

Figure 1.20: Graphs showing linear regression model predictions (based on nutrient loads within 1 km of surface water) compared to observed concentrations.

CHAPTER 2

PREDICTING NUTRIENT LOADS AND SOURCES: A SPATIALLY EXPLICIT STATISTICAL MODEL

2.1 Introduction

Nutrient loading models are one tool used to help quantify how changes in land use, management practices, and nutrient sources will impact in-stream and coastal water quality. While trends in water quality can be observed through periodic sampling, observations are limited in spatial and temporal extent by expense and accessibility (*Smith et al.*, 1997; *Valiela et al.*, 1997; *Alexander et al.*, 2002; *Borah and Bera*, 2004). Cutbacks to state and federal monitoring programs have led to decreases in the frequency and geographic coverage of samples (*Robertson and Saad*, 2011). Models can be used to estimate nutrient loads at unmonitored locations increasing the spatial and temporal resolution of nutrient loading estimates (*Smith et al.*, 1997). They can also forecast trends in water quality under scenarios of changing land use and climate and have been used at various scales to assess the source of nutrients, target source areas for management, and predict the effectiveness of management strategies. Models are particularly useful to better understand the role of non-point sources to nutrient loads (*Nikolaidis et al.*, 1998; *Borah and Bera*, 2004).

Several nutrient load modeling approaches exist in the literature (as reviewed in *Alexander et al.* (2002), *Borah and Bera* (2004) and *Valiela* (2002)). These range from semi-distributed hydrologic models such as the Soil Water Assessment Tool (SWAT) to simple mass balance accounting (*Jaworski et al.*, 1992; *Alexander et al.*, 2002; *Boyer et al.*, 2002). Common among many existing approaches is a tendency to lump sources or assume nutrient loading rates based on factors such as land use or management practices rather than directly accounting for independent source contributions. Such methods generally assume that changes in land use or management will lead to a proportional response in source contribution to loading which

limits their transferability (*Zhang*, 2011; *Destouni et al.*, 2006). Detailed descriptions of each source independent of transport mechanisms are necessary to describe nutrient loads across highly variable watersheds and predict how nutrient loading will be impacted by changes in climate and land use.

This work was motivated by the need for a nutrient model that can accurately and consistently predict nutrient loads at a high level of spatial detail across diverse watersheds. The model described here is based on spatially detailed and temporally variable descriptions of all potential nutrient sources in Michigan's Lower Peninsula (as described in CHAPTER 1) to better understand the impact specific sources have on nutrient loading. These sources are related to stream water quality through a statistical model that provides insight to the importance of pathways and processes. This model improves on nutrient loading models (described below) by enhancing the spatial detail of individual sources at a regional scale while retaining the ability to predict source contributions to the observed load.

2.1.1 Review of Existing Approaches

Examples of nutrient models developed at scales similar to the Lower Peninsula of Michigan include the budget approach (*Jaworski et al.*, 1992; *Boyer et al.*, 2002), the use of export coefficients (*Johnes and Heathwaite*, 1997; *Johnes*, 1996), loading functions (Generalized Watershed Loading Functions-GWLF) (*Haith and Shoenaker*, 1987; *Evans et al.*, 2002; *Georgas et al.*, 2009) and statistical approaches such as the USGS SPARROW (Spatially-Referenced Regression on Watershed attributes) model (*Smith et al.*, 1997). These approaches are described below.

A budget approach examines the difference between the nutrient inputs and outputs to a watershed (*Boyer et al.*, 2002; *Jaworski et al.*, 1992). While applications of this approach can incorporate detailed sources, they give little information about pathways and processes (*Robertson and Saad*, 2011). In its simplicity, this type of model makes it difficult to understand the controls on nutrient reduction that occur as nutrients travel through the landscape.

While an attempt is made to identify the net inputs from each source, the relative proportion of the observed load cannot be attributed to a particular source. Depending on landscape and stream factors, the proportion of nutrients delivered to a stream from a particular source will vary (*Boyer et al.*, 2002; *Robertson and Saad*, 2011). These assumptions make it difficult to use this type of model to predict loading in the future or in unmonitored locations outside of the studied watershed.

The export coefficient method attempts to predict the nutrients derived from various land cover/land use types (*Johnes*, 1996; *Johnes et al.*, 1996). This method assumes that loading will be evenly distributed across a land cover and that all land covers will contribute nutrients at the same rate (*Johnes*, 1996; *Vadeboncoeur et al.*, 2010; *Zhang*, 2011). "Export Coefficients", the proportion of the initial applied source that is delivered to the stream, are estimated for various land uses, conditions, and management practices. This method is ideally suited to smaller watersheds where there is minimal variation across land cover types. This assumption becomes problematic at larger scales, where land use practices and land cover conditions, and how they affect nutrient export, are more variable (*Zhang*, 2011, 2010).

More physically based models such as SWAT and Generalized Watershed Loading Function (GWLF) use a process-based approach to calculate hydrologic and sediment fluxes within the system. GWLF uses water balance equations to simulate runoff and erosion from "subareas" within the basin of interest (*Haith and Shoenaker*, 1987; *Georgas et al.*, 2009) and estimates the concentrations of dissolved nutrients in runoff and baseflow depending on the proportion of various land uses in the subarea (*Haith and Shoenaker*, 1987; *Evans et al.*, 2002; *Alexander et al.*, 2002). SWAT uses a similar approach but includes additional, partially process-based descriptions of nutrient cycling and land management (*Grizzetti et al.*, 2005; *Arnold et al.*, 1998). SWAT has been applied with a highly detailed accounting of agricultural sources and management practices, but other sources such as urban fertilizer are less detailed, and atmospheric deposition is completely excluded (*Valigura et al.*, 2001).

Since other models have identified atmospheric deposition as a major source of nitrogen to watersheds, this is problematic (*Robertson and Saad*, 2011; *Valigura et al.*, 2001; *Boyer et al.*, 2002). Additionally, both SWAT and GWLF uniformly distribute sources in a sub-catchment unit within a basin.

The most geographically extensive statistical model that has been applied for the Major River Basins (MRBs) in the United States is SPARROW (*Robertson and Saad*, 2011), which relates nutrient loading in catchments and landscape factors to observed nutrient data via a statistical model that is process informed (*Smith et al.*, 1997; *Robertson and Saad*, 2011; *Preston and Brakebill*, 1999; *Moore et al.*, 2004; *Schwarz et al.*, 2006). This particular statistical approach allows for the explicit description of landscape factors and a better understanding of the magnitude of processing, but as applied, SPARROW lumps some nutrient sources into large categories such as "urban" or "agriculture" which include several potential sources of nutrients that are not uniformly distributed. In some cases a "surrogate", such as population or urban area is used to account for the loading from a particular source or land use. SPARROW only considers a single pathway for a particular basin, lumping overland flow and groundwater pathways into a single parameter, and similar to SWAT and GWLF, the sources are distributed evenly, throughout a sub-catchment (*Schwarz et al.*, 2006; *Robertson and Saad*, 2011).

With all of the approaches described above, there is a general tradeoff between the scale of the model and the level of detail regarding the individual sources of nutrients and their pathways. Another drawback of existing models is a lack of direct source accounting, which makes it difficult to apply these models consistently in highly variable watersheds (*Nikolaidis et al.*, 1998; *Destouni et al.*, 2006). Furthermore, with the exception of the process-based models, existing approaches are generally applied to yearly loading averages and do not consider seasonal variability in processes and pathways. Figure 2.1 is a qualitative comparison of existing models illustrating these compromises.

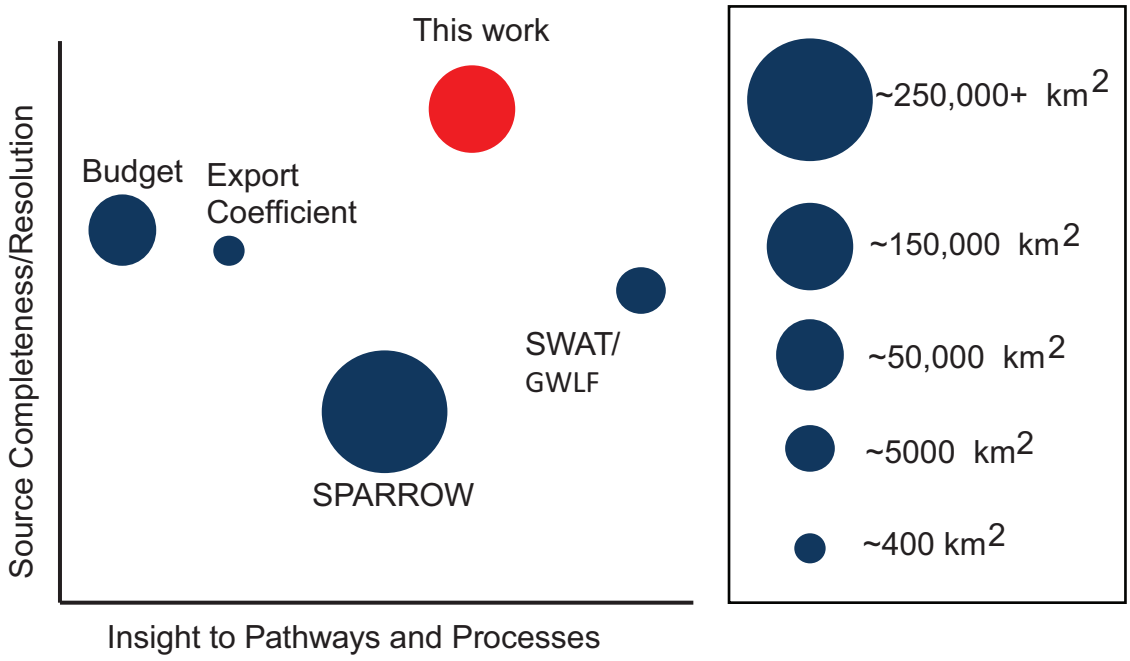

Figure 2.1: Qualitative comparison of nutrient modeling approaches.

2.2 Methods

2.2.1 Model Description

The model is a physically informed statistical model that uses a detailed and spatially explicit description of nutrient sources. The form of the model equation, similar to SPARROW, considers a simplified conceptual structure in which sources applied to the landscape experience attenuation along two pathways: travel within the upland portion of the basin and travel within the stream. This attenuation is described by statistically derived reduction factors that are functions of a basin's physical features.

At the foundation of the modeling approach is a spatially detailed description of nutrient sources. Nutrient applications are defined for each cell of the model using an estimation process described in CHAPTER 1. The load at an observation point is modeled by summing the contribution of nutrients from all cells that are upstream of the point and applying the

statistically derived reduction factors that are functions of a cell's position in the watershed. The functional form of the model is shown in Equation 2.1.

$$\sum_{i}^{sources} \sum_{j}^{cells} Q_{ij} R_j \left[Fgrd_j Bgrd_{ij} + \left(1 - Fgrd_j\right) Bsurf_j \right] \tag{2.1}$$

Q_{ij} is loading of source i to cell j, *Fgrd* is the fraction of nutrients entering the subsurface pathway, and *Bgrd*, *Bsurf*, and R are reduction factors that account for physical and biological attenuation in the watershed.

Bsurf and *Bgrd* describe attenuation that occurs as nutrients travel through the landscape to surface water; *Bsurf* represents the surface pathway and *Bgrd* represents the groundwater pathway. *Bsurf* and *Bgrd* are exponential functions of travel distance from cell j to surface water. These factors are calculated as

$$Bsurf_j = e^{(\alpha_1 * D_j)} \tag{2.2}$$

$$Bgrd_j = e^{(\alpha_2 * D_j)} \tag{2.3}$$

where α_1 and α_2 are empirically derived coefficients and D is flow distance from cell j to the nearest stream. The values of α_1 and α_2 are constrained between -1 and 0.

R describes attenuation that occurs during the in-stream portion of the pathway and is an exponential function of both travel time and basin yield. The equation for R is shown in Equation 2.4.

$$R_j = e^{(\alpha_3 * T_j)} * \alpha_4 * BY_j \tag{2.4}$$

T represents the in-stream travel time from cell j to the downstream observation point, α_3 is an empirically derived coefficient constrained between -1 and 0, α_4 is an empirically derived coefficient constrained between 0 and 1, and BY_j is the basin yield defined for each sub-watershed. Basin yield, which is the total discharge of a basin divided by the basin area, is a surrogate for recharge. Rivers with slow moving water and/or small, shallow channels,

may experience more biologic and physical processing due to increased interaction between the channel bed, the hyporheic zone, and the biota in the stream (*Alexander et al.*, 2000; *Mainston and Parr*, 2002). These watersheds tend to have low basin yields.

One alternative groundwater pathway (septic plumes) and one alternative surface pathway (tile drains) were also considered in the model. Since attenuation in septic plumes occurs differently than attenuation in other areas (*Valiela et al.*, 1997; *Robertson and Cherry*, 1992; *Reneau and Pettry*, 1976; *Gilliom and Patmont*, 1983), *Bsep*, which describes septic plume attenuation, is substituted for *Bgrd* for the septic source. *Bsep* has the same form as *Bsurf* and *Bgrd* ($Bsep = e^{(\alpha 7 * D_j)}$). In the Lower Peninsula model, the coefficient for *Bsep* was fixed based on analysis done by *Valiela et al.* (1997) who compiled data from several studies sampling septic plumes and concluded that roughly 35% of loss occurred in the septic plume over a 200 meter distance with an exponential loss rate. Tiles alter the overland flow pathway, so *Btile* ($Btile = e^{(\alpha 5 * D_j)}$) was substituted for *Bsurf* in cells where tile drains exist.

Fgrd is a function of cell recharge and is calculated as

$$Fgrd = \alpha_6 * recharge_j \tag{2.5}$$

Since septic tank loading occurs in the subsurface, *Fgrd* is set to 1 for the septic source and the value of α_6 is constrained between 0 and 1. *Fgrd* is set to 0 for all surface water cells since atmospheric deposition falling directly on surface water experiences no landscape attenuation. Similarly, *Fgrd* is set to 1 for point sources and point sources are applied only to river cells, which leads to a basin travel distance D_j of 0 and a $Bsurf_j$ of 1. This ensures that point sources only experience attenuation along the river pathway. The conceptual model underlying the model equation is shown in Figure 2.2.

Several alternative parameters were considered in the modeling structure including travel through lacustrine and palustrine wetlands, in-stream travel distance, and depth to bedrock. These parameters were ultimately abandoned because models were relatively insensitive to

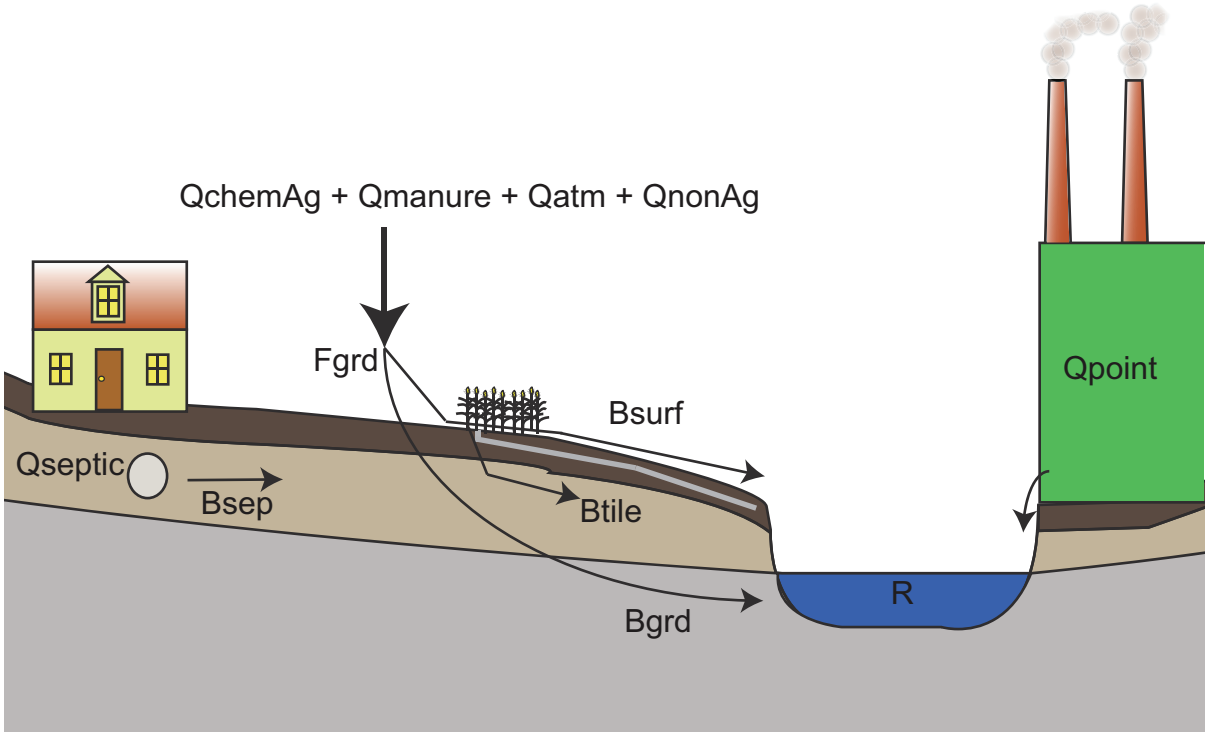

Figure 2.2: Conceptual model illustrating the sources and pathways described in the model. Nutrient sources include septic tanks (Qseptic), agricultural chemical fertilizer (QchemAg), manure (Qmanure), atmospheric deposition (Qatm), non-agricultural fertilizer (QnonAg), and point sources (Qpoint). R, Bgrd, Btile, Bsep, and Bsurf are the reduction factors and describe loss along the in-stream, groundwater, tile, septic, and surface runoff pathways, respectively.

them, and they did not improve model performance.

Unlike SPARROW, the model has a spatially explicit description of sources and basin factors, which includes within basin variability and the addition of travel distance and travel time as factors. This allows for an expanded process-based description of pathways. The differences between the spatially explicit model structure described here and a sub-basin based model such as SPARROW are illustrated in Figure 2.3.

2.2.2 Landscape and Pathway Descriptions

In the model landscape characteristics and travel pathways are used to predict the attenuation of nutrients in the watershed. Similar to nutrient sources, each landscape factor is

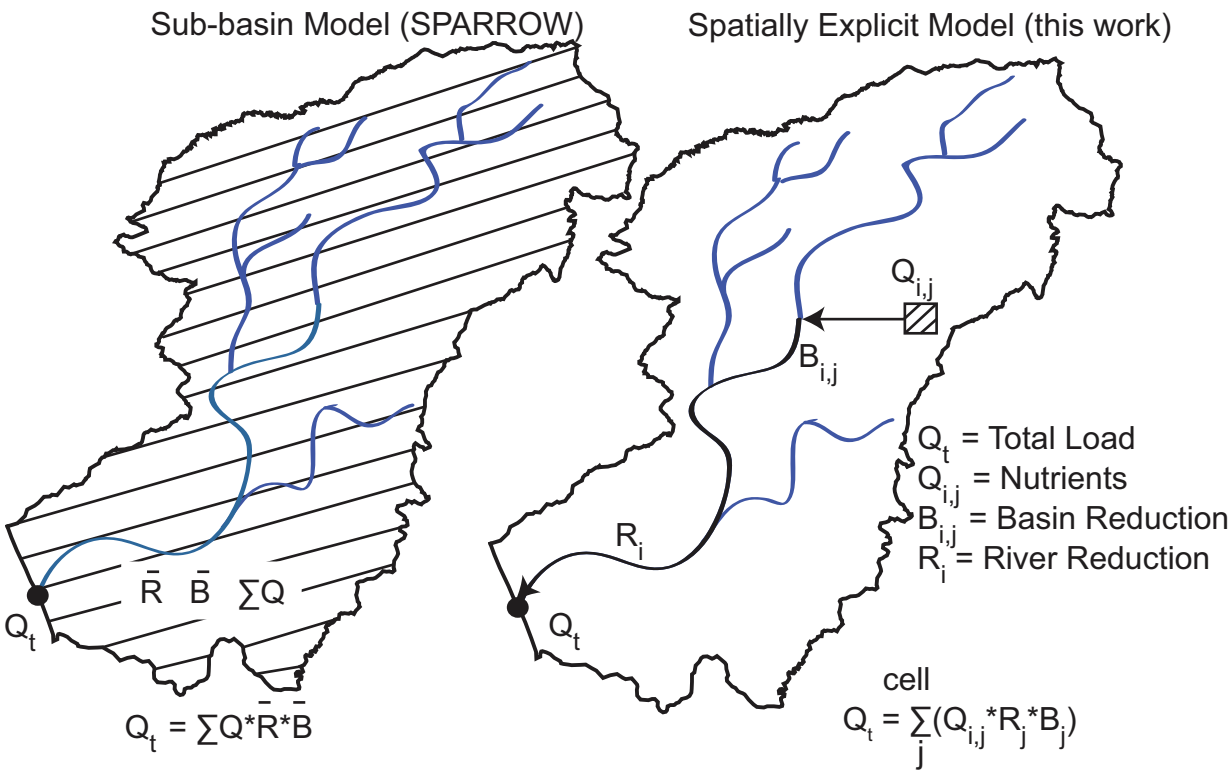

Figure 2.3: A comparison of a sub-basin based approach (such as the USGS SPARROW model) and the spatially explicit approach described here.

spatially explicit. The following sections describe the methods used to estimate these factors.

2.2.2.1 Watersheds and Travel Distance

Travel distance was calculated using the National Elevation Dataset (NED) (*Gesch et al.*, 2002; *Gesch*, 2007) and the ArcGIS Hydrology Toolbox, which calculates flow travel distance based on an elevation dataset. Sub-watersheds were generated using the ArcGIS Hydrology Toolbox. The points describing the outlet of the sub-watersheds coincide with sampling locations.

2.2.2.2 Recharge

Recharge was estimated using a physically based statistical model. The model, developed by *Hyndman et al.* (2007); *Kendall and Hyndman* (in review) for the Muskegon River wa-

tershed estimates the percentage of precipitation that becomes recharge from soil hydraulic conductivity values and land class. The Muskegon River watershed model was applied to the Lower Peninsula using soil hydraulic conductivity derived from the soil characteristics of the Soil Survey Geographic Database (SSURGO) (*Natural Resource Conservation Service*) and land class data from the National Land Cover Database (NLCD) (*Fry et al.*, 2011). Estimates of annual precipitation were downloaded from the PRISM climate group (*PRISM Climate Group*, 2011).

2.2.2.3 Tile Drainage

The tile drained area of Michigan was surveyed by the the NRCS during the 1992 National Resource Inventory (*NRCS*, 1995). These estimates were made on a county level and are not up to date. In order to derive an updated tile drainage layer, a 750 meter buffer was added to the Canal/Ditch feature of the National Hydrography Dataset (*Roth and Dewald*, 1999), and the NLCD classified agricultural cells were selected within each buffer. The Canal/Ditch feature includes features that do not drain tiles, and therefore, further classification was required. Within the canal ditch buffers, areas of low slope ($\leq$ 2 meter change in 30 meters) and/or low soil hydraulic conductivity ($\leq$5.0 x 10^{-6} cm/s) were selected as potentially tile drained areas. This dual attribute classification scheme ensured that areas that are extremely flat but with moderate drainage, based on SSURGO soil classification, such as those that exist in Saginaw Bay, were classified as tile drained areas. The resulting tile drainage map is shown in Figure 2.4.

2.2.2.4 Stream Velocity and Travel Time

Stream morphology plays a role in nutrient cycling by controlling the residence time of water in a watershed and the contact between water and the stream bed (*Mainston and Parr*, 2002; *Alexander et al.*, 2000). The model accounts for the effects of stream morphology using estimates of stream velocity, in-stream travel time, and basin yield.

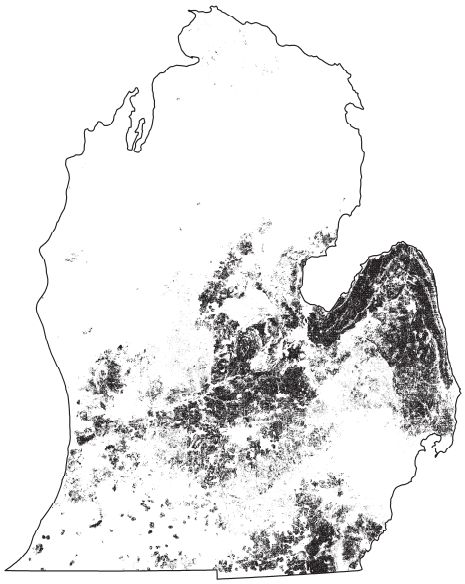

Figure 2.4: Estimated tile drained areas for the Lower Peninsula of Michigan (indicated in black).

Flow velocity was estimated using the relationship derived by *Leopold and Maddock* (1953) which relates channel area and depth to discharge:

$$A = aQ^b \tag{2.6}$$

where A is channel area, Q is discharge and a and b are empirically derived coefficients. A similar approach has been used to assess stream morphology and discharge in several studies (*Alexander et al.*, 2000; *Schulze and Hunger*, 2005; *Bjerklie et al.*, 2003). The relationship for channel area shown in Equation 2.6 was divided by Q and manipulated to estimate velocity from channel area and flow:

$$v = \frac{1}{a}Q^{1-b} \tag{2.7}$$

The coefficients for these relationships were derived empirically from channel area and discharge data available from USGS gauges for Michigan's Lower Peninsula (*USGS*, 2012). The site visit observations of channel area and discharge were averaged for each gauge.

Site visit data was filtered for observations collected during high flow conditions (discharge observation between the 75th and 90th percentile) and low flow (baseflow) conditions (discharge observations less than the 20th percentile). The 75th and 90th percentile were chosen for high flow so that the dataset did not include observations collected under flood conditions. The datasets for the two flow conditions were further subset based on the geology underlying the gauge location; three geologic models were fit for the two flow conditions: till, lacustrine, and outwash (Figure 2.5).

In order to apply these relationships to all stream cells, the discharge at every location in the Lower Peninsula was estimated from the flow accumulation derived using NED and the ArcGIS Hydrology Toolbox. USGS gauge data was used to derive empirical relationships between calculated cell flow accumulation and discharge. The 80th and 20th percentiles of discharge were used to create a high flow and low flow (baseflow) linear model. For the baseflow relationship, flow accumulation was multiplied by baseflow index. Baseflow index is the proportion of flow attributed to groundwater discharge and is estimated for gauges by the USGS (*Wolock*, 2003).

The in-stream velocity was estimated from the predicted discharge in each cell using Equation 2.7, and was then used to calculate travel time based on the flow length from a cell to the observation point. Calculated travel time to the Saginaw Bay watershed sample location is shown in Figure 2.6

2.2.3 Calibration/Validation Data

Flow measurements and nutrient samples were collected from the fall of 2010 to the spring of 2012 in 5 field campaigns intended to capture synoptic conditions during baseflow, melt, and spring rain. Sample locations for the 2010 baseflow, 2011 melt, and 2011 spring rain were chosen in an effort to capture most of the surface water outflow to the Great Lakes from the Lower Peninsula. Sites were located at the farthest accessible downstream sample point on most major and several minor streams and rivers discharging to the Great Lakes.

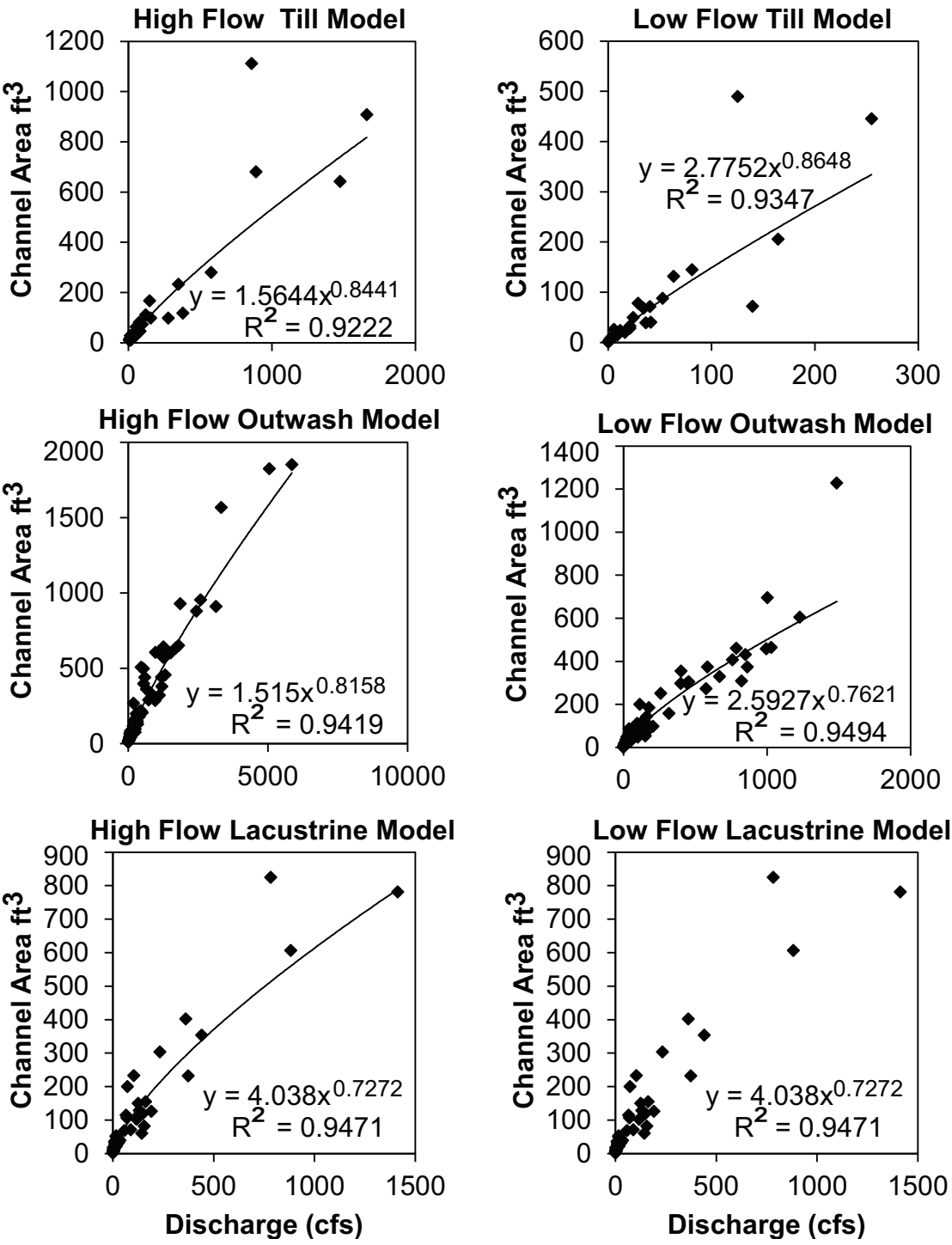

Figure 2.5: Graphs showing the relationship between discharge and channel area. Regressions were fit to USGS channel area and discharge data for observations between the 75th and 90th percentile for discharge (high flow) and observations less than the 20th percentile (low flow). Gauge data was subset by geology type (lacustrine, outwash, and till).

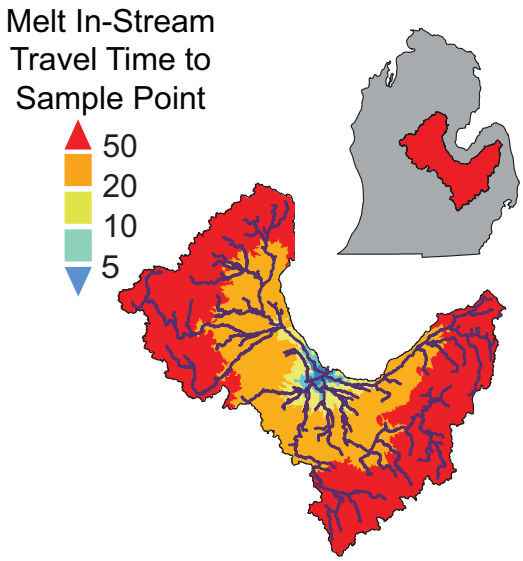

Figure 2.6: In-stream travel time to sample point for the Saginaw Bay watershed during snow melt.

A total of 67 locations were sampled.

The 2011 baseflow and 2012 melt sampling focused on 4 major watersheds in the Lower Peninsula of Michigan: Grand River in south central Michigan, Saginaw Bay in eastern Michigan, Muskegon River in north central Michigan, and Boardman-Charlevoix in northwest Michigan (Figure 2.7). Between 15 and 30 sites were sampled within each watershed for a total of 90 sites. Sites were chosen in an effort to evenly distribute samples throughout the watershed. This was accomplished by selecting points so that the area upstream of each sample point would have, approximately, the same incremental watershed area. The watersheds for the combined sampling covers over 70% of the land area of the Lower Peninsula.

The watersheds sampled represent a large range in watershed size, land use, and nutrient inputs. The samples also represent a large range of flow conditions. The datasets collected from June 2011- March 2012 were used to calibrate the models and October 2010-March 2011 datasets were used for validation. The methods used for measuring flow and analyzing nutrient concentrations are described in CHAPTER 1 and sample data is included in Appendix A.

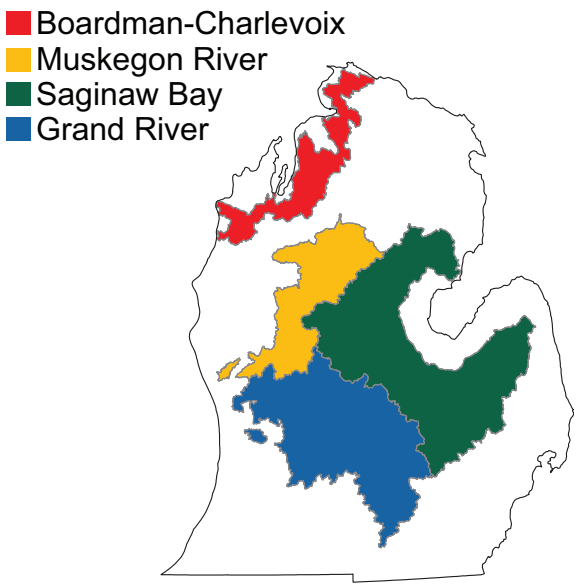

Figure 2.7: Location of Boardman-Charlevoix, Muskegon River, Saginaw Bay, and Grand River watersheds.

2.2.4 Optimization

The June 2010-March 2012 dataset was used as a training dataset for the optimization of the model. As discussed in Section 2.2.3 this dataset includes data from the Grand River, Muskegon River, Saginaw Bay, and Boardman-Charlevoix watersheds (Figure 2.7). The values of the coefficients for each model run were fit using the Matlab function fminseach, which uses the Nelder-Mead simplex algorithm (*Nelder and Mead*, 1965), a direct search algorithm. A total of 6 coefficients were optimized (*Bsurf, Bgrd, Btile, R, Fgrd,* and BY). The target of the optimization was the mean absolute difference between the natural logarithm of the observed area normalized load and the natural logarithm of the modeled area normalized load ($mean\left(abs\left[ln(\frac{load_{model}}{area}) - ln(\frac{load_{observed}}{area})\right]\right)$). Bounds were applied to the coefficients to reduce optimization time and ensure that the coefficients applied were in agreement with the process-based form of the statistical model. For instance, the coefficient that modifies distance in the exponential portion of basin reduction was limited between 0 and -1 since the basin reduction describes the distance based attenuation of nutrients. While in reality, depending on the time of year and the biologic and physical conditions, the basin

could become a source of stored nutrients, it was assumed that the net effect of these processes would be small over the 5 year period described by the model. The reduction factors describe permanent removal of nutrients relative to the time scale of the model.

2.3 Results

2.3.1 Sample Results

The results of the sampling showed that total nitrogen (TN) and total phosphorus (TP) concentrations decreased from southeast to northwest (Figure 2.8). Concentrations of nitrogen ranged from 64 to 5583 μg/L during baseflow and 179 to 7886 μg/L during melt. Phosphorus ranged from below detection limit to 476 μg/L for baseflow and from below detection limit to 395 μg/L for melt. The highest concentrations for nitrogen were observed during melt except for a few watersheds in the northeastern part of the state which had higher concentrations during spring rain of both TN and TP. For phosphorus, some watersheds showed higher melt concentrations while others showed higher baseflow concentrations.

2.3.2 Model Results

2.3.2.1 Model Performance

The results of the 6 models (Baseflow Total Nitrogen, Melt Total Nitrogen, Spring Rain Total Nitrogen, Baseflow Total Phosphorus, Melt Total Phosphorus, and Spring Rain Total Phosphorus) are shown in Tables 2.1 and 2.2. All models had adjusted R^2 values greater than 0.64 and all but the Melt Total Phosphorus model had an adjusted R^2 greater than 0.80. Overall, the nitrogen models performed the best. All nitrogen models had R^2 values greater than 0.86 and the baseflow model had the highest R^2 value of 0.95. Seasonally, the baseflow models were the most successful and the melt models were the least successful. However, within the validation sets, the TN melt model performed the best overall.

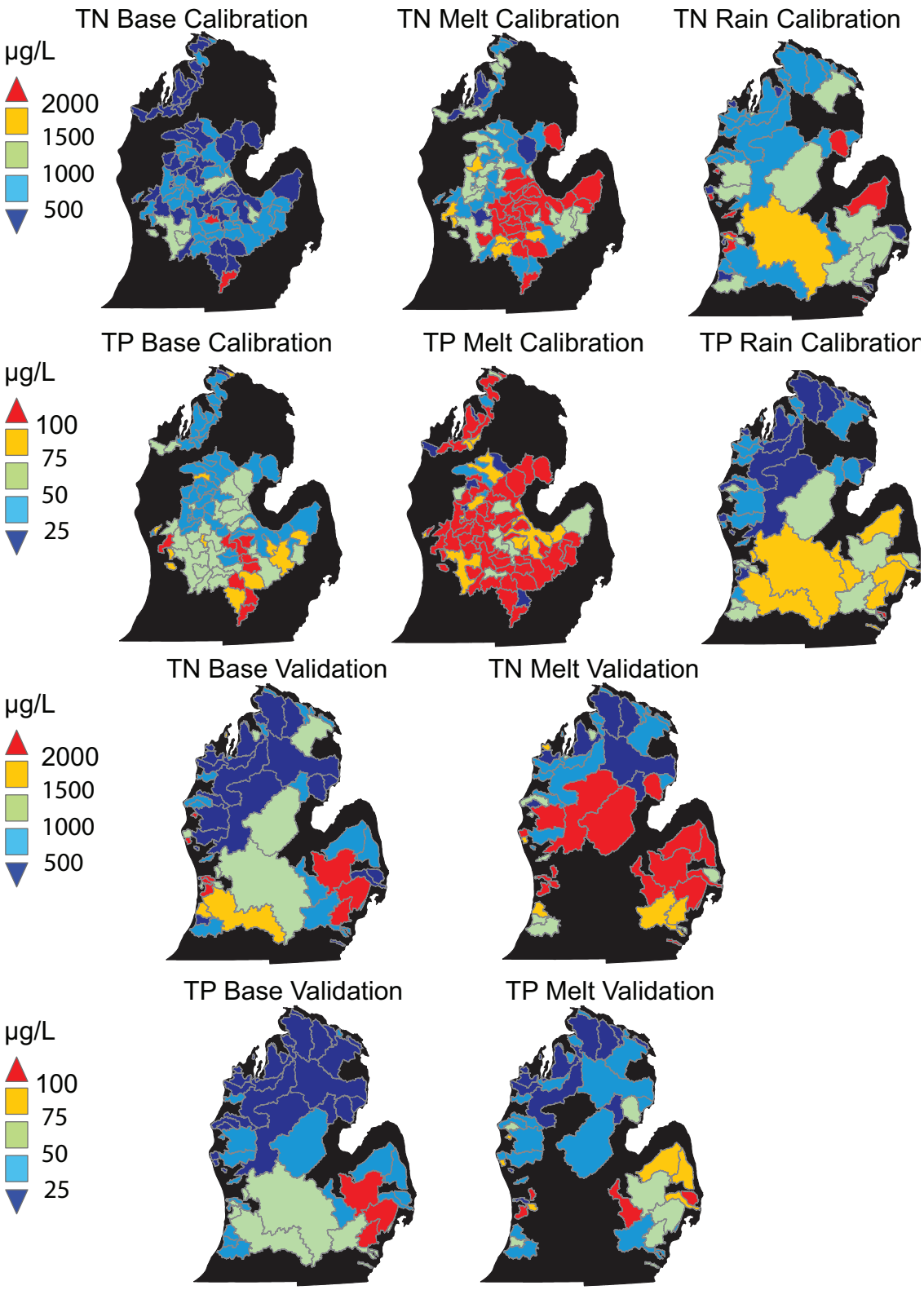

Figure 2.8: Sampled watersheds with concentration (μg/L) indicated for each sampling campaign.

Model	R^2	Adj R^2	Validation R^2	Optimization n	Validation n	Error
TN_Base	0.95	0.95	0.86	89	61	0.42
TP_Base	0.87	0.86	0.81	89	61	0.52
TN_Melt	0.85	0.84	0.90	88	64	0.45
TP_Melt	0.69	0.64	0.77	86	59	0.67
TN_Rain	0.88	0.87	NA	62	NA	0.47
TP_Rain	0.82	0.80	NA	62	NA	0.54

Table 2.1: Summary of estimated model parameters. R^2 values are for estimated and observed loads.

Model	Bsurf α_1	Btile α_5	Bgrd α_2	Fgrd α_6	R α_3	BY α_4
TN_Base	-4.03E-03	-1.28E-01	-4.59E-02	5.44E-01	-1.87E-10	9.93E-01
TP_Base	-2.14E-03	-9.90E-01	-8.97E-01	9.99E-01	-9.04E-07	1.00E+00
TN_Melt	-6.26E-05	-3.98E-10	-7.04E-05	8.34E-05	-1.15E-10	1.00E+00
TP_Melt	-4.64E-10	-9.78E-03	-9.39E-08	4.24E-03	-3.62E-10	1.00E+00
TN_Rain	-1.18E-03	-2.87E-02	-3.81E-11	1.00E+00	-8.69E-08	1.00E+00
TP_Rain	-4.27E-04	-2.14E-03	-4.26E-02	9.99E-01	-1.15E-08	5.41E-01

Table 2.2: Summary of coefficients associated with each basin parameter.

With the exception of the rain event data, the calibration dataset consists only of data collected from the Grand River, Saginaw Bay, Boardman-Charlevoix, and Muskegon River watersheds while the validation dataset contains samples covering nearly the entire Lower Peninsula. The validation dataset has high R^2 values and closely follows the 1:1 line, demonstrating the geographic and temporal transportability of the model. The rain models do not have a validation dataset because the spring rain was only sampled in 2011.

The R^2 values shown in Table 2.1 are for predicted and observed loads. The target of the model optimization was area normalized loads. Comparisons of model results for both loads and area normalized loads are shown in Figures 2.9 and 2.10. Plots of the area normalized loads indicate how consistently the models predict loads across watersheds irrespective of watershed size. The baseflow models best predict area normalized loads. The melt and rain models show a greater degree of variability in predicted area normalized loads for watersheds

with relatively small per unit area loads.

2.3.2.2 Sensitivity

The sensitivity for each parameter is shown in Table 2.3. Sensitivity was calculated as

$$Sensitivity = \frac{abs\left(model_{optimized} - model_{optimized} * \Delta\right)}{\frac{\triangle}{model_{optimized}}} * 100 \qquad (2.8)$$

where $\triangle$ is the change in the function value (0.5%) and $\text{model}_{optimized}$ is the optimized value of the coefficient. These values were normalized to the maximum sensitivity value to indicate the relative sensitivity of each parameter. The results show that the models were generally sensitive to *Bsurf* and *BY*. These two factors account for the basin attenuation and in-stream attenuation respectively. The models are also generally sensitive to *Fgrd* which predicts the portion of the source that travels via the groundwater pathway. The results suggest that attenuation is relatively most important along the surface pathway and that, with the exception of TP during baseflow, in-stream processing is best predicted by basin yield. This agrees with the analysis by *Alexander et al.* (2000) who showed that in-stream loss was correlated with channel depth (approximated from flow rate). They suggest that depth was a surrogate for the ratio of water volume to stream benthic area. Basin yield can also be a surrogate for this.

The TP Melt model only shows sensitivity to basin yield and the TN Melt model only shows sensitivity to basin yield and *Bsurf*. The model predicts that almost all of the nutrients during melt are delivered via the surface pathway. Therefore, most of the nutrients are only impacted by surface processing. Additionally, the TP Melt model is the least successful of all the models. The model's low sensitivity to all but one parameter suggests that the model parameters do not adequately describe the dynamics of phosphorus during melt. The delivery of sediment is not directly described by the model but is an important transport mechanism for phosphorus (*Mainston and Parr*, 2002). Relatively large amounts

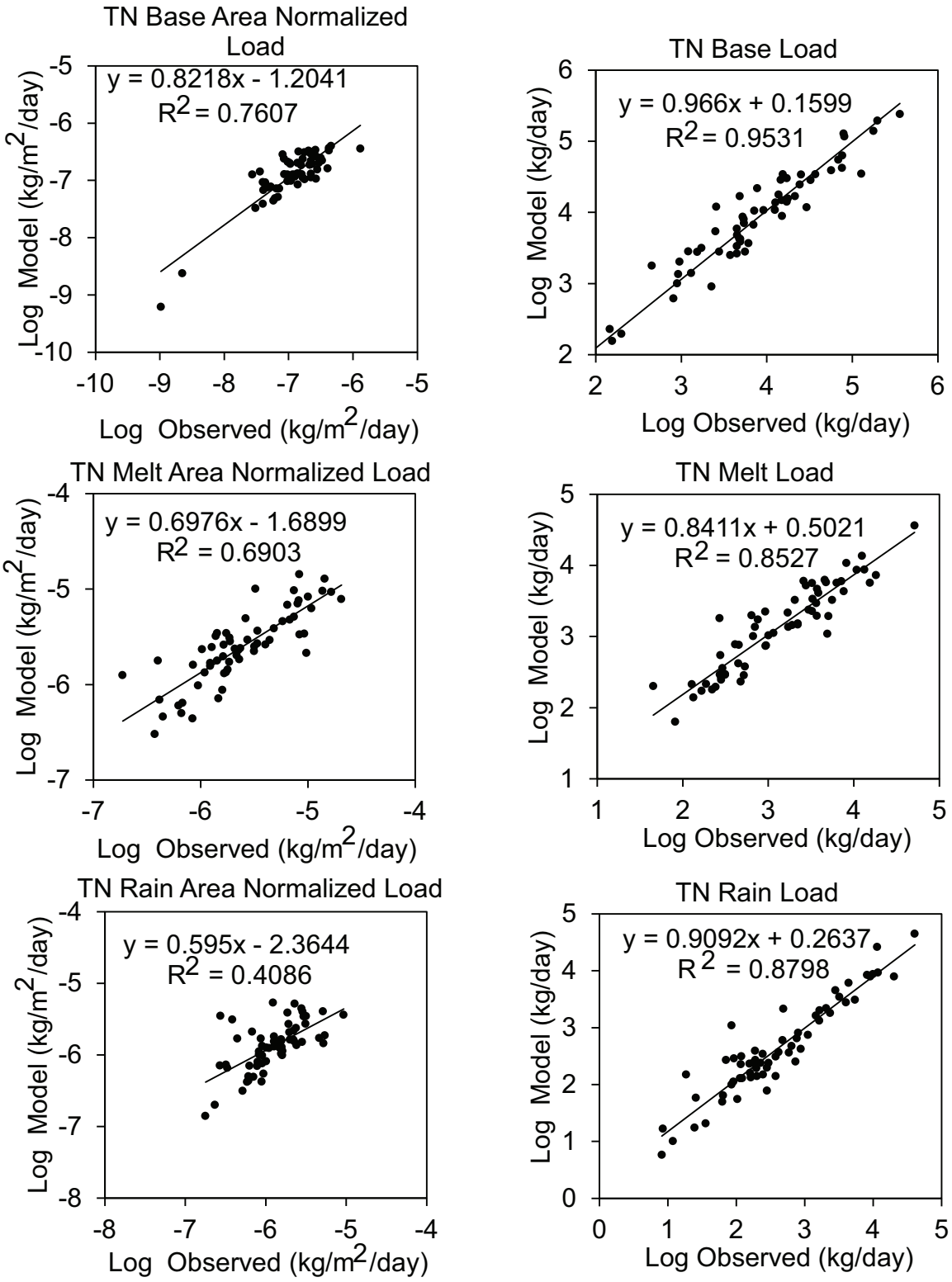

Figure 2.9: Graphs of observed and modeled TN loads and area normalized loads for the calibration dataset.

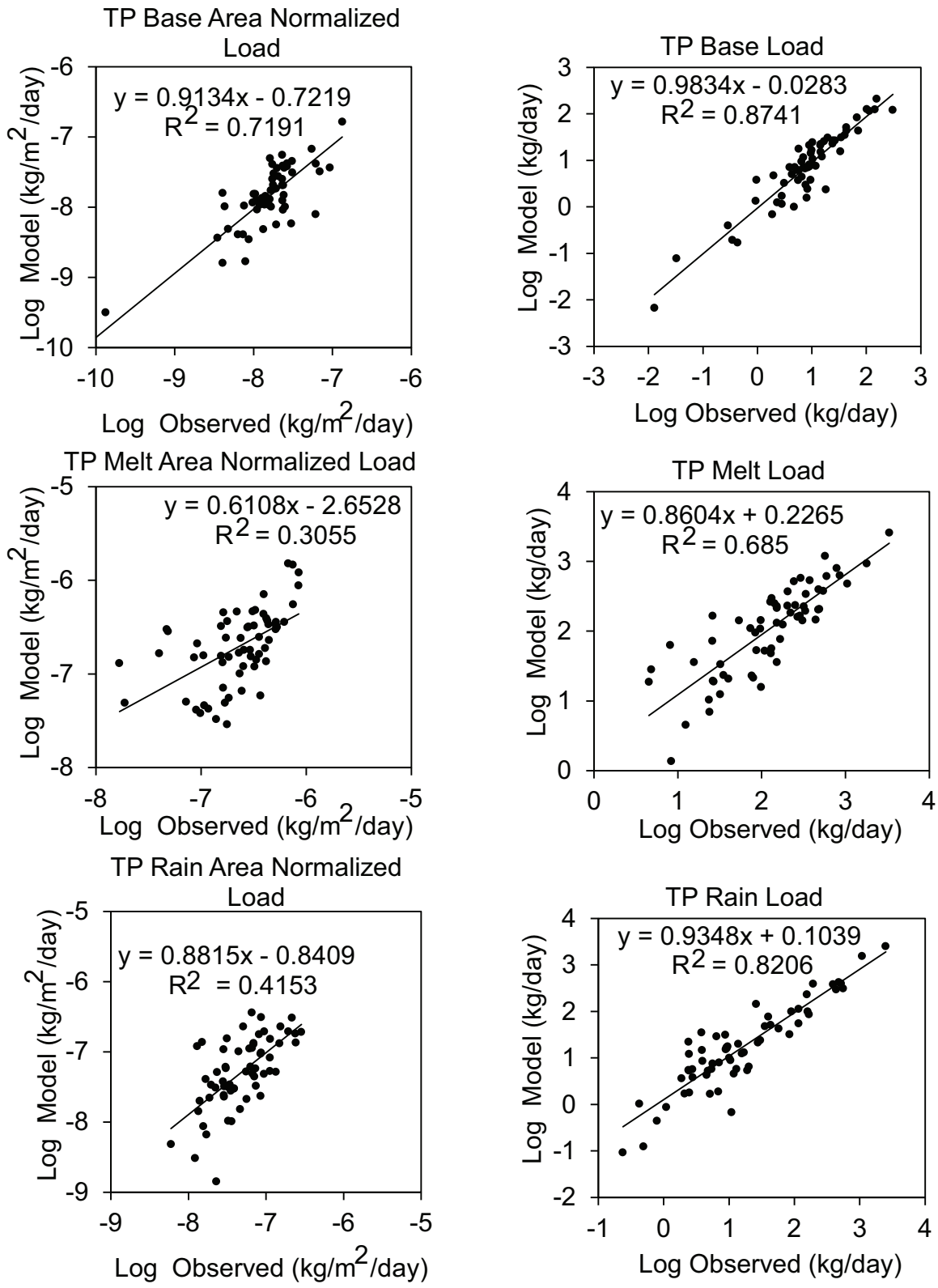

Figure 2.10: Graphs of observed and modeled TP loads and area normalized loads for the calibration dataset.

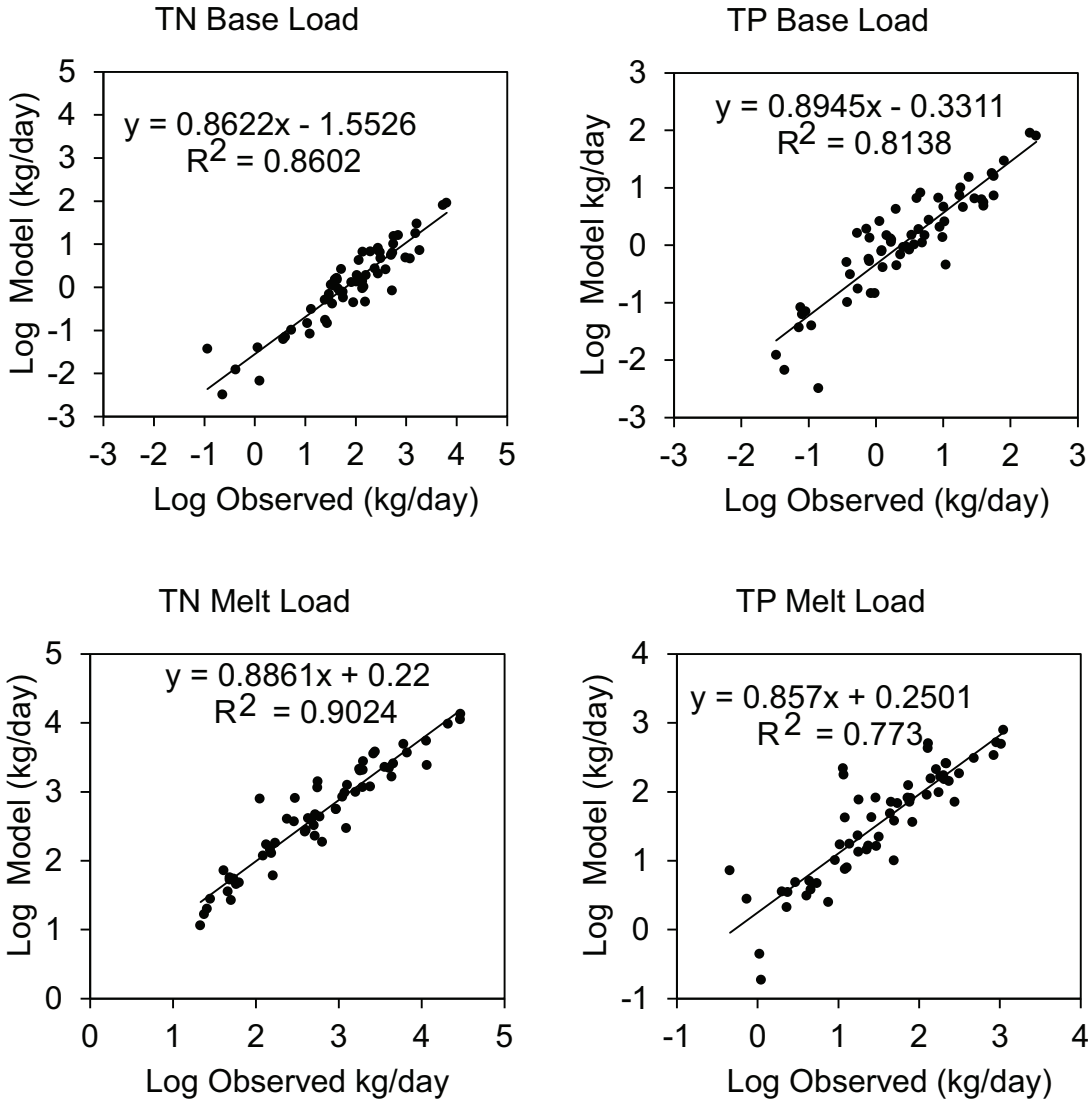

Figure 2.11: Graphs of observed and modeled loads for the validation dataset.

Model	Bsurf	Btile	Bgrd	Fgrd	R	BY
TN_Base	**1.000**	**0.051**	0.007	**0.134**	0.000	**0.674**
TP_Base	**1.000**	0.011	0.003	**0.182**	**0.351**	**0.313**
TN_Melt	**0.149**	0.000	0.000	0.000	0.000	**1.000**
TP_Melt	0.000	0.002	0.000	0.000	0.000	**1.000**
TN_Rain	**0.615**	**0.119**	0.004	**0.083**	0.006	**1.000**
TP_Rain	**1.000**	0.009	0.000	**0.450**	0.027	0.001

Table 2.3: Normalized sensitivity of model to each basin parameter coefficient. Sensitivity is calculated as the percent change in the model prediction per percent change in the parameter.

of sediments are mobilized during melt, and therefore, sediment delivery may be a sensitive parameter that is not included in the model.

2.3.3 Sources

A comparison of the total nutrient sources (as applied) relative to the total nutrients delivered downstream illustrates the importance of basin and river processing for attenuation of nutrient loads, the seasonal variability in pathways, and differences in the delivery of phosphorus and nitrogen. The results show that atmospheric deposition and commercial chemical fertilizer are the largest contributors to the in-stream nitrogen load. During melt, commercial fertilizer is the largest source of nitrogen while during baseflow and rain events, atmospheric deposition is the largest source of nitrogen. Point sources and direct atmospheric deposition become a relatively larger contributor to the total load when there is more basin processing (such as during baseflow). The model predicts that there is very little basin processing during the melt event so surface derived sources are relatively more important during melt.

The largest contributor of phosphorus to surface water based on this research is commercial chemical fertilizer followed by manure. Atmospheric deposition contributes a relatively small amount of phosphorus and is often considered effectively zero in many nutrient loading models. During baseflow, the model predicts that nearly 3% of total phosphorus delivered to streams is derived from atmospheric deposition, so ignoring atmospheric deposition as a

Model	Bsurf (% 1 km)	Btile (% 0.1 km)	Bgrd (% 0.1 km)	Fgrd max (%)	Rmin (%/day)	Rmax (%/km)
TN_Base	**2**	**0**	1	**54**	5	**99**
TP_Base	**12**	0	0	**100**	5	92
TN_Melt	**94**	100	99	0	**4**	**100**
TP_Melt	100	38	100	0	**4**	**100**
TN_Rain	**31**	**6**	100	**100**	**4**	**99**
TP_Rain	**65**	81	1	**100**	2	54

Table 2.4: Summary of calculated basin parameters. Reduction factor units (*Bsurf*, *Btile*, and *Bgrd*) are the percent of the nutrient load that remains after the first .1 kilometer (1 km for *Bsurf*) of travel. Units of *Rmin* and *Rmax* are the percent of the load that remains after the first day of in-stream travel for the sub-watershed with the highest relative basin yield (*Rmax*) and the lowest relative basin yield (*Rmin*). The bold values indicate the coefficients with relatively high model sensitivity.

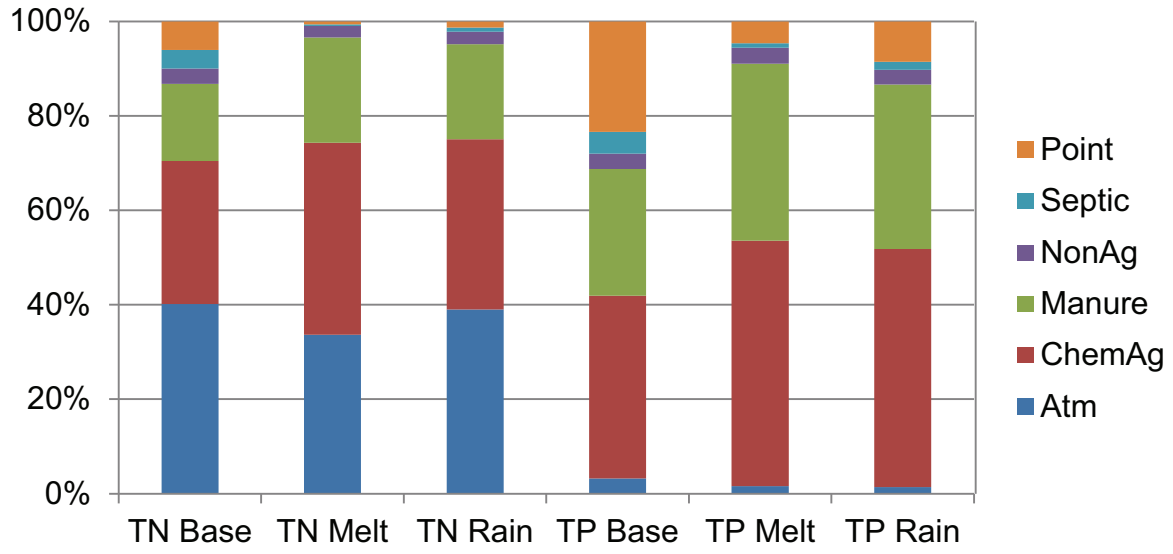

Figure 2.12: Source contributions to total loading to streams.

source of phosphorus may lead to up to 3% under-prediction of total phosphorus in these models. However, in watersheds that contain large amounts of unmanaged land (forest, range, grasslands), this percentage can be much larger. Figure 2.14 shows that atmospheric deposition contributes over 10% of the observed TP load in several sampled watersheds and in one sampled watershed, contributes up to 25% to the observed TP load.

The source contribution to total downstream load predicted by this model agrees well

with predictions from the SPARROW model constructed for the Great Lakes (*Robertson and Saad*, 2011). However, a few sources identified by the SPARROW model are surrogates for other sources. For instance, SPARROW attributes 15% of the total phosphorus load to an "urban" source. This model predicts that approximately 4-7% (depending on season) of total phosphorus is contributed by non-agricultural fertilizer and septic tanks and 3% of phosphorus is contributed by atmospheric deposition. Additionally, 4-24% is derived from point sources. Depending on the nature of the urban area being described, increases in urban area may not lead to proportional increases in the urban sources. For instance, low to medium density urban areas like Lansing may have a higher incidence of septic and lawn fertilizer use than a high density urban area such as downtown Detroit. The fact that these sources are not explicitly described in the SPARROW model may account for the urban bias observed in the SPARROW model (*Robertson and Saad*, 2011; *Alexander et al.*, 2002)

2.3.4 Pathways and Processes

2.3.4.1 Basin Processing

The parameter *Fgrd* describes the portion of the applied load entering the groundwater pathway. The model predicts that in basins with the largest recharge, nearly all nutrients enter the groundwater pathway during baseflow and rain while during melt, nearly all nutrients travel by the surface, runoff pathway and almost nothing enters the groundwater pathway. It is important to remember that this is for basins with the largest recharge, and therefore, this value varies between 0 and the maximum predicted value depending on the estimated recharge for a cell.

The groundwater basin reduction factors show that groundwater attenuation occurs over a much shorter distance than attenuation along the surface pathway. Almost all of the attenuation occurs in the first 0.1 kilometer of travel in the baseflow model. This suggests that the groundwater pathway only contributes nutrients to surface water if the nutrient

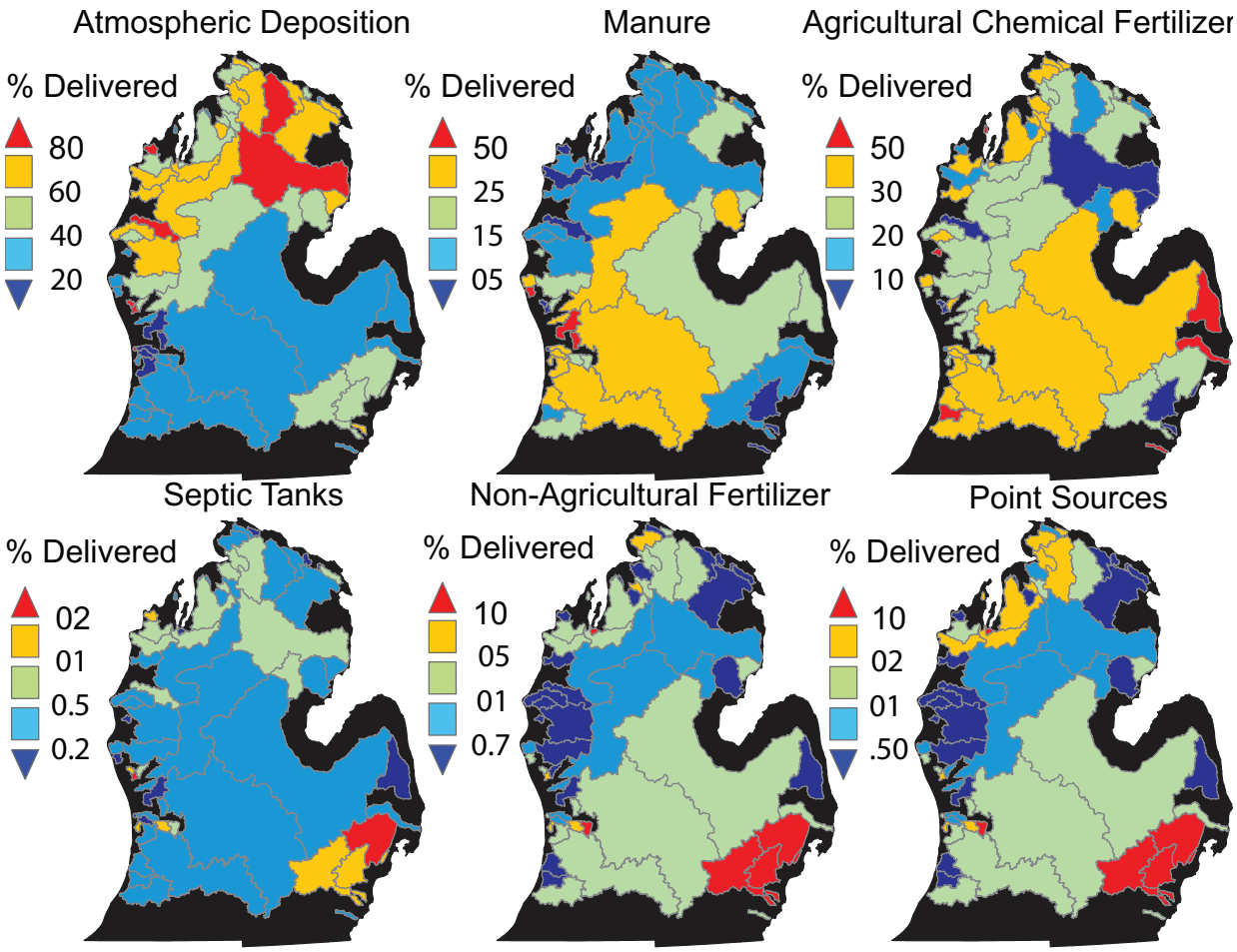

Figure 2.13: Percent of observed TN melt load derived from each source.

TN				TP	
Base	Melt	Rain	Base	Melt	Rain
8.4	0.4	58.6	7.8	1.1	3.4

Table 2.5: Percent of total load delivered to surface water via the groundwater pathway.

source is within a travel distance of 0.1 km. The TN Melt and TN Rain models predict that most of the nutrients persist in the groundwater beyond 0.1 kilometer. The proportion of nutrients delivered to streams via the groundwater pathway during each season are shown in Table 2.5. The models predict that relatively more nitrogen is delivered via the groundwater pathway relative to phosphorus. The model was relatively insensitive to the *Bgrd* parameter, so these predictions are potentially highly variable.

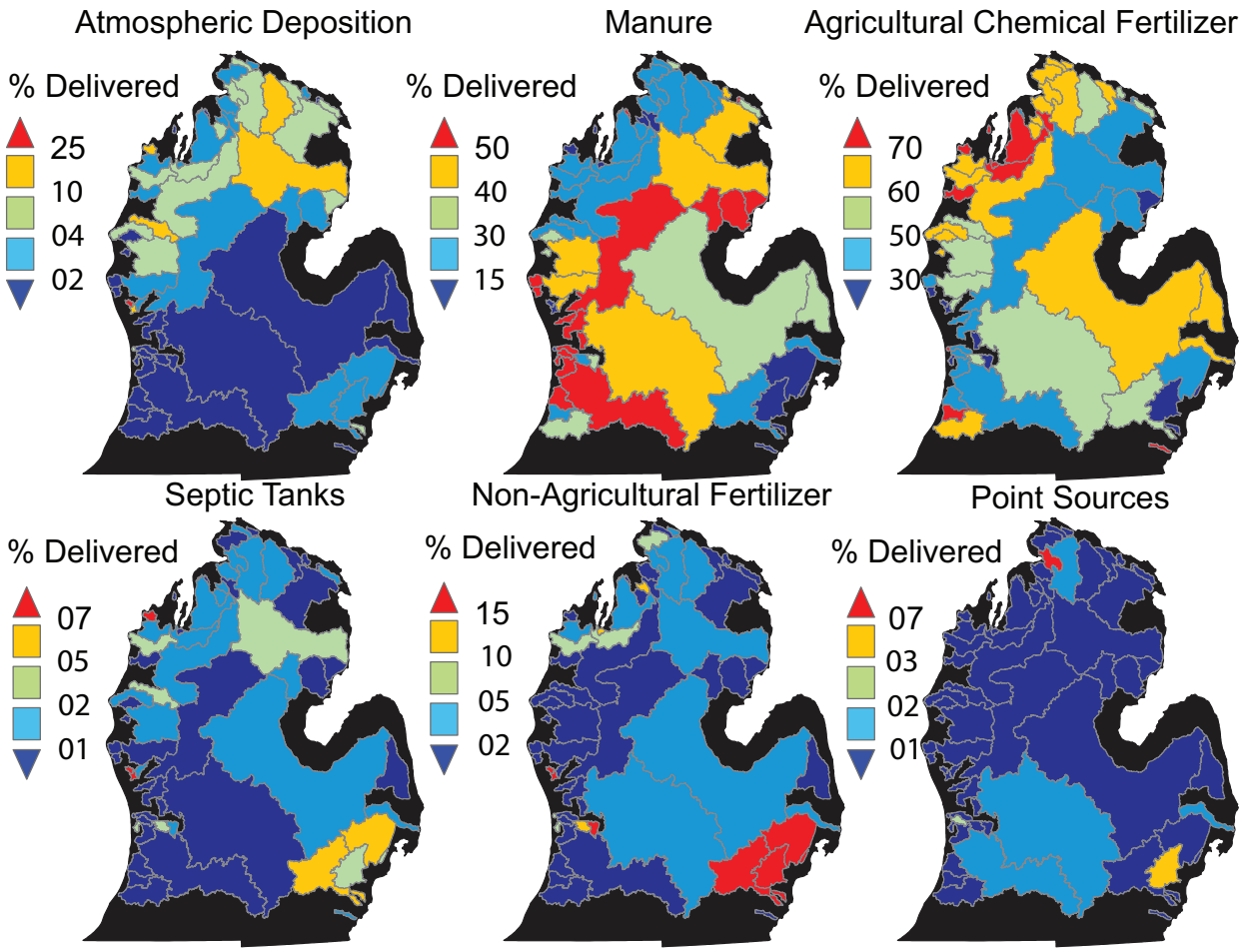

Figure 2.14: Percent of observed TP melt load derived from each source.

The results for the basin reduction factors indicate the differences in processes and pathways both seasonally and between nitrogen and phosphorus. The results show that phosphorus is more efficiently delivered to streams than nitrogen for all models. The largest attenuation along the surface pathway occurs during baseflow. This could be a result of lower temperatures or higher runoff rates.

The portion of each cell's applied load delivered to surface water is shown in Figure 2.15, which indicates that landscape retention of phosphorus and nitrogen during melt is different. Nitrogen derived in areas that are distant to surface water are retained while phosphorus is retained in areas with tile drainage. This is a result of *Btile* which indicates relatively more phosphorus is retained in tile drains during melt than nitrogen. This effect is reversed

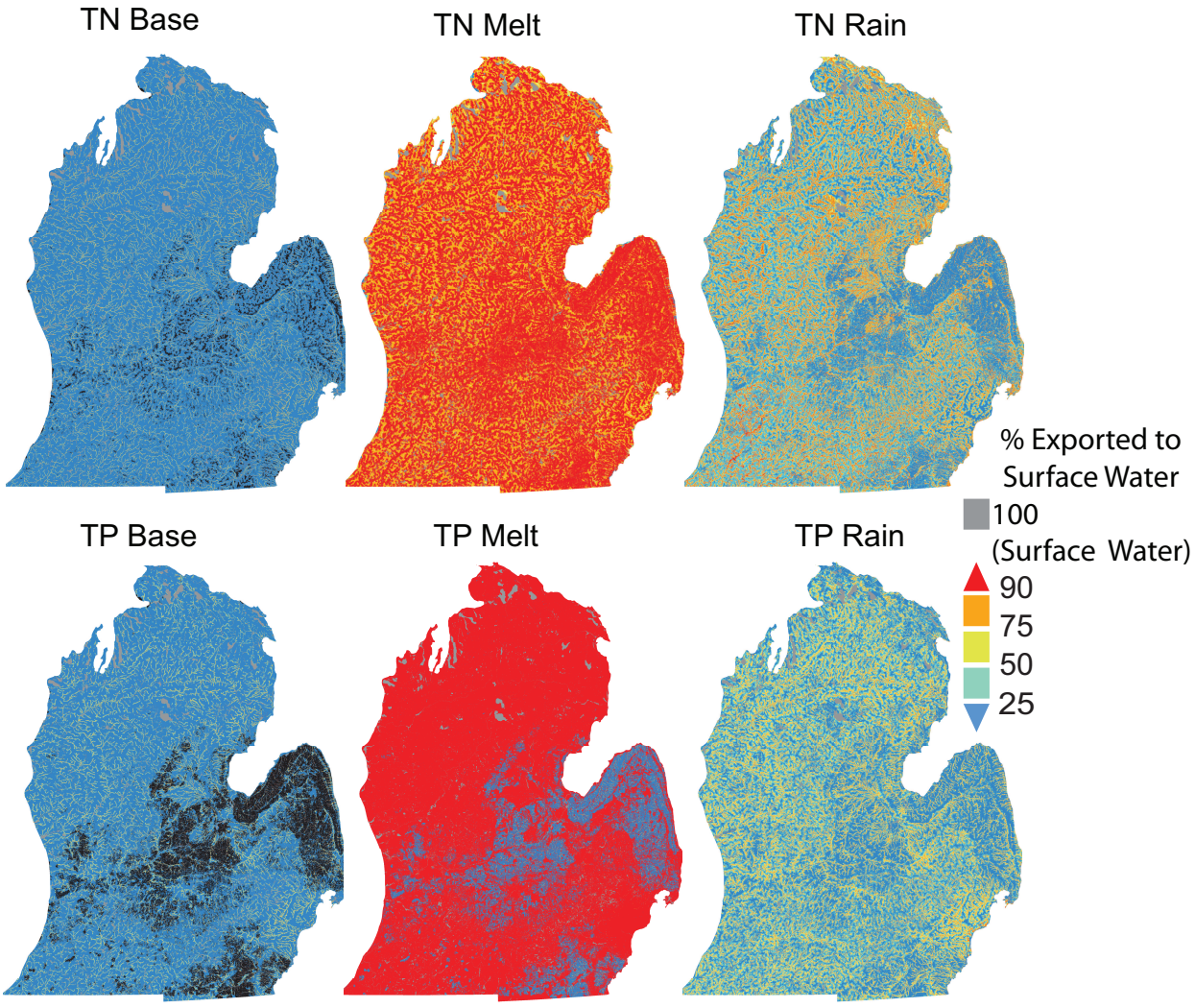

Figure 2.15: Percent of total applied load delivered to surface water.

during the spring rain event and no nutrients are delivered via tile during baseflow. Tile drains affect flow pathways and processes in several ways. Tile drains change the natural drainage pathway of water, decreasing the travel time to surface water and decreasing the amount of time available for physical and chemical processes that remove nutrients from agricultural runoff (*Robertson and Saad*, 2011). Several different physical and biological processes that affect nutrients differently may be affecting the delivery of nutrients in tile drains.

2.3.4.2 In-stream Processing

The results for in-stream processing show that in basins with the largest basin yield (Rmax), very little in-stream attenuation occurs. This is consistent with other studies that have shown that a higher rate of attenuation occurs in small, slow moving streams where there is more time for water to interact with the stream bed (*Robertson and Saad*, 2011; *Mainston and Parr*, 2002; *Alexander et al.*, 2000). The model also predicts that slightly more attenuation occurs during baseflow when discharge is lower.

2.3.5 Land use Export Rates

Table 2.6 shows the average export rate of nutrients from agriculture, urban, and unmanaged (forest, grasslands, shrublands) and pasture cells. Several studies have attempted to estimate annual nutrient exports rates as a means of quantifying and predicting non-point source contribution of nutrients. *Beaulac and Reckhow* (1982) compiled several studies estimating export rates. They found values for phosphorus ranging from 0 to 1 kg/ha/year for forest, ∼0 to 18 kg/ha/year for agriculture, and ∼0 to 6 kg/ha/year for urban, and values for nitrogen from ∼0 to 6 kg/ha/year for forest, ∼0 to 80 kg/ha/year for agriculture, and ∼0 to 40 kg/ha/year for urban. The seasonal values predicted by this model are similar to these values, but slightly higher rates are predicted for nitrogen export from forested and agricultural land.

There is a high degree of seasonal variability in the estimates of nutrients exported from each land type. The export rate for urban land appears to be higher than cropland during baseflow for nitrogen. This could be primarily due to the relative increase in point source delivery during baseflow (Figure 2.16). The melt export rates are 2 to 15 times greater than baseflow rates for total nitrogen and 0 to 9 times higher for phosphorus.

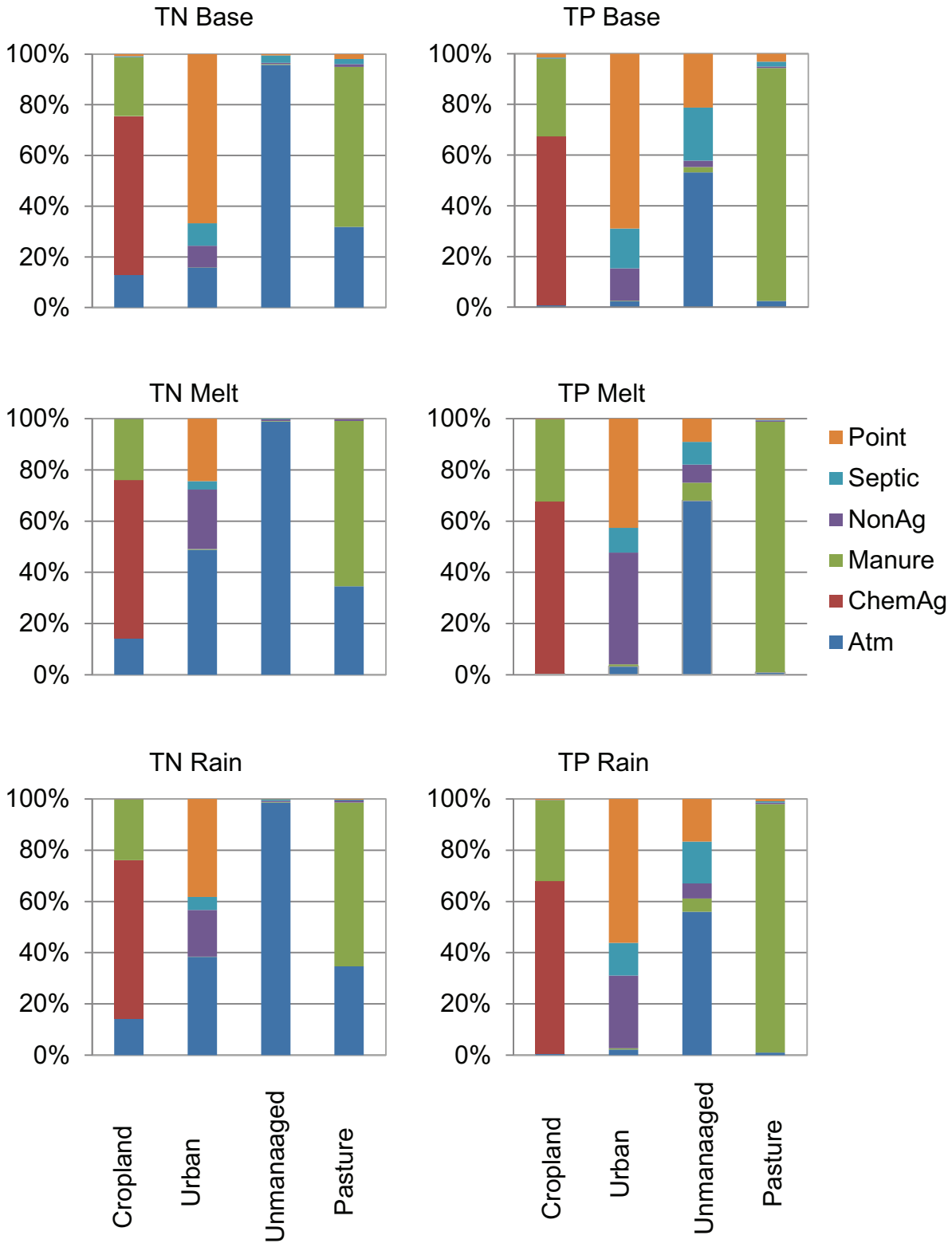

Figure 2.16: Source contributions to total stream loading within different land use classes.

	TN			TP		
	Base	Melt	Rain	Base	Melt	Rain
Cropland	6	92	35	1	9	5
Urban	10	27	17	1	2	1
Unmanaged	1	13	7	0	0	0
Pasture	3	41	18	1	4	2

Table 2.6: Estimated nutrient exports from each land use in kg/ha/year.

2.3.6 Residuals

For the residual analysis, error was calculated as

$$Error = log(load_{model}) - log(load_{observed}) \tag{2.9}$$

A residual of 1 indicates an order magnitude over prediction by the model. The model residuals are plotted in Figure 2.17.

Figure 2.17 indicates that the medians of the model residuals are close to 0. Additionally, with few exceptions, model residuals are less than an order of magnitude. In fact, only one model, TN Rain, had an observation with a residual greater than 1. TP Rain had two residuals of 0.96 and TN Rain has a single residual of 0.98. The spatial distribution of the model residuals is shown in Figure 2.18.

Alexander et al. (2002) compared regional nutrient loading models in terms of percent error where error is calculated as

$$Error = \frac{S - O}{O} * 100 \tag{2.10}$$

Here, S is the simulated value and O is the observed value (*Alexander et al.*, 2002). They observed that if the model errors are less than the standard error of the observations, model error is indistinguishable from zero. The median percent error, minimum percent error, and maximum percent error (following Alexander (2002)) for each model are shown in Table 2.7 along with the average percent difference between samples with duplicates. The model median percent error is less than the percent sample difference for all models except the TP

Melt model. The median percent errors were comparable or less than the median percent error of models compared in *Alexander et al.* (2002) which ranged from -0.6 to 46.5 %. The minimum and maximum percent error were also comparable or less than other model residuals (*Alexander et al.*, 2002).

2.3.6.1 Residuals and Land Use

To assess the model's ability to perform in watersheds of different land uses, model residuals were compared to watershed urban, agricultural, and forested area. Linear regressions were fit to the percent area of each land use in the watershed and log model error.

The results of the regressions show that nitrogen models have no apparent land use biases. All the regressions show that the residuals and the watershed land use have very little correlation. Total phosphorus, however, shows agricultural bias. In all of the models, loading was slightly overestimated in watersheds with a high proportion of agricultural land and slightly underestimated in watersheds dominated by forest. The effect is strongest during rain and melt seasons. This suggests that the model may not be accurately capturing the effect of sediment bound phosphorus. Delivery via sediment is an important transport mechanism for phosphorus as more sediment is mobilized during the melt and spring rain seasons (*Withers and Jarvie*, 2008).

2.3.6.2 Model Bias

A regression of prediction errors and watershed characteristics was used to further explore potential model bias. This approach was used by *Alexander et al.* (2002) who compared several large basin statistical nitrogen loading models. The same watershed characteristics that were used in their analysis were used to assess model bias here including basin area, runoff (basin yield), cultivated area, and urban area. The regression equation is as follows:

$$E = \beta_0 + \beta_1 * C + \beta_2 * U + \beta_3 * BA + \beta_4 * R \tag{2.11}$$

where C is the percent of the watershed that is cultivated, U is the percent of the watershed that is urban land, BA is watershed area in m^2, R is runoff in m^3/year, and β_0, β_1, β_2, β_3, and β_4 are the regression coefficients. E is the percent error (Equation 2.10).

This approach provides an indication of model bias and a comparison of the performance of this model with other regional scale statistical nutrient loading models. The value of the model slope indicates the percentage increase in model residual that results from an increase in the basin factor. The p-value is the significance of the predicted slope; p-value indicates the level of confidence in the influence of the parameter on the model residual. The results of the analysis are shown in Table 2.8.

The results show that the models have very little bias. When compared to the other nitrogen loading models studied by *Alexander et al.* (2002), these models show the smallest bias (lowest R^2, slopes, and least amount of significance attributed to model parameters). The only model that shows significant bias is the TP Base model. Again, this may be due to an inability of the model to accurately account for nutrients delivered via sediment. Another potential source of bias may be recycling and re-suspension of phosphorus during high melt flows; this effect is also not accounted for by the model.

2.4 Discussion

This work demonstrates the value of a spatially explicit description of nutrient sources. Not only does the model perform well in watersheds with diverse conditions and scales, it also provides information beyond a prediction of nutrient load including seasonal dynamics, and source apportionment. It performs as well as or better than other regional scale models and has less land use bias than other regional nitrogen models (*Alexander et al.*, 2002; *Robertson and Saad*, 2011). The model performed consistently across diverse watersheds with little to no land use bias (particularly the TN models) and performs consistently across three different seasons. This suggests that this model has the potential to perform well in other regions and for other time periods.

The model indicates that atmospheric deposition is the largest source of nitrogen to surface water in the Lower Peninsula and chemical agricultural fertilizer is the most significant source of total phosphorus. Atmospheric deposition contributes, on average, 3% of phosphorus to the in-stream load and was as much as 25% in sampled watersheds during melt. Most models do not account for atmospheric deposition of phosphorus and may be attributing this phosphorus to another source, particularly in forested watersheds where atmospheric deposition is a more significant source of phosphorus.

The results also indicate that nitrogen export rates can be more than 15 times larger during melt than baseflow and 2.5 times larger during spring rain. For phosphorus, as much as 9 times more phosphorus can be exported during melt. There is a significant amount of variation in export rates between seasons and between land uses. This has implications for management strategies. Resources for water quality should be allocated based on the anticipated improvement in water quality (*Destouni et al.*, 2006). Depending on the time of year and the dominant nutrient source in a watershed, the effectiveness of different management strategies may vary. Spatially explicit nutrient models provide a method to estimate the efficiency of different strategies and the potential areas and sources that should be targeted.

The results show that the groundwater pathway (depending on season) accounts for 0.4-59% of total nitrogen and 1-8% of total phosphorus delivered to the stream. The model can be improved with an expanded description of the groundwater pathway. Currently the model uses a surface travel distance to describe groundwater attenuation and uses a surface watershed boundary to determine nutrient inputs to the groundwater pathway. A better description of groundwater travel pathway may improve model predictions in watersheds that have groundwatersheds that are significantly different from surface watersheds. The addition of travel time in the groundwater pathway may also improve performance since groundwater residence time can be highly variable.

The presented model cannot describe the effect of wetlands and impoundments which have been shown to impact the ability of watersheds to retain nutrients (*Robertson and*

Saad, 2011). A spatially explicit description of these features should improve the model performance and provide insight to to their impact on nutrient loading. Finally, the bias of the phosphorus models needs be explored further; perhaps a better description of sediment delivery is needed.

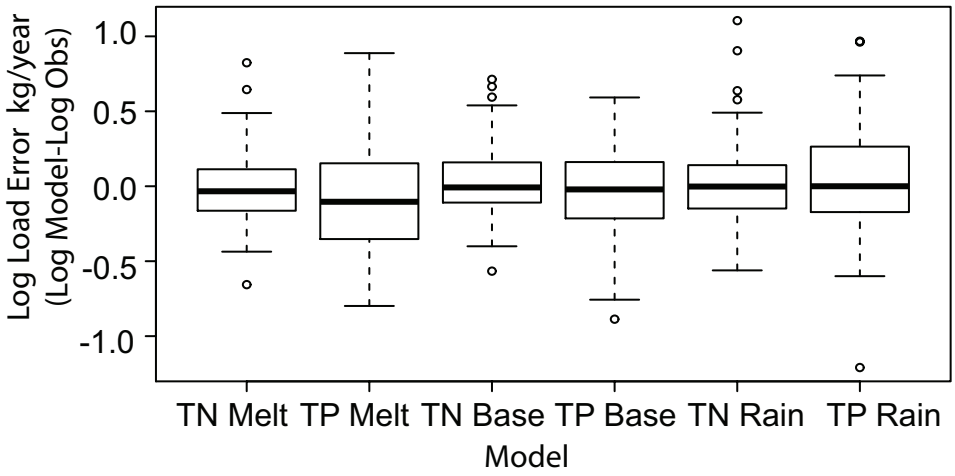

Figure 2.17: Box plots of model residuals.

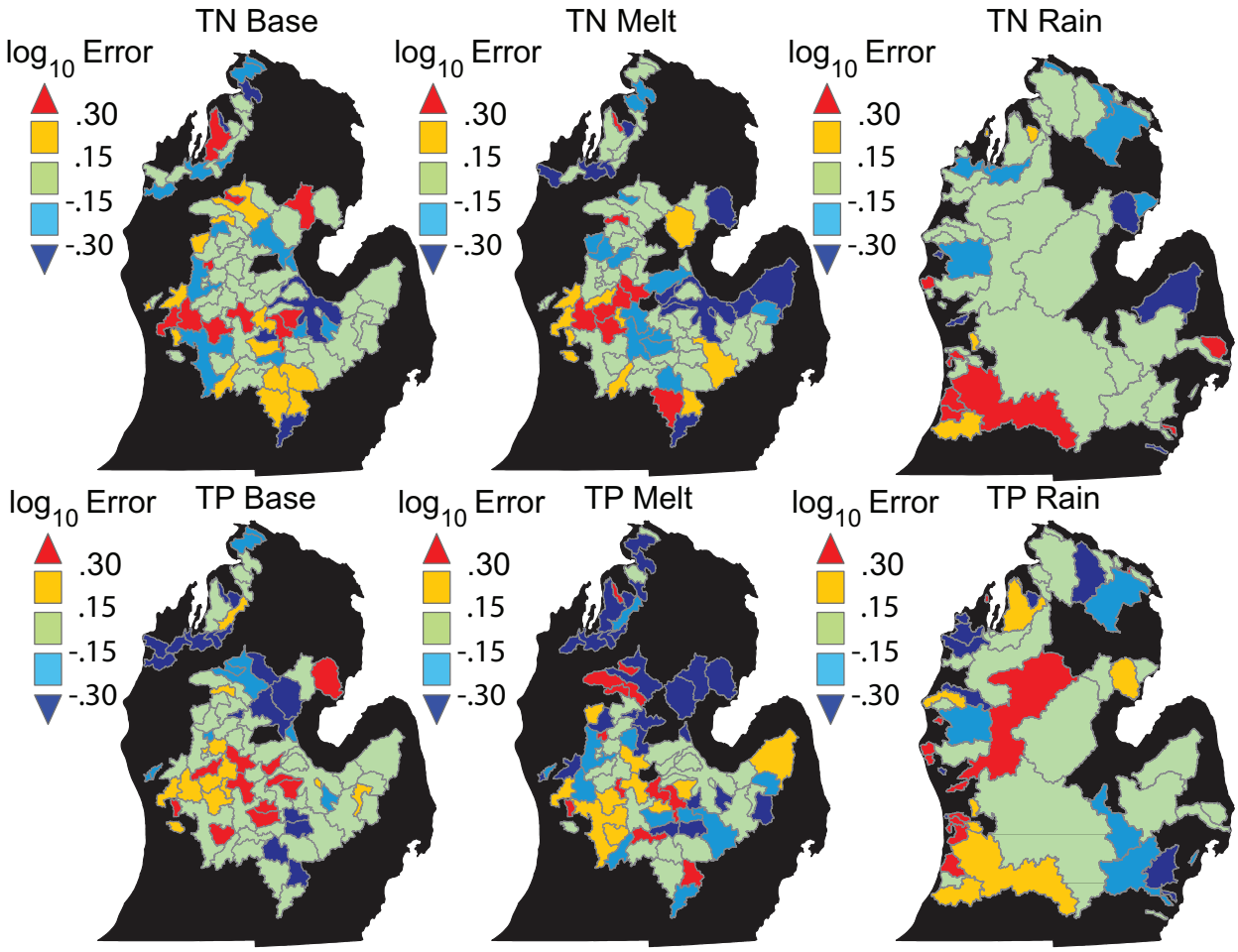

Figure 2.18: Model residuals for sampled watersheds (Equation 2.9). Only incremental watershed area is shown.

Model	Median %	Mean %	Min %	Max %	Sample Diff. %
TN_Base	-1.78	25	-72.85	416.45	-6
TP_Base	-4.7	11	-87.02	291.10	8
TN_Melt	-7.4	14	-77.95	566	-10
TP_Melt	-21.2	19	-84.10	672.66	18
TN_Rain	-0.42	46	-72.53	1172.7	-28
TP_Rain	-5.6E-05	60	-93.82	827.90	-18

Table 2.7: Model errors calculated as percent of observed loads. Sample Diff. is the mean percent difference between samples and duplicates.

Model	Value	Cultivated (%)	Urban (%)	Basin (km^2)	Runoff (m^2/year)	Intercept	R^2
TN_Melt	slope	24.87	27.44	0.00	-0.13	18.72	0.01
	p-value	0.64	0.84	0.45	0.53	0.47	0.90
TP_Melt	slope	84.62	-264.10	0.00	0.14	5.37	0.04
	p-value	0.28	0.17	0.81	0.64	0.89	0.54
TN_Base	slope	33.82	-162.80	-0.01	-0.48	42.81	0.05
	p-value	0.52	0.21	0.18	0.45	0.07	0.31
TP_Base	slope	**172.50**	-170.20	0.00	-0.53	-14.78	**0.26**
	p-value	**0.00**	0.08	0.25	0.26	0.40	**0.00**
TN_Rain	slope	12.13	14.93	0.00	0.07	-5.53	0.06
	p-value	0.29	0.23	0.47	0.30	0.34	0.49
TP_Rain	slope	18.01	3.73	0.00	-0.39	38.84	0.04
	p-value	0.75	0.95	0.51	0.25	0.18	0.65

Table 2.8: Results of the residual regressions. Slope indicates the percent change in the model error per unit change in the parameter. Bold values indicate significant parameters at a 95% confidence level.

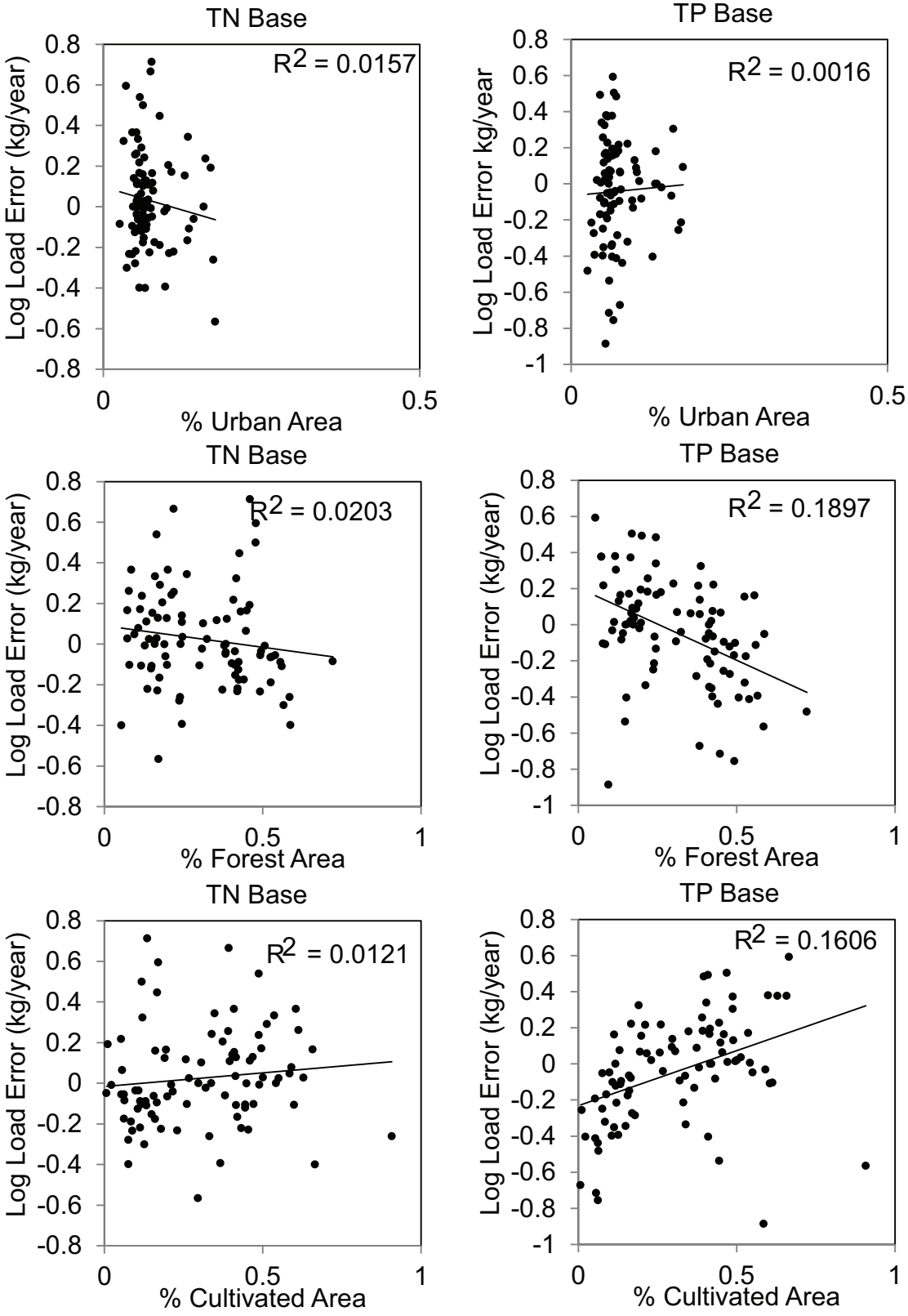

Figure 2.19: Baseflow model residuals and land use regression results.

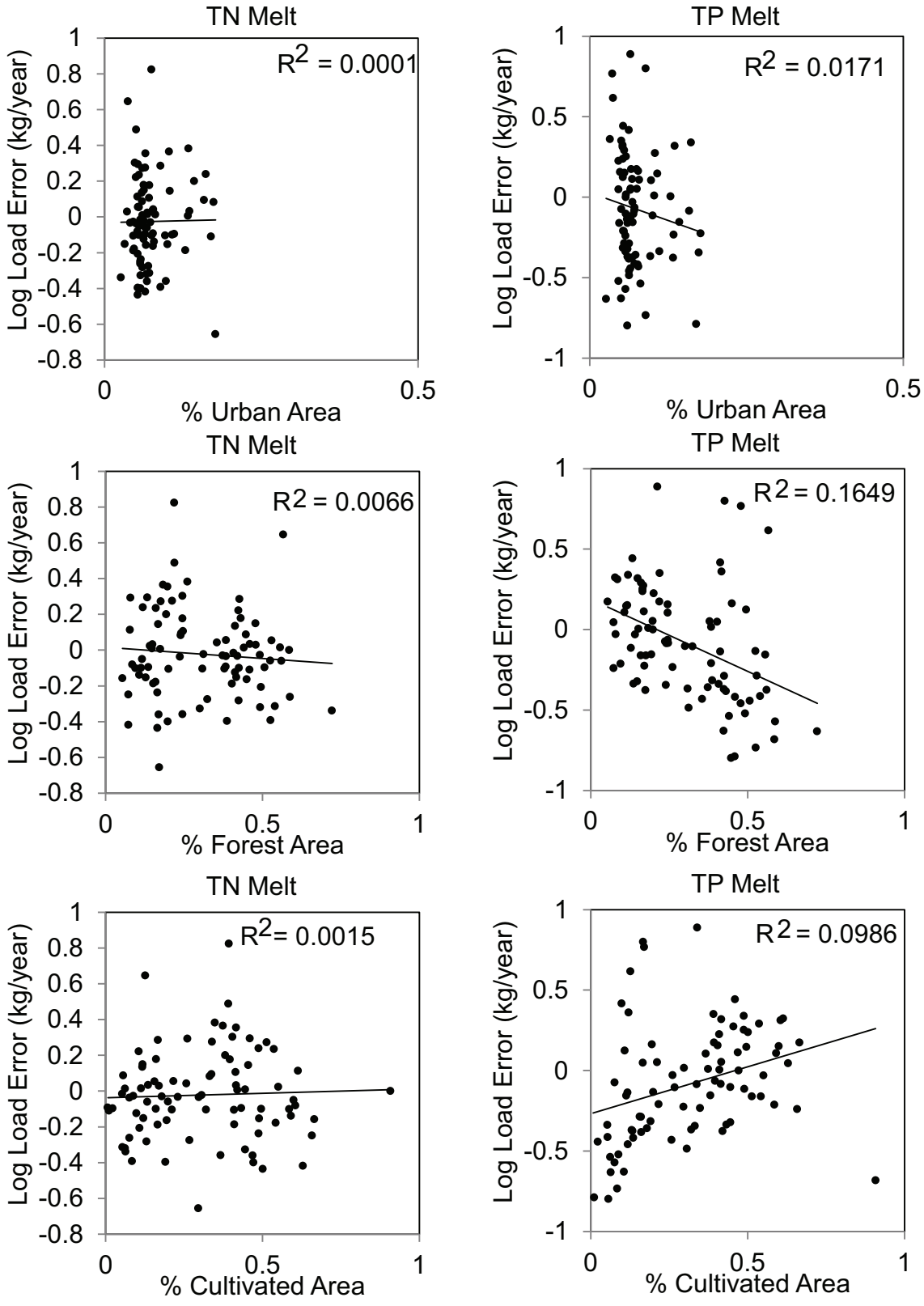

Figure 2.20: Melt model residuals and land use regression results.

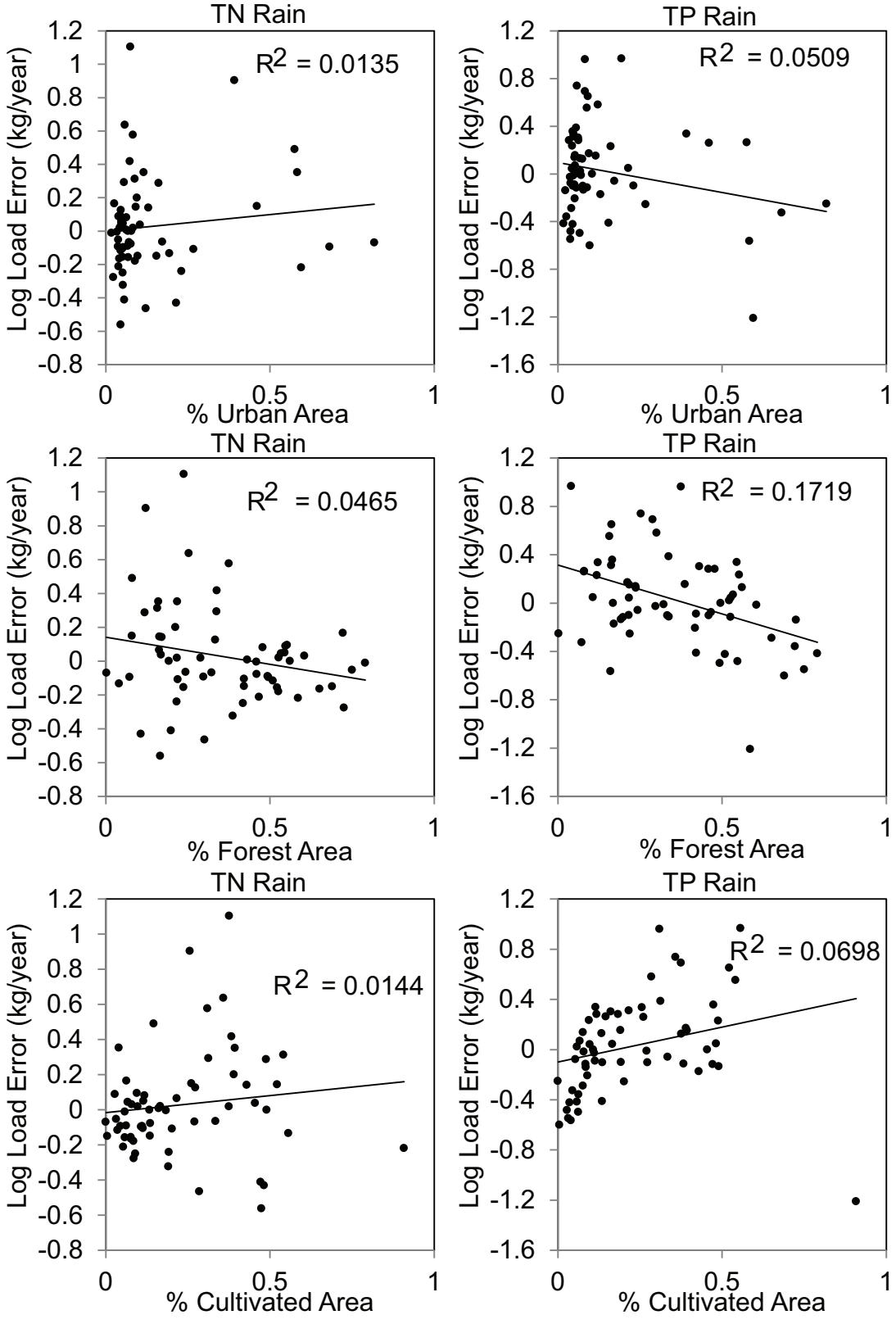

Figure 2.21: Rain model residuals and land use regression results.

CHAPTER 3

USING NITRATE ISOTOPE DATA TO VALIDATE A REGIONAL NUTRIENT SOURCE MODEL

3.1 Introduction

With coastline on four of the five Great Lakes, Michigan has a significant influence on the ecological health of the Great Lakes. Elevated levels of nitrate are a threat to both human and ecosystem health (*Davidson et al.*, 2012), and therefore, legislation in the Great Lakes and elsewhere has attempted to limit and control sources of nitrate. Correlations between nitrate and human disturbance and population have been observed in several major river basins worldwide (*Howarth et al.*, 1996; *Vitousek et al.*, 1997; *Hatfield and Keeney*, 2008), and a substantial amount of effort has focused on quantifying and understanding links between landscape processes and lake water quality. Of particular concern to environmental managers, are non-point sources of nitrate, which are difficult to quantify (*Dolan and McGunagle*, 2005; *PLUARG*, 1983; *Nikolaidis et al.*, 1998). Non-point sources of nitrate and the retention processes that occur within watersheds are spatially variable which makes identification and control of nitrate a challenge (*Hatfield and Keeney*, 2008).

Isotopic analysis of dissolved nitrate can provide insight to both sources and pathways of nutrients in surface water (*Kendall et al.*, 2007). Due to fractionation processes, nitrate derived from atmospheric deposition, waste (human or manure), nitrate stored in soil, and commercial fertilizer (derived from chemical fixation of N_2) have distinct isotopic signatures (*Chang et al.*, 2003; *Kendall et al.*, 2007; *Mayer et al.*, 2002). Isotope values for oxygen in nitrate derived from atmospheric deposition generally have values between 60 and 100 ‰while oxygen isotope values for septic and manure waste, ammonium fertilizer, and soil derived nitrate are generally between -15 and 15 ‰. Nitrate-nitrogen is greater for septic and manure waste (between 0 and 25 ‰) than it is for ammonium fertilizer (between -10 and

5 ‰) (*Kendall et al.*, 2007). Advances in analysis and the use of dual isotope techniques, specifically oxygen and nitrogen, have led to the growing popularity of the use of isotopes to identify sources of nitrogen in rivers, streams, lakes and groundwater (*Xue et al.*, 2009; *Kendall et al.*, 2007).

Interpretation of isotopic data is often complicated by microbial processes, mixing of multiple distinct sources, and/or the existence of sources with overlapping isotopic signatures that alter or obscure the the signature of the nitrate source. For these reasons, in the absence of additional data, isotopic analysis is often applied to small watersheds and/or those that are dominated by a single land use (*Chang et al.*, 2003; *Xue et al.*, 2009; *Burns et al.*, 2009). Land use can be an indication of the dominant nutrient sources, particularly in homogeneous watersheds, but some land uses contribute nutrients from several distinct sources. For instance, urban areas can contribute nutrients through wastewater effluent from treatment systems, direct wastewater contributions from leaky sewer systems, fertilizer from commercial and residential lawn application, and atmospheric deposition. The importance of each source contribution can vary from watershed to watershed or within a single watershed. In a state like Michigan where land use is highly variable across the state and includes both heavily farmed areas in addition to pristine forests and sprawling urban/suburban centers, source apportionment based on land use data alone may not adequately describe the sources of nutrients.

Here we use nitrogen isotopic data from four major watersheds in Michigan in conjunction with spatially explicit descriptions of nutrient sources and a process inferred statistical nutrient loading model to gain insight into, and quantify the sources contributing to, nitrate loading across the Lower Peninsula of Michigan. The model predicts nitrate loading and the source of nitrate. A mixing model using the results of the nitrate model is compared to isotope sample results. The use of isotopic data with the source model validates the model and provides clarification of isotopic data that alone would be difficult to interpret due to the diversity of some of Michigan's largest watersheds. The isotopic data provides additional

Watershed	Percent Land Use			Population Density	Sampled Area
	Ag	Urban	Forest	people/km^2	km^2
Grand River	65	15	20	86	13,520
Saginaw Bay	53	14	33	62	17,300
Muskegon River	28	11	61	23	6,560
Boardman-Charlevoix	16	11	73	26	4,720

Table 3.1: Watershed characteristics

information about landscape, in-stream processes, and storage of nitrate in soils that the nutrient model does not directly provide.

3.2 Methods

3.2.1 Sample Watersheds

Four watersheds in the Lower Peninsula of Michigan were sampled: Grand River, Saginaw Bay, Muskegon River, and Boardman-Charlevoix (Boardman). The Grand River watershed drains to Lake Michigan from the center of the Lower Peninsula. It has several large urban centers including Lansing and Grand Rapids and is the most densely populated watershed in the study. The watershed is dominated by agricultural land which is primarily row crop agriculture. The Saginaw Bay watershed in eastern Michigan is also dominated by agricultural land; it drains to Lake Huron and contains a large amount of tile drainage due to low slopes and poorly drained soils (CHAPTER 2). The Muskegon River and Boardman watersheds are much smaller than the Grand River and Saginaw Bay watersheds. Located in west-central and northwest Michigan, these watersheds drain to lake Michigan and are dominated by forested land (Table 3.1).

Fifteen to thirty sample points were selected in each watershed to sample approximately equal incremental watershed areas. The sample locations and incremental watershed areas are shown in Figure 3.1.

3.2.2 Sample Collection

Samples were collected during spring snow melt in March 2012. A total of 88 sites were visited over approximately 10 days. Flow was measured at each location using Acoustic Doppler Current Profiler (ADCP) or a Marsh-McBirney Flo-Mate. Some samples were collected at USGS gauge locations. Flows were downloaded from the USGS website to coincide with the time of the site visit. The locations of the USGS gauges are indicated in Figure 3.1. At all locations nitrate+nitrite samples were collected and filtered in the field with a 0.45 μm filter. The samples were then placed on dry ice and frozen. In addition to the 88 samples, blank and duplicate samples were collected approximately once a day or every 10-15 samples collected. Samples were analyzed in the Michigan State University Algae Laboratory using cadmium reduction. The nitrate+nitrite concentrations were combined with flow data to calculate NO_x fluxes.

Additional samples were collected in the spring of 2011. Samples were collected from the most downstream accessible point of most major and several minor watersheds that drain to the Great Lakes in the Lower Peninsula. The same sample collection methods were used. A total of 64 sites were visited.

Isotope samples were collected during the March 2012 field campaign. Samples were filtered in the field and frozen on dry ice. The samples were sent overnight to the Washington State University Isotope Laboratory, where they were analyzed using the "denitrifier method" (*Casciotti et al.*, 2002; *Sigman et al.*, 2001). Results are reported using delta notation where the ratio of ^{15}N to ^{14}N (in parts per thousand) is reported relative to the nitrogen isotopic ratio of N_2 in air, and the oxygen ^{18}O isotopic ratio is reported relative to Vienna Standard Mean Ocean Water. In addition to the internal quality assurance and quality control measures, duplicate and standard samples were sent for analysis. Data is included in Appendices B and C.

3.2.3 Statistical Nitrate Model

Results from the NO_x sampling were used to calibrate a statistical model that predicts nitrate loading and the sources of nitrate in sampled watersheds. The model is process-inferred; the structure of the model equation is based on nutrient pathways and processes. Fundamental to the basic structure of the model is a spatially detailed description of nutrient sources. These source inputs are combined with watershed factors such as recharge and travel distance and statistically optimized coefficients which describe attenuation of nutrients in the basin to predict nutrient fluxes at locations within the watershed. The model and the underlying equations are described extensively in CHAPTER 2.

The model was applied to total nitrogen loading to predict nitrate loads. The attenuation coefficients therefore, describe both loss of nitrate due to basin retention and the proportion of the total nitrogen pool that does not persist as nitrate. The values of the coefficients for the nitrate model were optimized using the Matlab function fminseach. The function uses the Nelder-Mead simplex algorithm (*Nelder and Mead*, 1965), a direct search algorithm that finds the minimum value of a function. The target of the optimization was the mean absolute difference between the natural logarithm of the observed area normalized load and the natural logarithm of the modeled area normalized load (see CHAPTER 2).

The 2012 nitrate data was used to optimize the model and the 2011 data was used to validate the model. A total of 6 coefficients were optimized including *Bsurf* (basin attenuation), *Fgrd* (the portion of the load entering the groundwater pathway), *Bgrd* (groundwater attenuation), *Btile* (attenuation in tile drains), and R and BY (in-stream attenuation).

3.3 Results

3.3.1 Nitrate Sample Results

The sampled watersheds have nitrate concentrations that range from 50 to 10,123 μg/L. The highest concentrations are in the Grand River and Saginaw Bay watersheds. The northern

Watershed	Average	Min	Max
	kg/day		
Grand	4,007	88	13,151
Muskegon	1,043	20	7,332
Saginaw	6,299	120	57,031
Boardman-Charlevoix	186	33	788

Table 3.2: Total NO_x loads for each sampled watershed.

R^2	Adj R^2	Validation R^2	n	Error
0.86	0.87	0.81	88	0.53

Table 3.3: Summary of model fit parameters.

portions of the Muskegon watershed and the Boardman-Charlevoix watersheds had relatively low concentrations of nitrate (Figure 3.2).

Saginaw Bay had the highest nitrate fluxes ranging from 120 to 57,031 kg/day and averaging 6,299 kg/day. Grand River had the second highest fluxes followed by the Muskegon River and Boardman-Charlevoix, which had the smallest fluxes. A summary of the watershed results are presented in Table 3.2.

3.3.2 Model Results

The nitrate sample data was used to optimize the nitrate loading model. The summary statistics and optimized parameters are shown in Tables 3.3 and 3.4. The model performed well with an R^2 of 0.86. The R^2 for the validation dataset was 0.81, illustrating the consistent performance of the model. The model was only sensitive to attenuation along the surface pathway and basin yield.

The model predicts that chemical fertilizer and manure are the dominant sources of nitrate in the Saginaw Bay and Grand River watersheds. Atmospheric deposition is the dominant source predicted by the model in the Muskegon River and Boardman-Charlevoix watersheds. Of the total atmospheric deposition, the model predicts that 5-12 % is deposited directly to surface water and wetlands. This deposition does not experience land-based

attenuation. The complete source apportionment for each watershed is shown in Figure 3.4.

The coefficients from the nitrate model indicate that during melt, in areas with the highest recharge nearly all of the nitrate infiltrates the soil (Table 3.5). The nitrate is not very persistent in the groundwater pathway; most nitrate is removed after 1 km of travel. Additionally, nitrate is more persistent in tile drains than in the surface runoff pathway; all of the nitrate remains after 1 km of travel. Attenuation during in-stream travel occurs relatively rapidly in the watershed with the lowest basin yield, but there is very little attenuation in the watershed with the largest basin yield.

The results for the nitrate loading model are similar to those found for the total nitrogen melt model (CHAPTER 2). Both models were sensitive to *Bsurf* and *BY*. The total nitrogen model estimates that all nitrogen persists in tile drains after 0.1 km; the nitrate model predicts that all nitrogen persists as nitrate in tile drains. Both models predict that in areas with the highest recharge, no nitrogen (nitrate) travels via the groundwater pathway. The largest difference between the models is that the total nitrogen model predicts that total nitrogen is more persistent in the surface pathway than nitrate. This is likely due to the fact that the nitrate model parameters describe only the portion of total nitrogen that persists as nitrate after 1 km and the total nitrogen model includes all nitrogen species.

3.3.3 Isotope Sample Results

The isotope results are indicated by watershed in Figure 3.5. There are some general watershed patterns evident in the isotope data. The Muskegon River has values ranging from the highest observed value of 61.3 ‰to 2.61 ‰. Both the Muskegon and Boardman-Charlevoix samples had generally higher oxygen values and lower nitrogen values than samples from Saginaw Bay and Grand River watersheds. Saginaw Bay showed the most variable nitrogen values with $\delta^{15}\mathrm{N}_{NO3}$ ranging from 1.32 to 8.4 ‰.

Only one sample had a $\delta^{18}\mathrm{O}_{NO3}$ value greater than 30 ‰. Since this sample was significantly higher than other results, it was analyzed a second time. The result of the reanalysis

was within 6.5 % of the original sample. The sample was from the most upstream sample location in the Muskegon River watershed located downstream of Houghton Lake, a 81 km^2 lake in north central Michigan.

As is common with large, mixed land use watersheds, much of the isotope data plots in the overlapping portion of the graph where source is indistinguishable without additional information (*Burns et al.*, 2009; *Chang et al.*, 2003). By plotting the isotope data along with the predominant nitrate source as predicted by the model, some trends are evident (Figure 3.6). Watersheds with manure as the predominant source, all have $\delta^{15}N_{NO3}$ values greater than 5. On average, watersheds dominated by atmospheric deposition have relatively heavier oxygen and the watershed with the heaviest oxygen sampled has the greatest contribution of atmospheric deposition at 95%. Samples dominated by fertilizer have low oxygen values and slightly lower nitrogen isotopic values (relative to watersheds with manure as a dominant source.

Dominant source is not perfectly predicted by isotopic ratio. This can be a result of fractionation processes that lead to further fractionation of the original source signature, nitrate derived from the soil which includes mineralization and nitrification of nitrate in the soil, mixing of several sources, or model error. This is why the use of isotopic data to infer source is difficult in large, mixed land use watersheds (*Xue et al.*, 2009).

Using the results from the statistical model and the observed isotope values, a simple mixing model can be constructed to predict isotopic ratios of source end members (manure/septics, ammonium fertilizer, soil, and direct atmospheric deposition). The model assumes that the isotopic value can be predicted from the proportion of the nitrate load each source contributes to the observed load. This is described by Equations 3.1.

$$\delta X = \alpha_1 (\%DirAtm) + \alpha_2 (\%Sep + \%Man) + \alpha_3 (\%IndAtm) + \alpha_4 (NonAg + ChemAg) \tag{3.1}$$

Each term contains the proportion of the total load contributed by the sources direct

atmospheric deposition (DirAtm), septic tanks (Sep), manure (Man), indirect atmospheric deposition (IndAtm), non-agricultural fertilizer (NonAg) and chemical agricultural fertilizer (ChemAg) and X is the isotopic ratio (delta notation) of nitrogen or oxygen. The coefficients α_1, α_2, α_3, and α_4 are the end member isotope values for atmospheric deposition, septic and manure waste, soil, and ammonium fertilizer derived nitrate respectively. The model assumes that atmospheric deposition that falls on the landscape is transformed by attenuation processes occurring in the soil (*Burns et al.*, 2009).

The predicted end member values are shown in Table 3.6. The values agree well with observed end member values compiled by *Kendall et al.* (2007). The R^2 value is 0.32 for the nitrogen isotope mixing model and 0.58 for the oxygen isotope mixing model. The model does a good job of predicting the the highest observed $\delta^{18}O_{NO3}$ value (observed in the Muskegon River watershed). There are no major outliers in the model. Mixing model error may be due to variability in end member values (as shown by *Kendall et al.* (2007)). For instance, values of $\delta^{15}N_{NO3}$ for the Lower Peninsula range from approximately -3.4-0.6 (*Kendall et al.*, 2007). Other sources of mixing model error could be nitrate loading model error or that the mixing model does not consider processes such as denitrification that may alter isotopic signatures.

For oxygen, due to high overland flow rates during melt, some atmospheric deposition that falls on the landscape may not experience a significant amount of processing. Higher $\delta^{18}O_{NO3}$ values have been correlated with higher runoff rates (*Burns et al.*, 2009; *Mayer et al.*, 2002), so it has been concluded that the dominant source of atmospheric deposition is primarily runoff. This assumption has been used to construct simple mixing models to determine contribution of atmospheric deposition for isotope data. However, the results of this mixing model suggest that atmospheric deposition directly to surface water predicted by surface water and wetland area is a good predictor of the elevated oxygen isotope values (as in the Muskegon River watershed). Ignoring this source increases uncertainty in these predictions.

3.4 Discussion

3.4.1 Soil Source

Direct atmospheric deposition to surface water is indicated in samples with higher $\delta^{18}O_{NO3}$ values. It is evident from Figure 3.6 that though some samples, on average, have higher $\delta^{18}O_{NO3}$ values, all but one sample plot outside the range expected for atmospherically derived oxygen. However, many plot in the soil nitrate range. Soil nitrate cannot be directly estimated from land use, which can make it difficult to determine dominant source from isotope data. Other studies have found that soil derived nitrate can be a significant influence on the isotopic ratio in watersheds (*Piatek et al.*, 2005; *Chang et al.*, 2003; *Spoelstra et al.*, 2001). *Burns et al.* (2009) found that isotopic data derived from forested land had an isotopic signature consistent with soil nitrate (derived from atmospheric deposition) and is an indication of the transformation of atmospherically derived nitrogen.

The model predicted source apportionment does not directly estimate the portion of nitrate derived from soil nitrification. However, the model can be used to estimate the percentage of atmospherically derived nitrogen that is deposited directly to surface water. Assuming that all atmospheric deposition that falls on the landscape experiences a cycle of soil nitrification before it reaches surface water, and therefore, will have the signature of soil derived nitrate, the contribution of soil derived nitrate can be estimated for each watershed using the model. The results of the mixing model suggest that this estimate is a good predictor of nitrate derived from soil.

3.4.2 Denitrification

Denitrification has been observed in nitrate isotope data surface water samples in other studies (*Kaushal et al.*, 2011; *Anisfeld et al.*, 2007). This process leads to relatively heavier nitrogen and oxygen which may be apparent in the dual isotope plot (*Bottcher et al.*, 1990). *Kaushal et al.* (2011) observed a strong 2:1 relationship between $\delta^{15}N_{NO3}$ and $\delta^{18}O_{NO3}$ in

rural watersheds where the dominant source was wastewater or manure. This effect is not apparent in the results from this study. However, in large watersheds where there is a large contribution from soil sources, the effect may be muted due to mixing (*Chang et al.*, 2003).

Another means of assessing the impact of from isotope data is through the relationship between nitrate and $\delta^{15}N_{NO3}$. Increasing values of nitrate should result in increasing values of $\delta^{15}N_{NO3}$ (*Chang et al.*, 2003). Plots of nitrate and $\delta^{15}N_{NO3}$ for each watershed show a weak relationship between nitrate and $\delta^{15}N_{NO3}$, so denitrification is not evident in this data.

This agrees well with *Kaushal et al.* (2011) who concluded, based on isotopic data, that denitrification occurred predominantly during summer baseflow. The slight negative relationship between nitrate and $\delta^{15}N_{NO3}$ could be the result of mixing of a heavy source such as atmospheric deposition and lighter source such as organic waste, soil derived nitrate, or fertilizer. In addition to the isotope data, the results from the model suggest that relatively little in-stream attenuation (denitrification and physical attenuation) occurs during spring melt, particularly in watersheds with high basin yields where the model predicts that nearly all nitrate persists after 1 week of in-stream travel time. During melt, discharge is high resulting in high flows and increased stream depths. Water traveling in-stream has less contact with stream biota so denitrification is expected to occur at lower rates (*Alexander et al.*, 2000).

3.5 Conclusions

The isotopic data suggests that in large watersheds, a significant portion of soil derived nitrate contributes to the nitrate load. As *Burns et al.* (2009) suggested, $^{18}O_{NO3}$ may be a good indication of the processes occurring in the soil that transform atmospherically derived nitrogen. Previous studies (*Kaushal et al.*, 2011; *Anisfeld et al.*, 2007) that have used isotope data and land use to estimate the contribution of sources to the nitrate load may be overestimating the contribution of organic waste and/or fertilizer if soil derived nitrate is

not considered, especially for samples during non-storm events. Using isotopic data in large, mixed land-use watersheds can provide some insight to nutrient sources, but it is limited. Even in small watersheds with a single land use, the variability in nitrogen sources (see CHAPTER 1) may make the application of isotope data to infer source, challenging. For instance, all sub-watersheds in the Boardman-Charlevoix are dominated by forest, but most of the isotope sample results plot in an intermediate range that indicates mixing of several sources.

In addition the isotope analysis helped confirm the results of the source apportionment model. The model successfully predicted dominant source as predicted by the isotope data (with the addition of the estimate of direct atmospheric deposition). Unlike isotope data alone, the model can be applied in large watersheds with diverse sources to predict the contributions of nitrate sources to the in-stream load.

Indirect atmospheric deposition is not the only source that is transformed by soil processes. A portion of the other sources may also be impacted by soil nitrification and mineralization, but these sources have overlapping isotopic signatures with the soil source, so their transformation is not evident in this analysis. In addition, groundwater nitrate may be impacted by these processes. Additional isotope sampling, particularly during baseflow, should help clarify this effect.

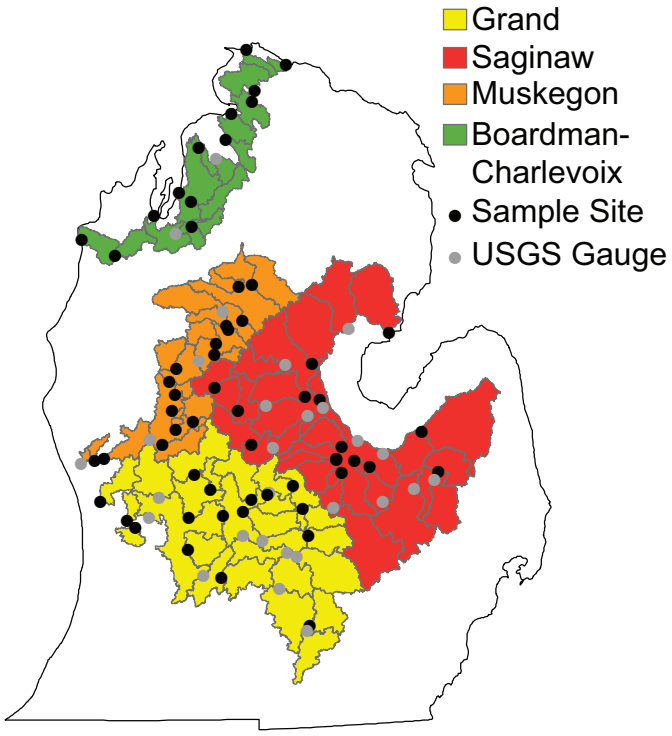

Figure 3.1: Sample locations and incremental watersheds.

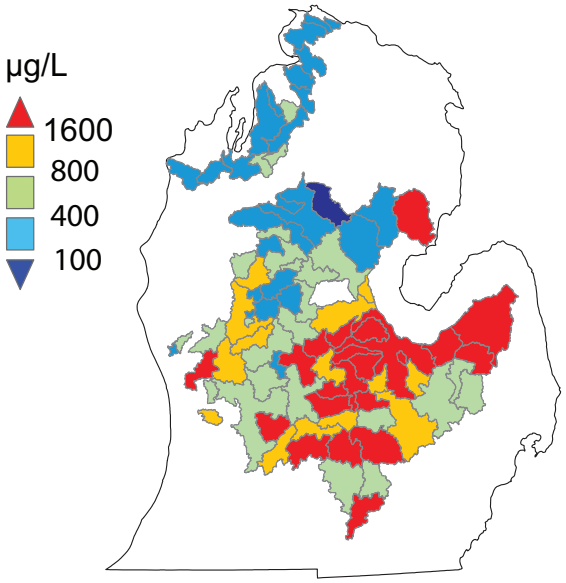

Figure 3.2: NO_x concentrations for sampled sub-watersheds. Incremental watershed areas are shown.

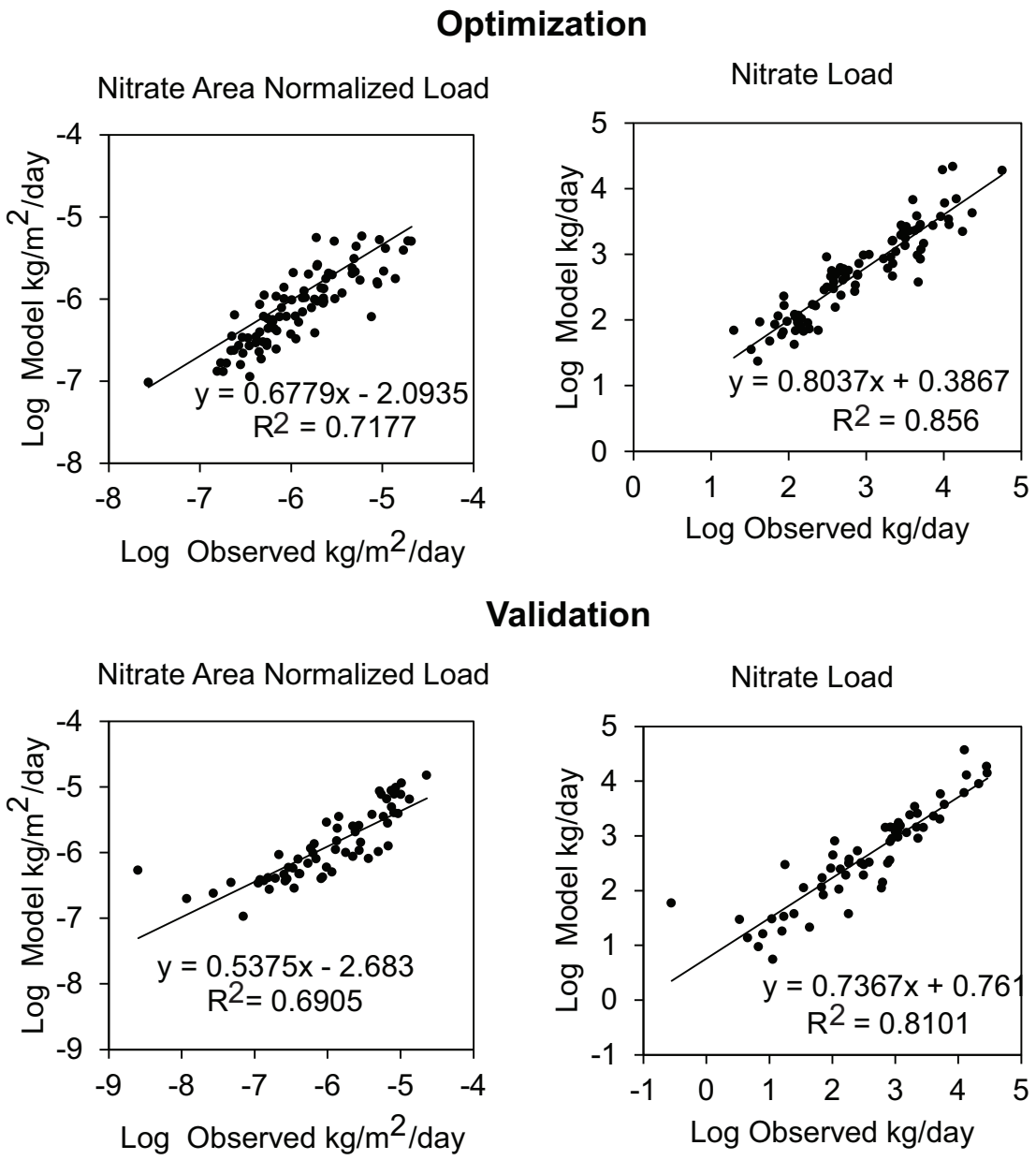

Figure 3.3: Graphs of observed and modeled nitrate loads and area normalized loads for the calibration and validation data sets.

Bsurf	Btile	R	BY	Fgrd	Bgrd
-8.71E-04	-3.78E-12	-6.18E-14	1.00E+00	4.26E-08	-3.96E-03
Sensitivity					
37.38	0.00	0.00	0.00	0.00	-82.95

Table 3.4: Summary of coefficients associated with each basin parameter.

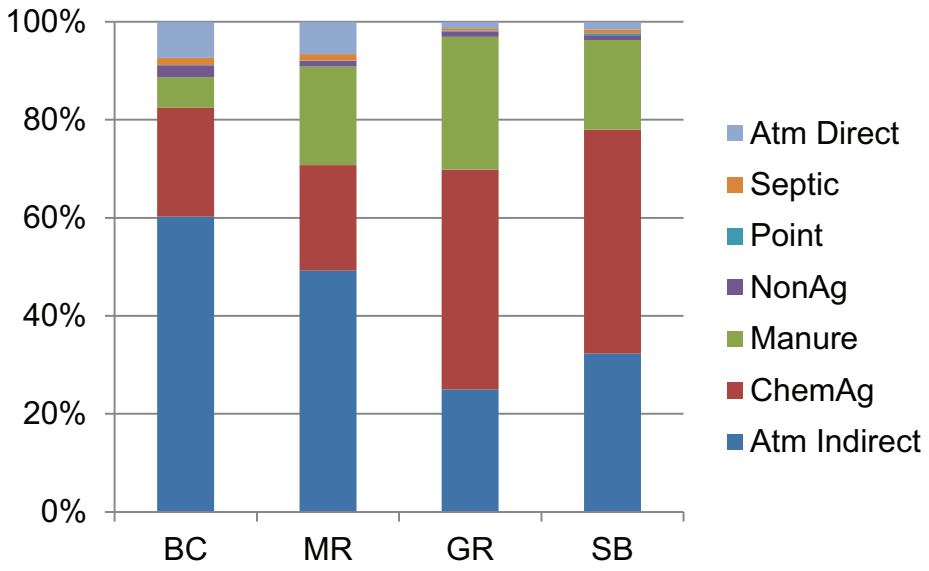

Figure 3.4: Model predicted source of exported nitrate in watersheds.

Bsurf (%/km)	Btile (%/km)	Rmin (%/day)	Rmax (%/day)	Fgrdmax (%)	Bgrd (%/km)
42	100	4	100	0	2

Table 3.5: Summary of calculated basin parameters. Reduction factor units (*Bsurf*, *Btile*, and *Bgrd*) are the percent of the nutrient load that remains after the first kilometer of travel. Units of *Rmin* and *Rmax* are the percent of the load that remains after the first day of in-stream travel for the sub-watershed with the highest relative basin yield (*Rmax*) and the lowest relative basin yield (*Rmin*). The bold values indicate the coefficients with relatively high model sensitivity.

Source	Model Predicted		Reported by *Kendall et al.* (2007)	
	$\delta^{15}N_{NO3}$	$\delta^{18}O_{NO3}$	$\delta^{15}N_{NO3}$	$\delta^{18}O_{NO3}$
Septic and Manure Waste	8.27	2.57	0-25	-15-15
Atmospheric Deposition	0.00	100.39	-15-15	60-98
Fertilizer	5.74	0.00	-10-5	-15-15
Soil	2.68	3.75	2-8	-15-15

Table 3.6: End member isotope values predicted by mixing model and compared to *Kendall et al.* (2007).

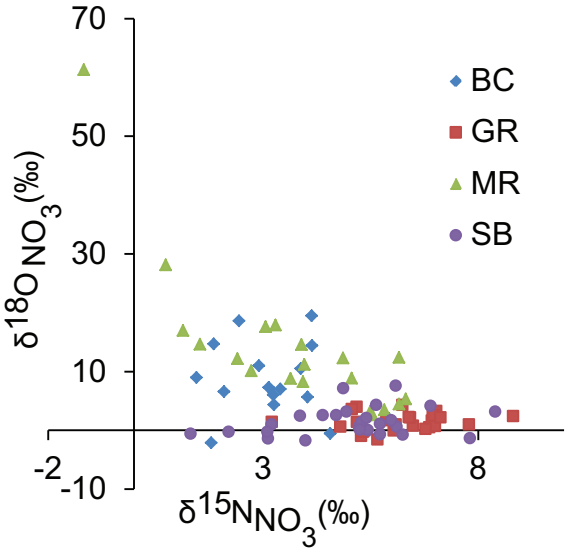

Figure 3.5: Measured isotopes by watershed

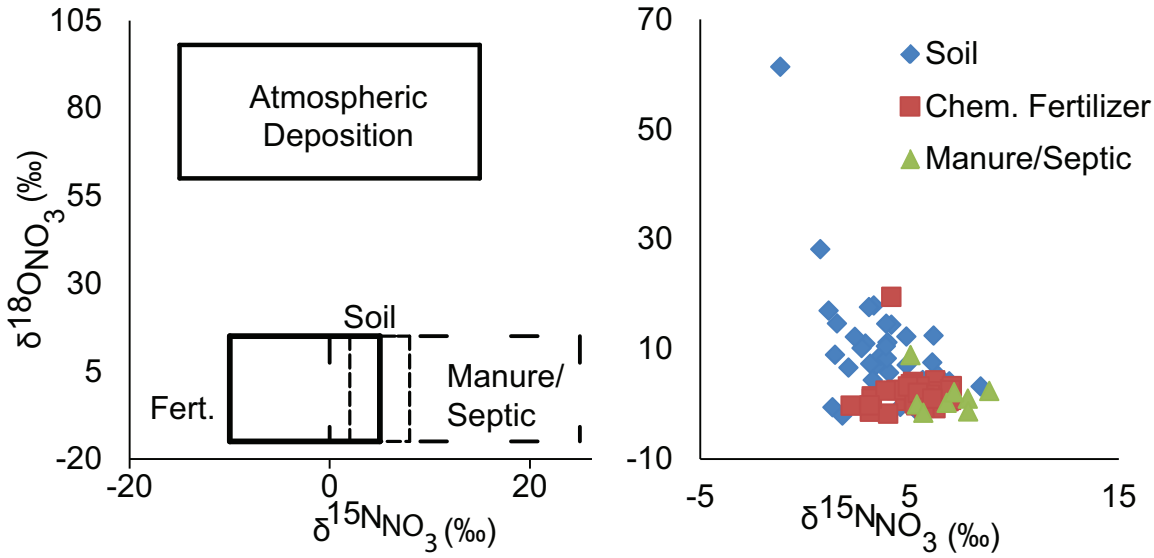

Figure 3.6: Isotope data with dominant source indicated (isotopic classification from *Kendall et al.* (2007)).

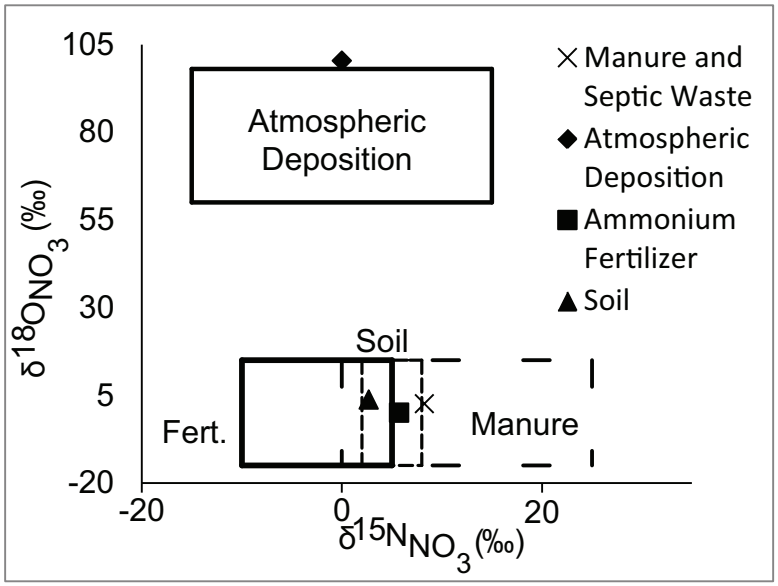

Figure 3.7: Predicted isotope values plotted with values reported by *Kendall et al.* (2007)

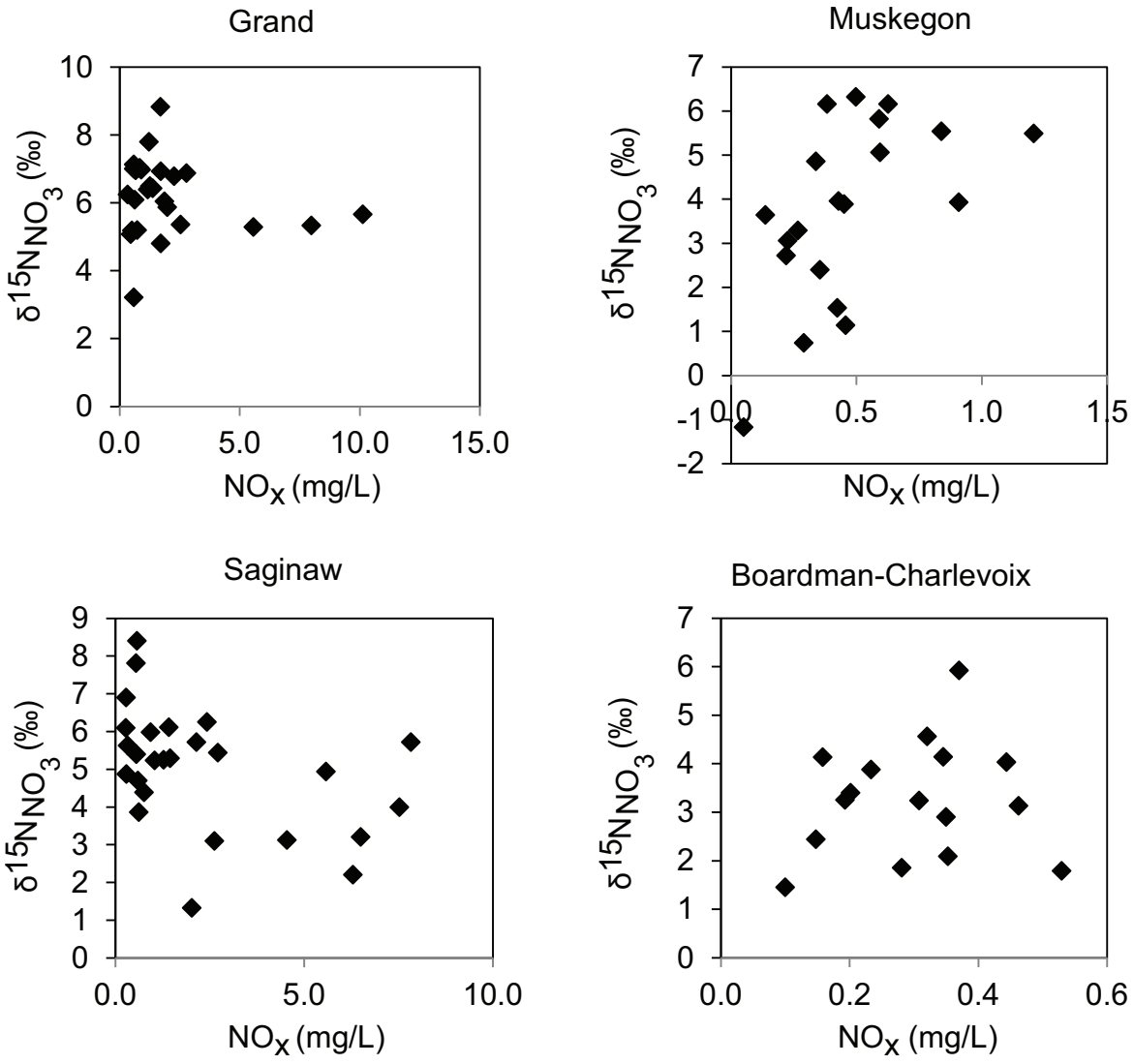

Figure 3.8: Nitrate vs. $\delta^{15}\mathrm{N}_{NO3}$.

APPENDICES

Appendix A

Total Nitrogen, Total Phosphorus, and Discharge Results

ID	Lat	Long	Date	Sample Type	Flow cfs	TN μg/L	TP μg/L
SW-1	42.087	-86.476	10/1/10		2022.82	1828.07832	49.71576
SW-10	44.259	-85.939	10/2/10		1510	190.00984	15.37661
SW-101	43.327	-83.746	10/15/10		69	940.17968	25.47636
SW-102	43.310	-83.956	10/13/10		223	3376.59024	104.25441
SW-103	43.245	-84.100	10/13/10		154	827.32592	27.09232
SW-104	43.589	-84.221	10/12/10		617	1013.70352	35.17212
SW-11	44.356	-86.049	10/2/10		106.3	525.48952	37.59606
SW-12	44.623	-86.223	10/3/10		806.23	492.87344	20.22449
SW-13	44.715	-86.125	10/3/10		170.22	329.79304	9.72075
SW-14	44.765	-85.621	10/3/10		235.9	483.55456	15.37661
SW-15	44.900	-85.411	10/3/10		452.73	176.03152	7.7008
SW-16	45.595	-84.474	10/3/10		919.95	250.58256	8.10479
SW-17	45.559	-84.403	10/3/10		408.94	395.0252	10.52873
SW-18	45.068	-83.436	10/4/10		444.61	1097.57344	18.20454
SW-19	44.415	-83.331	10/4/10		1146.31	180.69096	14.16464
SW-2	42.184	-86.371	10/1/10		283	818.00704	34.76813
SW-20	44.050	-83.688	10/4/10		37.79	352.06304	18.20454
SW-21	44.072	-84.019	10/4/10		178	553.44616	14.16464
SW-23	43.064	-82.597	10/12/10		23.41	519.80288	40.42399
SW-24	42.858	-82.538	10/12/10		1.659860294	283.19864	27.09232
SW-25	42.749	-82.490	10/12/10		48.03	362.40912	45.27187
SW-26	42.596	-82.909	10/12/10		0	3544.33008	160.00503
SW-27	42.297	-83.191	10/12/10		11.3	5583.1104	395.5312
SW-28	42.064	-83.253	10/4/10		271.92	809.71536	56.1796
SW-29	41.964	-83.546	10/4/10		167	1293.26992	97.38658
SW-3	42.646	-86.118	10/1/10		1540	1688.29512	51.73571

Table A.1: 2010 Baseflow Results. ND = Non Detect. DUP = Duplicate Sample.

ID	Lat	Long	Date	Sample Type	Flow cfs	TN μg/L	TP μg/L
SW-31	42.417	-86.241	10/1/10		38.14344	421.6116377	36.38409
SW-32	42.421	-86.245	10/1/10		68.940736	1656.70624	27.49631
SW-33	42.799	-86.059	10/1/10		5.6	4131.41952	57.39157
SW-34	42.797	-86.144	10/1/10		9.65	1218.71888	33.96015
SW-35	42.916	-86.147	10/1/10		2.79	3607.50784	53.75566
SW-36	42.907	-85.781	10/1/10		4.24	1265.31328	40.02
SW-37	42.904	-85.772	10/1/10		22.62	939.15248	20.62848
SW-39	42.949	-85.849	10/1/10		11.08	1330.54544	62.64344
SW-4	42.965	-85.675	10/2/10		1790	1237.35664	54.96763
SW-33	42.799	-86.059	10/1/10		5.6	4131.41952	57.39157
SW-34	42.797	-86.144	10/1/10		9.65	1218.71888	33.96015
SW-35	42.916	-86.147	10/1/10		2.79	3607.50784	53.75566
SW-36	42.907	-85.781	10/1/10		4.24	1265.31328	40.02
SW-37	42.904	-85.772	10/1/10		22.62	939.15248	20.62848
SW-39	42.949	-85.849	10/1/10		11.08	1330.54544	62.64344
SW-4	42.965	-85.675	10/2/10		1790	1237.35664	54.96763
SW-40	42.994	-86.018	10/1/10		7.08	2429.14608	30.32424
SW-41	42.962	-86.203	10/1/10		1.14	81.81552	50.52374
SW-43	43.197	-86.186	10/2/10		23.24	687.54272	25.47636
SW-51	43.490	-86.438	10/2/10		11.97	3611.61664	24.66838
SW-52	43.559	-86.503	10/2/10		44.44	1056.66568	18.20454
SW-55	43.905	-86.308	10/2/10		12.15	3460.46016	27.09232
SW-56	43.999	-86.372	10/2/10		23.36	855.28256	21.43646
SW-57	44.904	-85.975	10/2/10		55.47	255.242	9.31676

Table A.2: 2010 Baseflow Results (continued). ND = Non Detect. DUP = Duplicate Sample

ID	Lat	Long	Date	Sample Type	Flow cfs	TN μg/L	TP μg/L
SW-59	45.017	-85.618	10/2/10		2.95	1712.61952	10.52873
SW-6	43.463	-86.232	10/2/10		272	413.66296	26.28434
SW-60	44.745	-85.548	10/3/10		10.29	991.43352	21.43646
SW-62	45.100	-85.097	10/3/10		145	1488.9664	8.91277
SW-63	45.180	-85.164	10/3/10		2.94	562.76504	12.54868
SW-64	45.214	-85.013	10/3/10		61.66	548.78672	10.93272
SW-65	45.365	-84.962	10/3/10		55.79	409.00352	8.91277
SW-66	45.746	-84.828	10/3/10		62.31	590.72168	13.35666
SW-67	45.488	-84.076	10/3/10		84.39	655.95384	13.76065
SW-69	45.431	-83.839	10/2/10		14.32	780.73152	27.49631
SW-7	43.944	-86.278	10/2/10		431	287.85808	27.9003
SW-70	45.337	-83.685	10/3/10		2.2	683.91048	14.97262
SW-71	45.162	-83.410	10/4/10		0.92	553.44616	19.41651
SW-73	44.260	-83.527	10/4/10		56.12	325.1336	18.60853
SW-8	44.030	-86.506	10/2/10		101.35	576.74336	14.97262
SW-9	44.208	-86.246	10/2/10		158.56	92.1616	12.54868
SW-91	42.588	-82.903	10/12/10		0.24	716.52656	56.1796
SW-94	42.095	-83.211	10/4/10		4.72	948.47136	73.14718
SW-97	41.931	-83.340	10/3/10		0.54	87.50216	54.15965

Table A.3: 2010 Baseflow Results (continued). ND = Non Detect. DUP = Duplicate Sample

ID	Lat	Long	Date	Sample Type	Flow cfs	TN μg/L	TP μg/L
J-201	45.136	-85.081	3/19/11		69.49926407	717.883464	53.66032
J-202	45.033	-85.064	3/19/11		40.15277604	1637.296572	30.032944
J-203	45.036	-84.969	3/19/11		148.1097121	1755.6817	48.854752
SW-1	42.087	-86.476	3/5/11		6750.045393	3400.097016	118.535488
SW-10	44.259	-85.939	3/20/11		1360	532.877448	42.046864
SW-101	43.327	-83.746	3/7/11		2300	5195.23044	161.385136
SW-102	43.310	-83.956	3/6/11		3170	2683.292124	143.364256
SW-103	43.245	-84.100	3/22/11		1479.296073	3158.583016	232.667728
SW-104	43.589	-84.221	3/6/11		1160	2357.055488	75.68584
SW-11	44.356	-86.049	3/20/11		34.82026137	570.8274	63.67192
SW-11	44.356	-86.049	3/20/11	Blank		575.571144	43.64872
SW-11	44.356	-86.049	3/20/11	DUP		717.883464	61.6696
SW-12	44.623	-86.223	3/20/11		288.4855123	665.70228	45.250576
SW-13	44.715	-86.125	3/20/11		157.8212455	290.946504	29.63248
SW-14	44.765	-85.621	3/19/11		381.0452537	999.054532	52.859392
SW-15	44.900	-85.411	3/19/11		481.8333125	252.996552	38.042224
SW-15	44.900	-85.411	3/19/11	Blank		ND	8.808352
SW-15	44.900	-85.411	3/19/11	DUP		300.433992	29.63248
SW-16	45.595	-84.474	3/23/11		835.6862728	271.971528	38.442688
SW-17	45.559	-84.403	3/23/11		364.0942137	267.227784	33.236656
SW-18	45.068	-83.436	3/22/11		1555.893585	940.839432	82.493728
SW-19	44.415	-83.331	3/22/11		1722.543498	428.51508	65.67424
SW-2	42.184	-86.371	3/5/11		823	1238.218292	45.117088
SW-20	44.050	-83.688	3/22/11		646.8940646	2758.527272	148.570288
SW-21	44.072	-84.019	3/22/11		777	295.690248	38.843152
SW-21	44.072	-84.019	3/22/11	Blank		72.73428	8.808352
SW-21	44.072	-84.019	3/22/11	DUP		1373.019684	112.928992
SW-23	43.064	-82.597	3/7/11		2216.348482	5449.811368	191.8204
SW-24	42.858	-82.538	3/7/11			1413.966924	218.251024
SW-25	42.749	-82.490	3/22/11		1178.76826	2102.183484	166.190704

Table A.4: 2011 Melt Results (continued). ND = Non Detect. DUP = Duplicate Sample

ID	Lat	Long	Date	Sample Type	Flow cfs	TN μg/L	TP μg/L
SW-26	42.596	-82.909	3/4/11		739.135974	2249.365416	113.329456
SW-27	42.297	-83.191	3/4/11		438.2550137	1819.930716	116.533168
SW-28	42.064	-83.253	3/4/11		969.7407476	1919.54934	77.287696
SW-29	41.964	-83.546	3/4/11		3630	7045.416468	213.445456
SW-3	42.646	-86.118	3/6/11		3060	2243.21	85.3
SW-3	42.646	-86.118	3/6/11	Blank		1.57812	8.808352
SW-3	42.646	-86.118	3/6/11	DUP		2129.355776	87.299296
SW-31	42.417	-86.241	3/5/11		686.7643233	1181.688676	129.74848
SW-32	42.421	-86.245	3/5/11		573.5101872	1969.358652	92.505328
SW-33	42.799	-86.059	3/5/11		140	7013.66564	512.992528
SW-34	42.797	-86.144		DUP		3158.583016	149.371216
SW-34	42.797	-86.144	3/5/11		47.32165338		
SW-35	42.916	-86.147	3/5/11		118.3041334		
SW-36	42.907	-85.781	3/6/11		187.5561948	3485.901352	166.591168
SW-37	42.904	-85.772	3/6/11		199.1747202	2284.817628	111.327136
SW-39	42.949	-85.849	3/6/11		132.7831468	3652.514544	221.8552
SW-4	42.965	-85.675	3/6/11		6970		
SW-40	42.994	-86.018	3/6/11		165.2726402	3140.190192	28.831552
SW-40	42.994	-86.018	3/6/11	Blank		82.221768	8.407888
SW-40	42.994	-86.018	3/6/11	DUP		2649.42116	114.931312
SW-41	42.962	-86.203	3/6/11		7.416080007	1181.688676	58.065424
SW-43	43.197	-86.186	3/21/11		79.74051741	1486.078916	62.070064
SW-48	43.416	-86.277	3/21/11		12.67796535	765.320904	35.63944
SW-5	43.318	-86.038	3/21/11		3386.676537		
SW-51	43.490	-86.438	3/21/11		71.75940273	2449.475892	165.389776
SW-52	43.559	-86.503	3/21/11		113.9604294	1863.706112	64.472848
SW-55	43.905	-86.308	3/21/11		55.16150939	2976.739496	191.8204
SW-56	43.999	-86.372	3/20/11		169.6869735	1425.200868	105.320176
SW-57	44.904	-85.975	3/20/11		66.00311206	252.996552	46.451968
SW-59	45.017	-85.618	3/19/11		6.356640006	1660.016196	47.252896
SW-6	43.463	-86.232	3/21/11		815	988.276872	82.093264
SW-6	43.463	-86.232	3/21/11	DUP		969.301896	73.68352
SW-60	44.745	-85.548	3/19/11		19.35243735	974.04564	49.65568
SW-62	45.100	-85.097	3/19/11		180	1172.991812	51.257536

Table A.5: 2011 Melt Results (continued). ND = Non Detect. DUP = Duplicate Sample

ID	Lat	Long	Date	Sample Type	Flow cfs	TN μg/L	TP μg/L
SW-63	45.180	-85.164	3/19/11		11.47726668	1002.508104	71.280736
SW-64	45.214	-85.013	3/23/11		94.78456542	575.571144	45.250576
SW-65	45.365	-84.962	3/23/11		109.8639281	637.239816	51.257536
SW-66	45.746	-84.828	3/23/11		36.72725337	698.908488	50.857072
SW-67	45.488	-84.076	3/23/11		115.6555334	528.133704	45.250576
SW-69	45.431	-83.839	3/23/11		33.5136187	660.958536	53.66032
SW-7	43.944	-86.278	3/20/11		1380	3430.431804	59.66728
SW-70	45.337	-83.685	3/23/11		21.01222669	943.71	8.808352
SW-71	45.162	-83.410	3/23/11		38.4929867	618.26484	42.847792
SW-73	44.260	-83.527	3/22/11		173.5715868	920.782756	55.66264
SW-8	44.030	-86.506	3/20/11		343.5763923	1103.4169	98.512288
SW-9	44.208	-86.246	3/20/11		256.5610536	798.527112	78.088624
SW-91	42.588	-82.903	3/4/11		9.888106676	2085.58038	94.507648
SW-94	42.095	-83.211	3/4/11		61.44752006	1025.145124	80.491408
SW-97	41.931	-83.340	3/4/11		63.91954673	7886.514536	111.327136

Table A.6: 2011 Melt Results (continued). ND = Non Detect. DUP = Duplicate Sample

ID	Lat	Long	Date	Sample Type	Flow cfs	TN μg/L	TP μg/L
J-201	45.136	-85.081	6/24/11		73.45450674	636.33824	13.5684
J-202	45.033	-85.064	6/24/11		38.9167627	1090.83456	25.8213
J-203	45.036	-84.969	6/24/11		164.9901228	489.35744	29.5343
SW-1	42.087	-86.476	6/3/11		9592.275713	1127.604916	91.1701
SW-10	44.259	-85.939	6/25/11		2220	594.37472	21.37
SW-10	44.259	-85.939	6/25/11	Blank		69.83072	0.2016
SW-10	44.259	-85.939	6/25/11	DUP		678.30176	25.8213
SW-101	43.327	-83.746	6/1/11		2370	3496.52608	89.6849
SW-102	43.310	-83.956	6/1/11		2990	1369.513367	65.5504
SW-102	43.310	-83.956	6/1/11	Blank		118.78816	0.5729
SW-102	43.310	-83.956	6/1/11	DUP		1015.962826	87.65
SW-103	43.245	-84.100	6/1/11		2010	895.0048	88.571
SW-104	43.589	-84.221	6/1/11		2880	1300.65216	55.5253
SW-11	44.356	-86.049	6/25/11		28.95802669	888.11936	29.5343
SW-12	44.623	-86.223	6/25/11		225.9079229	685.29568	36.589
SW-13	44.715	-86.125	6/25/11		166.5086535	608.36256	26.9352
SW-14	44.765	-85.621	6/25/11		522.3745498	874.13152	21.737
SW-15	44.900	-85.411	6/24/11		1216.37838	559.40512	13.39
SW-16	45.595	-84.474	6/27/11		1151.540652	517.4416	15.43
SW-17	45.559	-84.403	6/27/11		1467.889436	657.32	23.5935
SW-18	45.068	-83.436	6/28/11		1963.530783	1132.90656	33.2473
SW-18	45.068	-83.436	6/28/11	DUP		692.2896	24.3361
SW-19	44.415	-83.331	6/28/11		1624.933759		
SW-2	42.184	-86.371	6/3/11		991	1167.87616	64.4365
SW-2	42.184	-86.371	6/3/11	Blank		125.78208	0.2016
SW-2	42.184	-86.371	6/3/11	DUP		83.71008	53.2975
SW-20	44.050	-83.688	6/28/11		162.0590055	2231.886348	35.1038
SW-21	44.072	-84.019	6/28/11		340	930.08288	36.2177
SW-24	42.858	-82.538	6/1/11		112.0887521	433.40608	61.8374
SW-25	42.749	-82.490	6/1/11		247.9795896	1329.119968	94.8831
SW-26	42.596	-82.909	6/1/11		0	1112.616133	98.2248
SW-27	42.297	-83.191	6/2/11		479.0787685	1398.311145	98.9674
SW-28	42.064	-83.253	6/2/11		3446.570211	1404.59	66.293
SW-28	42.064	-83.253	6/2/11	Blank		160.75168	0.9442
SW-28	42.064	-83.253	6/2/11	DUP		1243.89	46.2428

Table A.7: 2011 Rain Results. ND = Non Detect. DUP = Duplicate Sample

ID	Lat	Long	Date	Sample Type	Flow cfs	TN μg/L	TP μg/L
SW-29	41.964	-83.546	6/2/11		3800	1845.96096	111.9629
SW-3	42.646	-86.118	6/3/11		5610	839.05344	78.9172
SW-31	42.417	-86.241	6/3/11		277.9264269	125.6736	52.1836
SW-32	42.421	-86.245	6/3/11		312.5348003	643.22368	34.18
SW-33	42.799	-86.059	6/3/11		74.8670934	3524.50176	20.6231
SW-34	42.797	-86.144	6/3/11		36.30347737	209.60064	44.3863
SW-35	42.916	-86.147	6/3/11		49.51116271	1562.607198	72.2338
SW-36	42.907	-85.781	6/4/11		60.67059739	1286.66432	61.8374
SW-37	42.904	-85.772	6/4/11		67.73353073	559.29664	57.3818
SW-39	42.949	-85.849	6/4/11		38.10452537	1258.68864	95.6257
SW-4	42.965	-85.675	6/4/11		10817.55339	1539.594191	94.5118
SW-40	42.994	-86.018	6/4/11		44.35522138	2257.13885	59.6096
SW-41	42.962	-86.203	6/4/11		4.237760004	790.20448	22.8509
SW-41	42.962	-86.203	6/4/11	Blank		83.81856	ND
SW-41	42.962	-86.203	6/4/11	DUP		888.11936	15.0536
SW-43	43.197	-86.186	6/26/11		58.51640272	5146.65728	26.9352
SW-48	43.416	-86.277	6/26/11		11.65384001	867.02912	17.2814
SW-5	43.318	-86.038	6/26/11		3368.242281	993.02816	23.5935
SW-51	43.490	-86.438	6/26/11		21.64789069	2307.275172	46.2428
SW-52	43.559	-86.503	6/26/11		64.97898673	447.39392	15.0536
SW-55	43.905	-86.308	6/26/11		14.83216001	7776.3712	65.92
SW-56	43.999	-86.372	6/25/11		89.69925342	811.07776	71.4912
SW-57	44.904	-85.975	6/25/11		88.56918408	419.52672	23.5935
SW-59	45.017	-85.618	6/25/11		6.709786673	517.33312	25.8213
SW-56	43.999	-86.372	6/25/11		89.69925342	811.07776	71.4912
SW-57	44.904	-85.975	6/25/11		88.56918408	419.52672	23.5935
SW-59	45.017	-85.618	6/25/11		6.709786673	517.33312	25.8213
SW-6	43.463	-86.232	6/26/11	DUP		1097.93696	40.302
SW-60	44.745	-85.548	6/24/11		13.06642668	1125.91264	34.3612
SW-62	45.100	-85.097	6/24/11		192	335.4912	27.68
SW-62	45.100	-85.097	6/24/11	Blank		132.776	1.6868
SW-62	45.100	-85.097	6/24/11	DUP		139.66144	28.7917
SW-63	45.180	-85.164	6/24/11		28.60488003	923.08896	26.9352
SW-64	45.214	-85.013	6/27/11		88.85170142	734.25312	25.8213

Table A.8: 2011 Rain Results (continued). ND = Non Detect. DUP = Duplicate Sample

ID	Lat	Long	Date	Sample Type	Flow cfs	TN μg/L	TP μg/L
SW-65	45.365	-84.962	6/27/11		148.0743975	825.17408	27.6778
SW-65	45.365	-84.962	6/27/11	Blank		ND	2.4294
SW-65	45.365	-84.962	6/27/11	DUP		797.1984	18.7666
SW-66	45.746	-84.828	6/27/11		96.93876009	846.15584	11.7119
SW-67	45.488	-84.076	6/27/11		255.2190962	948.966464	16.9101
SW-69	45.431	-83.839	6/27/11		77.40974941	867.1376	23.9648
SW-7	43.944	-86.278	6/25/11		1470	1118.91872	46.6141
SW-70	45.337	-83.685	6/27/11		38.03389604	923.08896	29.5343
SW-71	45.162	-83.410	6/27/11		167.0383735	559.40512	11.7119
SW-73	44.260	-83.527	6/28/11		118.2335041	979.04032	18.7666
SW-8	44.030	-86.506	6/25/11		345.730587	566.39904	10.9693
SW-9	44.208	-86.246	6/25/11		267.5792296	636.33824	29.163
SW-91	42.588	-82.903	6/1/11		3.53146667	1374.921506	91.5414
SW-94	42.095	-83.211	6/2/11		25.14404269	419.41824	111.5916
SW-97	41.931	-83.340	6/2/11		34.2552267	4503.65056	84.4867

Table A.9: 2011 Rain Results (continued). ND = Non Detect. DUP = Duplicate Sample

ID	Lat	Long	Date	Sample Type	Flow cfs	TN μg/L	TP μg/L
BC10	45.508	-84.763	8/19/11		75.92653236	498.89816	35.29952
BC11	45.440	-84.785	8/19/11		81.18841762	664.04	37.95798
BC12	45.166	-85.240	8/19/11		27.89858631	368.78792	41.376
BC13	44.846	-85.307	8/20/11		81.93002561	438.84728	32.26128
BC14	44.699	-85.306	8/20/11		25.07341301	386.3	30.74216
BC15	44.528	-85.949	8/20/11		65.33213249	263.69888	50.49072
BC17	44.657	-85.439	8/20/11		93	303.7328	33.7804
BC9	45.659	-84.493	8/19/11		-0.03	608.99144	78.21466
GR1	43.130	-85.174	10/9/11		24.40243435	664.03808	82.01246
GR11	43.015	-84.426	10/9/11		15.53845313	503.9024	475.84432
GR12	42.966	-85.352	10/9/11		105.1317613	153.6056	56.5672
GR13	43.067	-84.842	10/9/11		66.74471914	258.69464	55.04808
GR14	42.775	-85.359	10/8/11		56.39752194	1363.73008	74.03708
GR15	43.063	-86.067	10/8/11		28.81676763	543.03472	136.321
GR17	42.312	-84.387	10/8/11		108.4866546	322.84816	126.44672
GR20	42.283	-84.410	10/8/11		109	2493.256	253.82
GR21	42.536	-84.624	10/8/11		433	362.88208	96.82388
GR21	42.536	-84.624	10/8/11	Blank		8.48264	1.4991
GR21	42.536	-84.624	10/8/11	DUP		342.86512	82.01246
GR23	42.728	-84.478	10/10/11		70	442.94992	85.43048
GR24	42.750	-84.555	10/10/11		546	412.92448	229.45
GR25	42.857	-84.913	10/9/11		628	763.22128	74.79664
GR26	42.828	-84.759	10/9/11		49	883.32304	70.23928
GR27	43.109	-84.693	10/9/11		44	453.86	142.39748
GR28	42.971	-85.069	10/9/11		987	703.1704	64.1628
GR28	42.971	-85.069	10/9/11	Blank		ND	ND
GR28	42.971	-85.069	10/9/11	DUP		513.00928	72.13818
GR3	42.609	-85.094	10/8/11		49.5464767	503.9024	74.03708
GR30	42.616	-85.236	10/8/11		158	282.81424	63.02346
GR31	43.082	-85.590	10/9/11		121	313.74128	56.94698
GR5	43.097	-84.710	10/9/11		9.534959877	2710.77224	41.376
GR6	43.226	-85.302	10/9/11		128.545385	513.00928	62.2639
GR7	42.877	-84.384	10/8/11		15.5737678	659.03384	219.11304
GR8	43.000	-84.908	10/9/11		19.49369575	513.91088	41.75578
GR9	43.145	-84.503	10/9/11		33.9727089	343.76672	124.54782
MR10	43.402	-85.563	9/11/11		58.69297525	653.128	40.23666
MR10	43.402	-85.563	9/11/11	Blank		ND	1.11932
MR10	43.402	-85.563	9/11/11	DUP		593.08	33.02084
MR11	43.306	-86.114	9/11/11		30.51187161	553.9448	75.17642

Table A.10: 2011 Baseflow Results. ND = Non Detect. DUP = Duplicate Sample

ID	Lat	Long	Date	Sample Type	Flow cfs	TN μg/L	TP μg/L
MR13	43.699	-85.460	9/11/11		14.09055182	103.5632	67.20104
MR14	43.540	-85.305	9/11/11		62.71884719	518.91512	45.55358
MR15	44.336	-84.922	8/21/11		24.54369302	123.58016	47.0727
MR16	43.490	-85.449	9/11/11		2.419054636	463.86848	48.9716
MR17	43.608	-85.481	8/22/11		12.88985317	473.87696	29.60282
MR2	44.082	-85.014	8/21/11		331.7459744	443.85152	42.51534
MR20	44.201	-85.053	8/21/11		102	188.19	39.85688
MR21	43.901	-85.255	8/21/11		480	509.96772	37.19842
MR21	43.901	-85.255	8/21/11	Blank			3.398
MR21	43.901	-85.255	8/21/11	DUP		488.54992	37.5782
MR23	43.435	-85.666	8/21/11		1220	669.04232	48.21204
MR24	43.289	-86.223	9/11/11		3.4	273.70736	41.75578
MR3	44.139	-84.899	8/21/11		144.1897821	213.65648	33.40062
MR4	44.006	-85.111	8/21/11		28.07515964	629.0084	45.1738
MR5	43.853	-85.444	8/21/11		58.23388458	288.72008	37.19842
MR6	44.111	-85.028	8/21/11		16.09	533.92784	99.48234
MR7	43.934	-85.129	8/21/11		5.61	308.73704	31.50172
MR8	43.779	-85.500	9/11/11		556.9829155	498.89816	31.50172
MR9	44.409	-84.805	8/21/11		49.08738604	538.93208	39.09732
SB12	43.657	-84.267	9/17/11		0.0918	674.04656	57.32676
SB13	43.211	-83.315	10/7/11	10/3/10	32.34823425	611.5	89.98784
SB15	43.250	-83.873	10/7/11		303.3176681	1113.51808	96.06432
SB16	43.450	-83.441	10/7/11		47.56885539	438.84728	49.73116
SB17	43.872	-84.321	9/17/11		73.06604439	418.83032	53.14918
SB19	43.015	-84.180	10/7/11		169	651.53	58.08632
SB2	43.302	-84.144	10/7/11		0.3186	709.07624	42.13556
SB20	43.218	-84.106	10/7/11		214.9603732	824.17376	50.49072
SB21	43.160	-83.351	10/8/11		57	553.9448	64.54258
SB22	43.111	-83.519	10/8/11		121	543.93632	48.9716
SB24	43.038	-83.774	10/8/11		220	603.0856	75.17642
SB27	43.328	-83.758	10/7/11		89	618.99992	47.83226
SB28	43.867	-84.545	9/17/11		52	304.35684	34.16018
SB29	43.627	-84.708	9/17/11		132	383.80064	50.49072
SB3	43.675	-84.388	9/17/11		136.5618142	508.90664	56.94698
SB30	43.379	-84.656	9/17/11		119	634.02	64.54258

Table A.11: 2011 Baseflow Results (continued). ND = Non Detect. DUP = Duplicate Sample

ID	Lat	Long	Date	Sample Type	Flow cfs	TN μg/L	TP μg/L
SB31	43.563	-84.370	9/17/11		69	493.89392	26.1848
SB31	43.563	-84.370	9/17/11	Blank			1.87888
SB31	43.563	-84.370	9/17/11	DUP		498.89816	42.89512
SB32	43.610	-84.242	9/17/11		358	458.86424	51.63006
SB33	43.409	-83.964	10/7/11		5240	1388.09752	73.6573
SB33	43.409	-83.964	10/7/11	Blank		43.05968	6.05646
SB33	43.409	-83.964	10/7/11	DUP		1507.61786	78.97422
SB4	43.597	-84.944	9/17/11		96.55029743	458.86424	34.16018
SB5	43.397	-84.836	9/17/11		62.4010152	398.81336	35.29952
SB6	43.292	-83.992	10/7/11		19.45838108	649.03	46.69292
SB7	43.741	-85.127	9/17/11		32.24229025	523.91936	42.13556
SB8	43.298	-84.143	10/7/11		6.568527916	418.83032	36.43886
SB9	43.380	-84.094	10/7/11		9.358386546	684.05504	113.91398
SW-11	44.356	-86.049	8/20/11		6.82	483.88544	52.00984
SW-12	44.623	-86.223	8/20/11		153.2656514	383.80064	61.12456
SW-13	44.715	-86.125	8/20/11		99.58735872	306.24	23.14656
SW-13	44.715	-86.125	8/20/11	Blank			
SW-13	44.715	-86.125	8/20/11	DUP		214.40208	34.16018
SW-14	44.765	-85.621	8/20/11		235.195677	433.84304	33.02084
SW-15	44.900	-85.411	8/19/11		293.8180229	128.5844	34.91974
SW-20	44.050	-83.688	9/17/11		11.93635718	390.02804	25.42524
SW-21	44.072	-84.019	9/17/11		140	63.52928	34.16018
SW-36	42.907	-85.781	10/9/11		34.213	1124.42816	78.97422
SW-36	42.907	-85.781	10/9/11	DUP	22.036		
SW-39	42.949	-85.849	10/8/11		17.44544511	596.48	99.10256
SW-4	42.965	-85.675	10/9/11		2100	1183.57744	68.72016
SW-5	43.318	-86.038	9/11/11		1086.879482	313.74128	55.80764
SW-62	45.100	-85.097	8/19/11		156	228.6692	31.12194
SW-62	45.100	-85.097	8/19/11	Blank		3.4784	1.11932
SW-62	45.100	-85.097	8/19/11	DUP		202.7464	45.1738
SW-64	45.214	-85.013	8/19/11		72.14786307	388.80488	49.35138
SW-65	45.365	-84.962	8/19/11		35.63249821	278.7116	31.50172
SW-66	45.746	-84.828	8/19/11		6.886359911	433.84304	22.76678

Table A.12: 2011 Baseflow Results (continued). ND = Non Detect. DUP = Duplicate Sample

ID	Lat	Long	Date	Sample Type	Flow cfs	TN μg/L	TP μg/L
BC10	45.508	-84.763	3/9/12		166.1556635	694.2821739	188.477
BC11	45.440	-84.785	3/9/12		209.9812062	1014.359308	155.73
BC12	45.166	-85.240	3/10/12		116.2206777	159.3250521	15.9255
BC13	44.846	-85.307	3/10/12		104.531512	650.12676	105.35
BC14	44.699	-85.306	3/10/12		105.4850089	519.5445012	92.755
BC15	44.528	-85.949	3/11/12		300.0690059	397.5530834	134.3185
BC17	44.657	-85.439	3/10/12		172	1134.018126	76.3815
BC9	45.659	-84.493	3/9/12		110.4996963	475.2041344	130.54
GR1	43.130	-85.174	3/2/12		105.8734706	1069.67208	100.312
GR11	43.015	-84.426	3/4/12		248.0857675	2834.695063	143.135
GR11	43.015	-84.426	3/4/12	Blank		111.5100218	ND
GR11	43.015	-84.426	3/4/12	DUP		2051.64984	144.3945
GR12	42.966	-85.352	3/2/12		406.0484206	272.199	153.211
GR13	43.067	-84.842	3/4/12		698.3481925	3281.35164	120.464
GR14	42.775	-85.359	3/3/12		811.6024354	3194.54916	189.7365
GR15	43.063	-86.067	3/2/12		688.0363001	1940.218062	174.6225
GR17	42.312	-84.387	3/3/12		226.01408	743.65	14.666
GR20	42.283	-84.410	3/3/12		347	5797.249324	316.946
GR21	42.536	-84.624	3/3/12		1710	619.40892	143.135
GR23	42.728	-84.478	3/7/12		500	2427.79392	124.2425
GR24	42.750	-84.555	3/7/12		2200	2479.662271	146.9135
GR25	42.857	-84.913	3/2/12		3350	1530.83496	70.084
GR26	42.828	-84.759	3/3/12		660	2263.99101	190.996
GR27	43.109	-84.693	3/4/12		1350	2500.12932	73.8625
GR28	42.971	-85.069	3/2/12	DUP	4053		
GR28	42.971	-85.069	3/3/12		6740	3122.21376	202.3315
GR3	42.609	-85.094	3/3/12		855.5692369	1852.268658	120.464
GR30	42.616	-85.236	3/3/12		1160	978.04724	192.2555
GR30	42.616	-85.236	3/3/12	Blank		23.4055803	ND
GR30	42.616	-85.236	3/3/12	DUP		1187.863565	92.755
GR31	43.082	-85.590	3/2/12		536	706.2114	253.971
GR31	43.082	-85.590	3/2/12	DUP	508		
GR5	43.097	-84.710	3/4/12		224.6368067	5938.58406	134.3185
GR6	43.226	-85.302	3/2/12		398.6676483	777.55	208.629
GR7	42.877	-84.384	3/3/12		251.2287758	1646.5716	177.1415
GR8	43.000	-84.908	3/4/12		604.1638876	5185.537759	194.7745
GR9	43.145	-84.503	3/4/12		816.5818081	3599.6274	63.7865
MR10	43.402	-85.563	3/8/12		246.4612913	1111.28964	253.35

Table A.13: 2012 Melt Results. ND = Non Detect. DUP = Duplicate Sample

ID	Lat	Long	Date	Sample Type	Flow cfs	TN μg/L	TP μg/L
MR11	43.306	-86.114	3/8/12		80.6940895	956.64	203.591
MR13	43.699	-85.460	3/8/12		147.0857255	759.0642832	13.4065
MR14	43.540	-85.305	3/8/12		260.6931154	1481.998018	132.43
MR15	44.336	-84.922	3/9/12		176.926647	1239.831136	36.0775
MR16	43.490	-85.449	3/8/12		108.2395555	1185.40872	121.7235
MR17	43.608	-85.481	3/8/12		124.3783734	927.79	86.4575
MR2	44.082	-85.014	3/9/12		659.1841902	1185.40872	33.5585
MR20	44.201	-85.053	3/9/12		455	632.1800677	23.4825
MR20	44.201	-85.053	3/9/12	Blank		124.664293	ND
MR20	44.201	-85.053	3/9/12	DUP		1204.69816	70.084
MR21	43.901	-85.255	3/9/12		2820	663.9948998	124.2425
MR23	43.435	-85.666	3/8/12		3570	1239.83	206.11
MR24	43.289	-86.223	3/8/12		43	776.1831175	79.67
MR3	44.139	-84.899	3/9/12		697.9244161	678.9696771	97.793
MR4	44.006	-85.111	3/9/12		154.6430713	1185.40872	ND
MR5	43.853	-85.444	3/8/12		698.9132277	1296.38444	57.489
MR6	44.111	-85.028	3/9/12		321.8228611	813.0378375	168.325
MR7	43.934	-85.129	3/9/12		152.0650982	654.94912	33.56
MR8	43.779	-85.500	3/8/12		856.734622	1771.465534	226.262
MR9	44.409	-84.805	3/9/12		159.975591	568.0221807	3.3305
SB12	43.657	-84.267	3/6/12		116.0087895	1110.988734	83.31
SB12	43.657	-84.267	3/6/12	Blank		93.28865173	ND
SB12	43.657	-84.267	3/6/12	DUP		1545.30204	144.4
SB13	43.211	-83.315	3/7/12		334.077062	2711.0347	219.9645
SB15	43.250	-83.873	3/7/12		1881.178754	1035.91556	228.781
SB16	43.450	-83.441	3/7/12		1041.713021	6061.683402	56.2295
SB17	43.872	-84.321	3/5/12		446.4484374	415.6869564	139.3565
SB19	43.015	-84.180	3/7/12		956	879.81636	136.8375
SB19	43.015	-84.180	3/7/12	Blank		45.69708309	ND
SB19	43.015	-84.180	3/7/12	DUP		807.48096	149.4325
SB2	43.302	-84.144	3/6/12		279.2333329	7409.074632	141.8755
SB20	43.218	-84.106	3/7/12		911.2252041	1484.646015	219.9645
SB21	43.160	-83.351	3/7/12		275	1386.087721	194.7745
SB22	43.111	-83.519	3/7/12		634	1093.78388	143.135
SB24	43.038	-83.774	3/7/12		1520	1002.15904	129.28
SB27	43.328	-83.758	3/7/12		1470	5071.169951	94.0145
SB28	43.867	-84.545	3/5/12		308	1146.82984	172.1035
SB29	43.627	-84.708	3/6/12		538	1371.69708	337.098

Table A.14: 2012 Melt Results (continued). ND = Non Detect. DUP = Duplicate Sample

ID	Lat	Long	Date	Sample Type	Flow cfs	TN μg/L	TP μg/L
SB3	43.675	-84.388	3/5/12			793.69	180.92
SB3'	43.674	-84.390	3/5/12		367.5553976	3831.10068	70.084
SB30	43.379	-84.656	3/6/12			3388.374711	56.2295
SB31	43.563	-84.370	3/5/12		921	4950.48	150.692
SB32	43.610	-84.242	3/5/12		4660	2456.72808	116.6855
SB33	43.409	-83.964	3/6/12		9590	3570.69324	78.9005
SB4	43.597	-84.944	3/4/12		362.0109897	867.13296	153.211
SB5	43.397	-84.836	3/4/12		437.4785036	807.48096	131.7995
SB6	43.292	-83.992	3/7/12		136.314742	3382.6212	126.7615
SB7	43.741	-85.127	3/4/12		176.7500735	1355.52	76.3815
SB8	43.298	-84.143	3/6/12		324.4714636	2592.768879	78.91
SB9	43.380	-84.094	3/6/12		298.3385856	3174.7521	116.6855
SW-12	44.623	-86.223	3/11/12		391.5340789	1159.593125	ND
SW-13	44.715	-86.125	3/11/12		211.9235147	190.4448152	253.971
SW-14	44.765	-85.621	3/10/12		525.3061625	1493.57	223.743
SW-15	44.900	-85.411	3/10/12		912.1433863	496.8799603	177.14
SW-20	44.050	-83.688	3/5/12		444.5767583	2644.80012	189.7365
SW-21	44.072	-84.019	3/5/12		297	698.35036	174.6225
SW-21	44.072	-84.019	3/5/12	Blank		61.06631888	ND
SW-21	44.072	-84.019	3/5/12	DUP		823.73172	207.3695
SW-36	42.907	-85.781	3/2/12		158.0332825	1125.75672	168.96
SW-36	42.907	-85.781	3/2/12	Blank		79.80486507	ND
SW-39	42.949	-85.849	3/2/12		217.0794609	1763.17	116.6855
SW-4	42.965	-85.675	3/2/12		8540	1487.43372	87.717
SW-5	43.318	-86.038	3/8/12		2955.451928	663.9948998	260.2685
SW-5	43.318	-86.038	3/8/12	Blank		46.72766878	ND
SW-5	43.318	-86.038	3/8/12	DUP		732.88	230.0405
SW-62	45.100	-85.097	3/10/12		187	1151.6522	144.3945
SW-62	45.100	-85.097	3/10/12	Blank		111.5100218	ND
SW-62	45.100	-85.097	3/10/12	DUP		1267.38884	203.591
SW-64	45.214	-85.013	3/10/12		113.5720752	867.13296	178.401
SW-65	45.365	-84.962	3/10/12		214.5721172	1109.007188	49.932
SW-66	45.746	-84.828	3/10/12		92.0654229	593.9317825	51.1915

Table A.15: 2012 Melt Results (continued). ND = Non Detect. DUP = Duplicate Sample

Appendix B

Nitrate Results

ID	Date	Lat	Long	Sample Type	NOx μg/L
J-201	3/19/11	45.13562	-85.080693		427.767458
J-202	3/19/11	45.032895	-85.063817		1851.246197
J-203	3/19/11	45.03636	-84.968732		1667.68841
SW-1	3/5/11	42.087101	-86.476194		4050.106798
SW-10	3/20/11	44.258801	-85.939177		297.5626204
SW-101	3/7/11	43.3274	-83.745823		5173.973871
SW-102	3/6/11	43.3102	-83.955886		2756.87437
SW-103	3/22/11	43.245098	-84.100284		3431.876158
SW-104	3/6/11	43.5891	-84.221356		2131.036822
SW-11	3/20/11	44.356201	-86.049494		290.3843768
SW-11	3/20/11	44.356201	-86.049494	Blank	0
SW-11	3/20/11	44.356201	-86.049494	DUP	208.1199606
SW-12	3/20/11	44.6231	-86.223457		134.5879328
SW-13	3/20/11	44.715099	-86.125244		267.7311532
SW-14	3/19/11	44.7649	-85.620741		880.204067
SW-15	3/19/11	44.899799	-85.410914		215.0131516
SW-15	3/19/11	44.899799	-85.410914	Blank	0
SW-15	3/19/11	44.899799	-85.410914	DUP	214.1276146
SW-16	3/23/11	45.595299	-84.474136		54.0583336
SW-17	3/23/11	45.559101	-84.403295		19.9472548
SW-18	3/22/11	45.067799	-83.436025		319.615808
SW-19	3/22/11	44.415401	-83.330781		199.5583534
SW-2	3/5/11	42.183998	-86.371158		1114.479413
SW-20	3/22/11	44.049599	-83.687858		1786.539089

Table B.1: 2011 Melt Results. ND = Non Detect. DUP = Duplicate Sample

ID	Date	Lat	Long	Sample Type	NOx μg/L
SW-21	3/22/11	44.072399	-84.019051		582.329744
SW-21	3/22/11	44.072399	-84.019051	Blank	0
SW-21	3/22/11	44.072399	-84.019051	DUP	574.040537
SW-23	3/7/11	43.064301	-82.596818		5246.979864
SW-24	3/7/11	42.858002	-82.538059		840.519428
SW-25	3/22/11	42.749001	-82.489671		1830.196192
SW-26	3/4/11	42.5956	-82.90946		2843.695708
SW-27	3/4/11	42.297001	-83.191016		2150.059286
SW-28	3/4/11	42.064201	-83.252775		1725.959648
SW-29	3/4/11	41.963902	-83.546067		6870.21722
SW-3	3/6/11	42.645599	-86.11776		1813.656845
SW-3	3/6/11	42.645599	-86.11776	Blank	0
SW-3	3/6/11	42.645599	-86.11776	DUP	2174.57366
SW-31	3/5/11	42.417099	-86.240863		1024.512725
SW-32	3/5/11	42.420502	-86.244757		1463.308406
SW-33	3/5/11	42.798698	-86.059097		6415.757696
SW-34	3/5/11	42.796902	-86.144102		597.35
SW-35	3/5/11	42.916199	-86.146693		2878.826848
SW-36	3/6/11	42.9067	-85.781123		3312.82708
SW-37	3/6/11	42.903801	-85.772215		1829.74652
SW-39	3/6/11	42.949299	-85.849483		3119.809048
SW-4	3/6/11	42.964901	-85.675129		736.185749
SW-40	3/6/11	42.994202	-86.017657		2712.64591
SW-40	3/6/11	42.994202	-86.017657	Blank	0
SW-40	3/6/11	42.994202	-86.017657	DUP	506.1554223

Table B.2: 2011 Melt Results (continued). ND = Non Detect. DUP = Duplicate Sample

ID	Date	Lat	Long	Sample Type	NOx μg/L
SW-41	3/6/11	42.962399	-86.203368		629.6350532
SW-43	3/21/11	43.1973	-86.186454		947.345192
SW-48	3/21/11	43.415699	-86.276515		146.3274533
SW-51	3/21/11	43.490299	-86.437662		1818.582592
SW-52	3/21/11	43.558998	-86.50317		1385.594066
SW-55	3/21/11	43.904999	-86.308022		2330.333634
SW-56	3/20/11	43.999401	-86.37208		694.004186
SW-57	3/20/11	44.9035	-85.975496		1046.19
SW-59	3/19/11	45.016899	-85.617735		430.965114
SW-6	3/21/11	43.462601	-86.232338		350.561
SW-6	3/21/11	43.462601	-86.232338	Blank	0
SW-6	3/21/11	43.462601	-86.232338	DUP	452.8562568
SW-60	3/19/11	44.745098	-85.54849		337.1871848
SW-62	3/19/11	45.099899	-85.096655		1446.991298
SW-63	3/19/11	45.179501	-85.16416		283.0044534
SW-64	3/23/11	45.2141	-85.013231		293.0023468
SW-65	3/23/11	45.3647	-84.961607		130.8706485
SW-66	3/23/11	45.745998	-84.827748		37.7721952
SW-67	3/23/11	45.488098	-84.07552		453.9696752
SW-69	3/23/11	45.431099	-83.839247		135.0776396
SW-7	3/20/11	43.943802	-86.278413		335.2380356
SW-70	3/23/11	45.337299	-83.684801		331.8488
SW-71	3/23/11	45.1623	-83.410055		ND
SW-73	3/22/11	44.259602	-83.52734		386.9901728
SW-8	3/20/11	44.030201	-86.50636		221.8486875
SW-9	3/20/11	44.208199	-86.246047		215.6857726
SW-91	3/4/11	42.588402	-82.903226		1812.766291
SW-94	3/4/11	42.0951	-83.211266		ND
SW-97	3/4/11	41.931301	-83.34023		4877.812554

Table B.3: 2011 Melt Results (continued). ND = Non Detect. DUP = Duplicate Sample

ID	Date	Lat	Long	Sample Type	NOx μg/L
BC10	3/9/12	45.50764	-84.76265		349.8131862
BC11	3/9/12	45.44003	-84.78534		345.5550495
BC12	3/10/12	45.165655	-85.239769		201.3527037
BC13	3/10/12	44.845585	-85.307429		320.5209196
BC14	3/10/12	44.69917	-85.30557		462.5068334
BC15	3/11/12	44.52819	-85.94865		100.1715435
BC17	3/10/12	44.65679	-85.43884		443.6154012
BC9	3/9/12	45.65927	-84.49263		158.4701182
GR1	3/2/12	43.12973	-85.17377		340.6451801
GR11	3/4/12	43.01474	-84.42586		2790.784189
GR11	3/4/12	43.01474	-84.42586	Blank	ND
GR11	3/4/12	43.01474	-84.42586	DUP	616.3103177
GR12	3/2/12	42.96558	-85.35174		519.2301768
GR13	3/4/12	43.06736	-84.84189		1873.358544
GR14	3/3/12	42.77521	-85.35897		2543.062047
GR15	3/2/12	43.0631	-86.06651		1700.159858
GR17	3/3/12	42.312	-84.38722		676.139703
GR20	3/3/12	42.28331	-84.41029		5572.808401
GR21	3/3/12	42.53555	-84.62442		731.2201456
GR23	3/7/12	42.727659	-84.477961		1991.868993
GR24	3/7/12	42.750321	-84.555337		1709.356954
GR25	3/2/12	42.85708	-84.91265		1263.441766
GR26	3/3/12	42.82789	-84.75898		1377.895405
GR27	3/4/12	43.10872	-84.69332		1222.814129
GR28	3/3/12	42.97123	-85.06897		592.1609789
GR3	3/3/12	42.60863	-85.09383		1716.115662
GR30	3/3/12	42.61599	-85.23645		1168.266882
GR30	3/3/12	42.61599	-85.23645	Blank	12.75670951
GR30	3/3/12	42.61599	-85.23645	DUP	1156.519452
GR31	3/2/12	43.08217	-85.59049		837.8317027
GR5	3/4/12	43.09736	-84.70956		10123.03868
GR6	3/2/12	43.22578	-85.30203		459.4064666
GR7	3/3/12	42.87736	-84.38425		589.1411178
GR8	3/4/12	42.99961	-84.90849		7988.841806
GR9	3/4/12	43.14473	-84.50335		2264.088764
MR10	3/8/12	43.40164	-85.5628		1207.829928
MR11	3/8/12	43.30589	-86.11443		626.7997862

Table B.4: 2012 Melt Results. ND = Non Detect. DUP = Duplicate Sample

ID	Date	Lat	Long	Sample Type	NOx μg/L
MR13	3/8/12	43.69864	-85.46043		266.5138838
MR14	3/8/12	43.5399	-85.30548		136.9166199
MR15	3/9/12	44.33609	-84.9216		290.2351194
MR16	3/8/12	43.48959	-85.4486		497.5192703
MR17	3/8/12	43.60761	-85.480685		219.4142962
MR2	3/9/12	44.08187	-85.01359		337.8536637
MR20	3/9/12	44.20086	-85.05293		450.5869143
MR20	3/9/12	44.20086	-85.05293	Blank	25.08646871
MR20	3/9/12	44.20086	-85.05293	DUP	573.8087129
MR21	3/9/12	43.90098	-85.25467		427.8774506
MR23	3/8/12	43.43517	-85.66613		838.8409191
MR24	3/8/12	43.28875	-86.22311		381.978334
MR3	3/9/12	44.13933	-84.8994		225.0605142
MR4	3/9/12	44.00591	-85.11092		354.6508668
MR5	3/8/12	43.85285	-85.444458		457.2180539
MR6	3/9/12	44.111408	-85.028132		594.0207878
MR7	3/9/12	43.93358	-85.12883		422.8037192
MR8	3/8/12	43.77874	-85.49961		907.7956489
MR9	3/9/12	44.40864	-84.80501		50.40907302
SB12	3/6/12	43.65714	-84.26715		1415.21538
SB12	3/6/12	43.65714	-84.26715	Blank	ND
SB12	3/6/12	43.65714	-84.26715	DUP	1315.1161
SB13	3/7/12	43.21095	-83.3146		2717.858351
SB15	3/7/12	43.24987	-83.87269		1041.177877
SB16	3/7/12	43.45034	-83.44139		4542.886475
SB17	3/5/12	43.871818	-84.321231		288.2179637
SB19	3/7/12	43.01495	-84.17964		934.257909
SB19	3/7/12	43.01495	-84.17964	Blank	ND
SB19	3/7/12	43.01495	-84.17964	DUP	588.5110585
SB2	3/6/12	43.30233	-84.14385		7527.484258
SB20	3/7/12	43.21777	-84.10555		1453.012232
SB21	3/7/12	43.15983	-83.35131		567.9800556
SB22	3/7/12	43.11134	-83.51899		596.9733799
SB24	3/7/12	43.03844	-83.77401		762.71316
SB27	3/7/12	43.32754	-83.75812		6501.721677
SB28	3/5/12	43.86695	-84.54549		542.4893401
SB29	3/6/12	43.62684	-84.70802		619.5699381
SB3	3/5/12	43.67512	-84.38839		468.4208956

Table B.5: 2012 Melt Results (continued). ND = Non Detect. DUP = Duplicate Sample

ID	Date	Lat	Long	Sample Type	NOx μg/L
SB3'	3/5/12	43.674173	-84.389555		5578.086968
SB30	3/6/12	43.378977	-84.65597		3237.105255
SB31	3/5/12	43.5634	-84.36966		7826.53935
SB32	3/5/12	43.61029	-84.24164		1280.02009
SB33	3/6/12	43.40875	-83.96436		2429.042143
SB4	3/4/12	43.59702	-84.94359		326.1504248
SB5	3/4/12	43.3973	-84.83624		554.8123137
SB6	3/7/12	43.292201	-83.992242		2148.330772
SB7	3/4/12	43.74069	-85.12742		277.0606123
SB8	3/6/12	43.29845	-84.14273		2624.742406
SB9	3/6/12	43.37951	-84.094		6291.419834
SW-12	3/11/12	44.6231	-86.223457		233.4763823
SW-13	3/11/12	44.715099	-86.125244		193.038179
SW-14	3/10/12	44.7649	-85.620741		370.0861244
SW-15	3/10/12	44.899799	-85.410914		352.8817201
SW-20	3/5/12	44.049599	-83.687858		2024.657205
SW-21	3/5/12	44.072399	-84.019051		281.4512779
SW-21	3/5/12	44.072399	-84.019051	Blank	ND
SW-21	3/5/12	44.072399	-84.019051	DUP	278.917344
SW-36	3/2/12	42.9067	-85.781123		908.7460593
SW-36	3/2/12	42.9067	-85.781123	Blank	ND
SW-36	3/2/12	42.9067	-85.781123	DUP	985.1694554
SW-39	3/2/12	42.949299	-85.849483		589.0212381
SW-4	3/2/12	42.964901	-85.675129		628.9688034
SW-5	3/8/12	43.3181	-86.03813		590.7124537
SW-5	3/8/12	43.3181	-86.03813	DUP	825.3481123
SW-62	3/10/12	45.099899	-85.096655		529.6767952
SW-62	3/10/12	45.099899	-85.096655	Blank	ND
SW-62	3/10/12	45.099899	-85.096655	DUP	531.4229666
SW-64	3/10/12	45.2141	-85.013231		307.8048816
SW-65	3/10/12	45.3647	-84.961607		281.0861289
SW-66	3/10/12	45.745998	-84.827748		147.6876311

Table B.6: 2012 Melt Results (continued). ND = Non Detect. DUP = Duplicate Sample

Appendix C

Isotope Results

ID	Date	Lat	Long	Sample Type	$\delta^{15}N_{NO3}$	$\delta^{18}O_{NO3}$
BC10	3/9/12	45.50764	-84.76265		2.9	10.96
BC11	3/9/12	45.44003	-84.78534		4.14	14.42
BC12	3/10/12	45.165655	-85.239769		3.4	7
BC13	3/10/12	44.845585	-85.307429		4.56	-0.53
BC14	3/10/12	44.69917	-85.30557		3.13	7.31
BC15	3/11/12	44.52819	-85.94865		1.45	8.95
BC17	3/10/12	44.65679	-85.43884		4.03	5.68
BC9	3/9/12	45.65927	-84.49263		4.13	19.49
GR1	3/2/12	43.12973	-85.17377		6.24	4.28
GR11	3/4/12	43.01474	-84.42586		6.87	0.49
GR11	3/4/12	43.01474	-84.42586	DUP	6.83	0.41
GR12	3/2/12	42.96558	-85.35174		5.18	3.98
GR13	3/4/12	43.06736	-84.84189		6.04	-0.07
GR14	3/3/12	42.77521	-85.35897		5.36	-0.08
GR15	3/2/12	43.0631	-86.06651		8.82	2.37
GR17	3/3/12	42.312	-84.38722		6.95	2.67
GR20	3/3/12	42.28331	-84.41029		5.28	-0.96
GR21	3/3/12	42.53555	-84.62442		5.19	1.39
GR23	3/7/12	42.727659	-84.477961		5.87	1.67
GR24	3/7/12	42.750321	-84.555337		6.93	1.65
GR25	3/2/12	42.85708	-84.91265		6.49	0.78
GR26	3/3/12	42.82789	-84.75898		6.42	2.19
GR27	3/4/12	43.10872	-84.69332		7.79	0.96
GR28	3/3/12	42.97123	-85.06897		7	0.73
GR3	3/3/12	42.60863	-85.09383		4.8	0.58
GR30	3/3/12	42.61599	-85.23645		6.39	2.23
GR30	3/3/12	42.61599	-85.23645	DUP	7.16	3.01
GR31	3/2/12	43.08217	-85.59049		7.03	3.24
GR5	3/4/12	43.09736	-84.70956		5.66	-1.58
GR6	3/2/12	43.22578	-85.30203		5.07	3.61
GR7	3/3/12	42.87736	-84.38425		3.21	1.4
GR8	3/4/12	42.99961	-84.90849		5.33	-0.28
GR9	3/4/12	43.14473	-84.50335		6.78	0.2
MR10	3/8/12	43.40164	-85.5628		5.49	3.18
MR11	3/8/12	43.30589	-86.11443		6.16	4.45
MR13	3/8/12	43.69864	-85.46043		3.29	17.92
MR14	3/8/12	43.5399	-85.30548		3.64	8.79
MR15	3/9/12	44.33609	-84.9216		0.74	28.14

Table C.1: 2012 Melt Results. ND = Non Detect. DUP = Duplicate Sample

ID	Date	Lat	Long	Sample Type	$\delta^{15}N_{NO3}$	$\delta^{18}O_{NO3}$
MR20	3/9/12	44.20086	-85.05293		3.89	14.6
MR20	3/9/12	44.20086	-85.05293	DUP	3.85	14.89
MR21	3/9/12	43.90098	-85.25467		3.96	11.22
MR23	3/8/12	43.43517	-85.66613		5.54	2.61
MR24	3/8/12	43.28875	-86.22311		6.16	12.41
MR3	3/9/12	44.13933	-84.8994		3.06	17.62
MR4	3/9/12	44.00591	-85.11092		2.4	12.18
MR5	3/8/12	43.85285	-85.444458		1.14	16.97
MR6	3/9/12	44.111408	-85.028132		5.06	8.88
MR7	3/9/12	43.93358	-85.12883		1.53	14.63
MR8	3/8/12	43.77874	-85.49961		3.93	8.28
MR9	3/9/12	44.40864	-84.80501		-1.17	61.31
SB12	3/6/12	43.65714	-84.26715		6.11	0.6
SB12	3/6/12	43.65714	-84.26715	DUP	5.34	0.34
SB13	3/7/12	43.21095	-83.3146		5.44	-0.01
SB15	3/7/12	43.24987	-83.87269		5.23	0.57
SB16	3/7/12	43.45034	-83.44139		3.12	-1.42
SB17	3/5/12	43.871818	-84.321231		4.87	7.11
SB19	3/7/12	43.01495	-84.17964		5.98	1.66
SB19	3/7/12	43.01495	-84.17964	DUP	7.4	1.82
SB2	3/6/12	43.30233	-84.14385		3.99	-1.75
SB20	3/7/12	43.21777	-84.10555		5.29	1.36
SB21	3/7/12	43.15983	-83.35131		8.4	3.16
SB22	3/7/12	43.11134	-83.51899		4.7	2.54
SB24	3/7/12	43.03844	-83.77401		4.39	2.54
SB27	3/7/12	43.32754	-83.75812		3.2	0.95
SB28	3/5/12	43.86695	-84.54549		7.81	-1.34
SB29	3/6/12	43.62684	-84.70802		3.86	2.44
SB3	3/5/12	43.67512	-84.38839		6.02	-0.62
SB3'	3/5/12	43.674173	-84.389555		4.94	3.17
SB30	3/6/12	43.378977	-84.65597		4.9	0.8
SB31	3/5/12	43.5634	-84.36966		5.72	1.06
SB32	3/5/12	43.61029	-84.24164		5.25	0.1
SB33	3/6/12	43.40875	-83.96436		6.25	-0.76
SB4	3/4/12	43.59702	-84.94359		5.63	4.32
SB5	3/4/12	43.3973	-84.83624		5.4	2.04
SB6	3/7/12	43.292201	-83.992242		5.72	-0.7
SB7	3/4/12	43.74069	-85.12742		6.09	7.57
SB8	3/6/12	43.29845	-84.14273		3.1	-0.26

Table C.2: 2012 Melt Results (continued). ND = Non Detect. DUP = Duplicate Sample

ID	Date	Lat	Long	Sample Type	$\delta^{15}N_{NO3}$	$\delta^{18}O_{NO3}$
SW-15	3/10/12	44.899799	-85.410914		2.09	6.59
SW-20	3/5/12	44.049599	-83.687858		1.32	-0.58
SW-21	3/5/12	44.072399	-84.019051		6.9	4.11
SW-21	3/5/12	44.072399	-84.019051	DUP	7.1	3.83
SW-36	3/2/12	42.9067	-85.781123		6.97	2.49
SW-36	3/2/12	42.9067	-85.781123	DUP	6.81	2.59
SW-39	3/2/12	42.949299	-85.849483		7.13	2.15
SW-4	3/2/12	42.964901	-85.675129		6.09	0.95
SW-5	3/8/12	43.3181	-86.03813		5.82	3.46
SW-5	3/8/12	43.3181	-86.03813	DUP	6.14	3.8
SW-62	3/10/12	45.099899	-85.096655		1.79	-2.12
SW-62	3/10/12	45.099899	-85.096655	DUP	0.98	-2.33
SW-64	3/10/12	45.2141	-85.013231		3.24	6.03
SW-65	3/10/12	45.3647	-84.961607		1.85	14.71
SW-66	3/10/12	45.745998	-84.827748		2.44	18.58
DR11				Standard	3.94	24.87
DR12				Standard	4.16	24.95
DR13				Standard	4.58	25.43

Table C.3: 2012 Melt Results (continued). ND = Non Detect. DUP = Duplicate Sample

BIBLIOGRAPHY

BIBLIOGRAPHY

Alexander, R. B., R. A. Smith, and G. E. Schwarz, Effect of stream channel size on the delivery of nitrogen to the Gulf of Mexico, *Nature*, *403*(6771), 758–761, 2000.

Alexander, R. B., P. J. Johnes, E. W. Boyer, and R. A. Smith, A comparison of models for estimating the riverine export of nitrogen from large watersheds, *Biogeochemistry*, *57/58*, 295–339, 2002.

Anderson, D. M., P. M. Gilber, and J. M. Burkholder, Harmful Algal Blooms and Eutrophication Nutrient Sources , Composition , and Consequences, *Estuaries*, *25*(4), 704–726, 2002.

Anisfeld, S. C., R. T. Barnes, M. a. Altabet, and T. Wu, Isotopic apportionment of atmospheric and sewage nitrogen sources in two Connecticut rivers., *Environmental science & technology*, *41*(18), 6363–9, 2007.

Arnold, J., R. Srinivasan, R. Muttiah, and J. Williams, Large Area Hydrologic Modeling and Assessment Part I: Model Development, *Journal of The American Water Resources Association*, *34*(1), 73–89, 1998.

Auer, M. T., L. M. Tomlinson, S. N. Higgins, S. Y. Malkin, E. T. Howell, and H. a. Bootsma, Great Lakes Cladophora in the 21st century: same algae-different ecosystem, *Journal of Great Lakes Research*, *36*(2), 248–255, doi:10.1016/j.jglr.2010.03.001, 2010.

Beaulac, M., and K. H. Reckhow, An Examination of Land Use-Nutrient Export Relationships, *18*(6), 1013–1024, 1982.

Beyer, H., Geospatial Modelling Environment, 2012.

Bjerklie, D. M., S. Lawrence Dingman, C. J. Vorosmarty, C. H. Bolster, and R. G. Congalton, Evaluating the potential for measuring river discharge from space, *Journal of Hydrology*, *278*(1-4), 17–38, doi:10.1016/S0022-1694(03)00129-X, 2003.

Borah, D. K., and M. Bera, Watershed-Scale Hydrologic and Nonpoint-Source Pollution Models: Review of Applications, *Transaction of the ASAE*, *47*(3), 789–804, 2004.

Bottcher, J., O. Strebel, S. Voerkelius, and H. Schmidt, Using Isotope Fractionation of Nitrate-Nitrogen and Nitrate-Oxygen for Evaluation of Microbial Denitrification in a Sandy Aquifer, *Journal of Hydrolo*, *114*, 413–424, 1990.

Boyer, E. W., C. L. Goodale, N. Jaworski, and R. W. Howarth, Anthropogenic nitrogen sources and relationships to riverine nitrogen export in the northeastern U . S . A ., *Biogeochemistry*, *57/58*, 137–169, 2002.

Burns, D. a., E. W. Boyer, E. M. Elliott, and C. Kendall, Sources and transformations of nitrate from streams draining varying land uses: evidence from dual isotope analysis., *Journal of environmental quality*, *38*(3), 1149–59, doi:10.2134/jeq2008.0371, 2009.

Carpenter, S. R., N. F. Caraco, D. L. Correll, R. W. Howarth, a. N. Sharpley, and V. H. Smith, Nonpoint Pollution of Surface Waters With Phosphorus and Nitrogen, *Ecological Applications*, *8*(3), 559–568, doi:10.1890/1051-0761(1998)008[0559:NPOSWW]2.0.CO;2, 1998.

Casciotti, K. L., D. M. Sigman, M. G. Hastings, J. K. Böhlke, and a. Hilkert, Measurement of the oxygen isotopic composition of nitrate in seawater and freshwater using the denitrifier method., *Analytical chemistry*, *74*(19), 4905–12, 2002.

Chang, C. C. Y., C. Kendall, S. R. Silva, W. A. Battaglin, and D. H. Campbell, Nitrate stable isotopes : tools for determining nitrate sources among different land uses in the Mississippi River Basin, *Water Resources*, *1885*(2002), 1874–1885, doi:10.1139/F02-153, 2003.

Cheng, J., Challenges of CAFO Waste Management, *Journal of Environmental Engineering*, *129*(5), 391, doi:10.1061/(ASCE)0733-9372(2003)129:5(391), 2003.

Correll, D. L., The Role of Phosphorus in the Eutrophication of Receiving Waters: A Review, *Journal of Environment Quality*, *27*(2), 261, doi:10.2134/jeq1998.00472425002700020004x, 1998.

Crumpton, W. G., T. M. Isenhart, and P. D. Mitchell, Nitrate and Organic N Analyses with Second-Derivative Spectroscopy, *Liminology and Oceanography*, *37*(4), 907–913, 1992.

Davidson, E. A., M. B. David, J. N. Galloway, C. L. Goodale, R. Haeuber, J. A. Harrison, R. W. Howarth, D. B. Jaynes, R. R. Lowrance, B. T. Nolan, J. L. Peel, R. W. Pinder, E. Porter, C. S. Snyder, A. R. Townsend, and M. H. Ward, Excess Nitrogen in the U.S. Environment: Trends, Risks, and Solutions, *Issues in Ecology*, (15), 2012.

Destouni, G., G. A. Lindgren, and I.-M. Gren, Policy Analysis Effects of Inland Nitrogen Transport and Attenuation Modeling on Coastal Nitrogen Load Abatement, *40*(20), 2006.

Dolan, D. M., Point Source Loadings of Phosphorus to Lake Erie : 1986-1990, *Journal of Great Lakes Research*, *19*(2), 212–223, doi:10.1016/S0380-1330(93)71212-5, 1993.

Dolan, D. M., and S. C. Chapra, Great Lakes total phosphorus revisited: 1. Loading analysis and update (1994-2008), *Journal of Great Lakes Research*, *38*(4), 730–740, doi:10.1016/j.jglr.2012.10.001, 2012.

Dolan, D. M., and K. P. McGunagle, Lake Erie Total Phosphorus Loading Analysis and Update: 1996-2002, *Journal of Great Lakes Research*, *31*, 11–22, doi:10.1016/S0380-1330(05)70301-4, 2005.

Dolan, D. M., A. K. Yui, and R. D. Geist, Evaluation of River Load Estimation Methods for Total Phosphorus, *Journal of Great Lakes Research*, *7*(3), 207–214, 1981.

Evans, B. M., D. W. Lehning, K. J. Corradini, G. W. Petersen, E. Nizeyimana, J. M. Hamlett, P. D. Robillard, and R. L. Day, A Comprehensive GIS-Based Modeling Approach for Prediciting Nutrient Loads in Watersheds, *Journal of Spatial Hydrology*, *2*(2), 2002.

Fry, J., G. Xian, S. Jin, J. Dewitz, C. Homer, L. Yang, C. Barnes, N. Herold, and J. Wickham, Completion of the 2006 National Land Cover Database for the Conterminous United States, *Photogrammetric Engineering & Remote Sensing*, *77*(9), 858–864, 2011.

Georgas, N., S. Rangarajan, K. J. Farley, and S. C. K. Jagupilla, AVGWLF-Based Estimation of Nonpoint Source Nitrogen Loads Generated within Long Island Sound Watersheds, *Journal Of The American Water Resources Association*, *45*(3), doi:10.1111/j.1752-1688.2009.00318.x, 2009.

Gesch, D., The National Elevation Dataset, in *Digital Elevation Model Technologies and Applications: The DEM Users Manual*, edited by D. Maune, 2nd ed., pp. 99–118, American Society for Photogrammetry and Remote Sensing, Bethesda, Maryland, 2007.

Gesch, D., M. Oimoen, S. Greenlee, C. Nelson, M. Steuck, and D. Tyler, The National Elevation Dataset, *Photogrammetric Engineering & Remote Sensing*, *68*(1), 5–11, 2002.

Gilliom, R. J., and C. R. Patmont, Lake phosphorus loading from septic systems by seasonally perched groundwater, *Journal (Water Pollution Control Federation)*, *55*(10), 1297–1305, 1983.

Grizzetti, B., F. Bouraoui, and G. Demarsily, Modelling nitrogen pressure in river basins: A comparison between a statistical approach and the physically-based SWAT model, *Physics and Chemistry of the Earth, Parts A/B/C*, *30*(8-10), 508–517, doi:10.1016/j.pce.2005.07.005, 2005.

Haith, D. a., and L. L. Shoenaker, Generalized Watershed Loading Functions for Stream Flow Nutrients, *Journal of the American Water Resources Association*, *23*(3), 471–478, doi:10.1111/j.1752-1688.1987.tb00825.x, 1987.

Hatfield, J. L., and D. R. Keeney, Chapter 1 . The Nitrogen Cycle , Historical Perspective , and, *Perspective*, pp. 1–18, 2008.

Hinderer, J. M., and M. W. Murray, Feast and Faimine in the Great Lakes-How Nutrients and Invasive Species Interact to Overwhelm the Coasts and Starve Offshore Waters, *Tech. rep.*, National Wildlife Federation, 2011.

Howarth, R. W., G. Billen, D. Swaney, A. Townsend, N. Jaworski, K. Lajtha, J. A. Downing, R. Elmgren, N. F. Caraco, T. E. Jordan, F. Berendse, J. Freney, V. Kudeyarov, P. Murdoch, and Z. Zhao-Lian, Regional nitrogen budgets and riverine N & P fluxes for the drainages to the Norh Atlantic Ocean: Natural and human influences, *Biogeochemistry*, *35*, 75–139, 1996.

Hyndman, D., A. Kendall, and R. Welty, Evaluating Temporal and Spatial Variations in Recharge and Streamflow Using the Integrated Landscape Hydology Model (ILHM), in *Geophysical Monograph Series*, vol. 171, pp. 121–141, 2007.

Jaworski, N. A., P. M. Groffman, A. A. Keller, and J. C. Prager, A Watershed Nitrogen and Phosphorus Balance: The Upper Potomac River Basin, *Estuaries*, *15*(1), 83–95, doi:10.2307/1352713, 1992.

Johnes, P., B. Moss, and G. Phillips, The determination of total nitrogen and total phosphorus concentrations in freshwaters from land use, stock headage and population data: testing of a model for use in conservation and water quality management, *Freshwater Biology*, *36*(2), 451–473, doi:10.1046/j.1365-2427.1996.00099.x, 1996.

Johnes, P. J., Evaluation and management of the impact of land use change on the nitrogen and phosphorus load delivered to surface waters: the export coefficient modelling approach, *Journal of Hydrology*, *183*(3-4), 323–349, doi:10.1016/0022-1694(95)02951-6, 1996.

Johnes, P. J., and A. L. Heathwaite, Modelling the Impact of Land Use Change on Water Quality in Agricultural Catchments, *Hydrological Processes*, *11*(3), 269–286, doi:10.1002/(SICI)1099-1085(19970315)11:3¡269::AID-HYP442¿3.0.CO;2-K, 1997.

Kaushal, S. S., P. M. Groffman, L. E. Band, E. M. Elliott, C. a. Shields, and C. Kendall, Tracking nonpoint source nitrogen pollution in human-impacted watersheds., *Environmental science & technology*, *45*(19), 8225–32, doi:10.1021/es200779e, 2011.

Kellogg, R. L., C. H. Lander, D. C. Moffitt, and N. Gollehon, Manure Nutrients Relative to the Capacity of Cropland and Pastureland to Assimilate Nutrients: Spatial and Temporal Trends for the United States, *Tech. rep.*, NRCS, 2000.

Kendall, A. D., and D. W. Hyndman, Simulating Spatial and Temporal Variability of Regional Evapotranspiration and Groundwater Recharge: In fluences of Land Use, Soils, and Lake-Effect Climate, *Advances in Water Resources*.

Kendall, C., E. M. Elliott, and S. Wankel, Tracing anthropogenic inputs of nitrogen to ecosystems, in *Stable Isotopes in Ecology and Environmental Science*, edited by R. Michener and K. Lajtha, pp. 375–449, 2007.

Law, N., L. Band, and M. Grove, Nitrogen input from residential lawn care practices in suburban watersheds in Baltimore county, MD, *Journal of Environmental Planning and Management*, *47*(5), 737–755, doi:10.1080/0964056042000274452, 2004.

Leopold, L. B., and T. Maddock, The Hydraulic Geometrv of Stream Channels and Some Physiographic Implications, *Geological Survey Professional Paper*, *252*, 1953.

Mainston, C. P., and W. Parr, Phosphorus in rivers–ecology and management., *The Science of the total environment*, *282-283*, 25–47, 2002.

Maupin, M. A., and T. Ivahnenko, Nutrient Loadings to Streams of the Continental United States From Municipal and Industrial Effluent, *JAWRA Journal of the American Water Resources Association*, *47*(5), 950–964, doi:10.1111/j.1752-1688.2011.00576.x, 2011.

Mayer, B., E. W. Boyer, N. A. Jaworski, N. V. A. N. Breemen, R. W. Howarth, S. Seitzinger, G. Billen, K. Lajtha, K. Nadelhoffer, D. Van Dam, L. J. Hetling, M. Nosal, and K. Paustian, Sources of nitrate in rivers draining sixteen watersheds in the northeastern U . S .: Isotopic constraints, *Biogeochemistry*, *57/58*, 171–197, 2002.

McMahon, G., L. Tervelt, and W. Donehoo, Methods for Estimating Annual Wastewater Nutrient Loads in the Southeastern United States, *Tech. rep.*, U.S. Geological Survey Open File Report 2007-1040, Reston, Virginia, 2007.

MDEQ, Wellogic Wells Summary, 2005.

Moon, J. B., and H. J. Carrick, Seasonal variation of phytoplankton nutrient limitation in Lake Erie, *Aquatic Microbial Ecology*, *48*(Carrick 2004), 61–71, 2007.

Moore, R. B., C. M. Johnston, K. W. Robinson, and J. R. Deacon, Estimation of Total Nitrogen and Phosphorus in New England Streams Using Spatially Referenced Regression Models, 2004.

NADP, National Atmospheric Deoposition Program (NRSP-3), *Tech. rep.*, NADP Program Office, Illinois State Water Survey, 2204 Griffith Dr., Champaign, Il 61820, 2007.

Natural Resource Conservation Service, S. S. S., Soil Survey Geographic (SSURGO) Database, *Tech. rep.*, United States Department of Agriculture.

Neff, J. C., E. A. Holland, J. Frank, W. H. Mcdowell, and K. M. Russell, The origin , composition and rates of organic nitrogen deposition : A missing piece of the nitrogen cycle ?, *Methods*, pp. 99–136, 2002.

Nelder, J., and R. Mead, A Simplex Method for Function Minimization, *The Computer Journal*, *7*(4), 308–313, 1965.

Nicholls, K. H., G. J. Hopkins, S. J. Standke, and L. Nakamoto, Trends in Total Phosphorus in Canadian Near-Shore Waters of the Laurentian Great Lakes: 1976-1999, *Journal of Great Lakes Research*, *27*(4), 402–422, doi:10.1016/S0380-1330(01)70656-9, 2001.

Nikolaidis, N., H. Heng, R. Semagin, and J. Clausen, Non-linear response of a mixed land use watershed to nitrogen loading, *Agriculture, Ecosystems & Environment*, *67*(2-3), 251–265, doi:10.1016/S0167-8809(97)00123-0, 1998.

NRCS, 1992 National REsource Inventory, *Tech. rep.*, Iowa State University, Statistical Laboratory, Ames, 1995.

NRCS, Agricultrual waste characteristics: Agricultural Waste Management Field Handbook, *Waste Management*, (March), 2008.

Piatek, K. B., M. J. Mitchell, S. R. Silva, and C. Kendall, Sources of Nitrate in Snowmelt Discharge: Evidence from Water Chemistry and Stable Isotopes of Nitrate, *Water, Air, and Soil Pollution*, *165*, 13–35, 2005.

PLUARG, Nonpoint Source Pollution Abatement in the Greate Lakes Basin: An Overview of Post-PLUARG Developments, *Tech. Rep. August*, Nonpoint Source Control Task Force of the Water Quality Board of the International Joint Commission, Windsor, Ontario, 1983.

Preston, S. D., and J. W. Brakebill, Application of Spatially Referenced Regression Modeling for the Evaluation of Total Nitrogen Loading in the Chesapeake Bay Watershed, *USGS Scientific Investigations Report*, *99-4054*, 1999.

PRISM Climate Group, PRISM Climate Group, 2011.

Reneau, R., and D. Pettry, Phosphorus Distribution from Septic Tank Effluent in Coastal Plain Soils, *Journal of Environment Quality*, *5*(1), 34–39, 1976.

Robertson, D. M., and D. a. Saad, Nutrient Inputs to the Laurentian Great Lakes by Source and Watershed Estimated Using SPARROW Watershed Models, *JAWRA Journal of the American Water Resources Association*, *47*(5), 1011–1033, doi:10.1111/j.1752-1688.2011.00574.x, 2011.

Robertson, W., and J. Cherry, Hydrogeology of an unconfined sand aquifer and its effect on the behavior of nitrogen from a large-flux septic system, *Hydrogeology Journal*, *0*, 32–44, 1992.

Roth, K. S., and T. Dewald, The National Hydrography Dataset, *Tech. rep.*, U.S. Geological Survey, U.S. Environmental Protection Agency, 1999.

Ruddy, B. C., D. L. Lorenz, and D. K. Mueller, County-Level Estimates of Nutrient Inputs to the Land Surface of the Conterminous United States , 1982 - 2001, *National Water-Quality Assessment Program: Scientific Investigations Report*, *2006-5012*, 2006.

Schulze, K., and M. Hunger, Simulating river flow velocity on global scale, *Advances In Geosciences*, *5*, 133–136, 2005.

Schwarz, G. E., A. B. Hoos, R. B. Alexander, and R. A. Smith, *The SPARROW Surface Water-Quality Model : Theory , Application and User Documentation*, book 6 ed., U.S. Geological Survey, Reston, Virginia, 2006.

Sigman, D. M., K. L. Casciotti, M. Andreani, C. Barford, M. Galanter, and J. K. Böhlke, A bacterial method for the nitrogen isotopic analysis of nitrate in seawater and freshwater., *Analytical chemistry*, *73*(17), 4145–53, 2001.

Smith, R. A., R. B. Alexander, and M. G. Wolman, Water-Quality Trends in the Nation's Rivers, *Science*, *235*(4796), 1607–1615, 1987.

Smith, R. A., G. E. Schwarz, and R. B. Alexander, Regional interpretation of water-quality monitoring data, *Water Resources Research*, *33*(12), 2781–2798, 1997.

Spoelstra, J., S. L. Schiff, R. J. Elgood, R. G. Semkin, and D. S. Jeffries, Tracing the Sources of Exported Nitrate in the Turkey Lakes Watershed Using 15 N/ 14 N and 18 O/ 16 O isotopic ratios, *Ecosystems*, *4*(6), 536–544, doi:10.1007/s10021-001-0027-y, 2001.

Throssell, C. S., G. T. Lyman, M. E. Johnson, G. A. Stacey, and C. D. Brown, Golf Course Environmental Profile Measures Nutrient Use and Management and Fertilizer Restrictions , Storage , and Equipment Calibration, *Applied Turfgrass Science*, doi:10.1094/ATS-2009-1203-01-RS.Abstract, 2009.

USDA, USDA National Agricultural Statistics Service Cropland Data Layer, 2011.

USEPA, Onsite Wastewater Treatment Systems Manual, *Tech. Rep. February*, U.S. Environmental Protection Agency, 2002a.

USEPA, National Water Quality Inventory: 1996 Report to Congress, *Tech. rep.*, United States Environmental Protection Agency Office of Water, Washington, D.C., 2002b.

USEPA, National Water Quality Inventory : Report to Congress 2004 Reporting Cycle, *Tech. Rep. January*, United States Environmental Protection Agency Office of Water, Washington, D.C., 2009.

USGS, Streamflow Measurements for the Nation, 2012.

Vadeboncoeur, M. a., S. P. Hamburg, and D. Pryor, Modeled Nitrogen Loading to Narragansett Bay: 1850 to 2015, *Estuaries and Coasts*, *33*(5), 1113–1127, doi:10.1007/s12237-010-9320-3, 2010.

Valiela, I., Assessment of models for estimation of land-derived nitrogen loads to shallow estuaries, *Applied Geochemistry*, *17*(7), 935–953, doi:10.1016/S0883-2927(02)00073-2, 2002.

Valiela, I., G. Collins, J. Kremer, K. Lajtha, M. Geist, B. Seely, J. Brawley, and C. H. Sham, Nitrogen Loading From Coastal Watersheds To Receiving Estuaries: New Method and Application, *Ecological Applications*, *7*(2), 358–380, doi:10.1890/1051-0761(1997)007[0358:NLFCWT]2.0.CO;2, 1997.

Valigura, R. A., R. B. Alexander, M. S. Castro, T. P. Meyers, H. W. Paerl, P. E. Stacey, and E. R. Turner, Atmospheric Nitrogen Flux from the Watersheds of Major Estuaries of the United States: An Application fo the SPARROW Watershed Model, *Coastal and Estuarine Studies*, pp. 119–170, 2001.

Verhougstraete, M. P., Measuring microbial water quality responses to land and climate using fecal indicator bacteria and molecular source tracking in rivers and near - shore waters of Michigan, Ph.D. thesis, Michigan State University, 2012.

Vitousek, P. M., J. D. Aber, R. W. Howarth, G. E. Likens, P. A. Matson, D. W. Schindler, W. H. Schlesinger, and D. G. Tilman, Human Alteration of the Global Nitrogen Cycle: Sources and Consequences, *Ecological Applications*, *7*(3), 737–750, 1997.

Warncke, D., J. Dahl, L. Jacobs, and C. Laboski, Nutrient Recommendations for Field Crops in Michigan, *Extension Bulletin*, *E2904*, 2004.

Withers, P. J. a., and H. P. Jarvie, Delivery and cycling of phosphorus in rivers: a review., *The Science of the Total Environment*, *400*(1-3), 379–95, doi:10.1016/j.scitotenv.2008.08.002, 2008.

Wolock, D. M., Base-flow Index Grid for the Conterminous United States. Open-File Report 03-236, *Tech. rep.*, U.S. Geological Survey, Reston, Virginia, 2003.

Xue, D., J. Botte, B. De Baets, F. Accoe, A. Nestler, P. Taylor, O. Van Cleemput, M. Berglund, and P. Boeckx, Present limitations and future prospects of stable isotope methods for nitrate source identification in surface- and groundwater., *Water research*, *43*(5), 1159–70, doi:10.1016/j.watres.2008.12.048, 2009.

Zhang, T., A Spatially Explicit Model for Estimating Annual Average Loads of Nonpoint Source Nutrient at the Watershed Scale, *Environmental Modeling & Assessment*, *15*(6), 569–581, doi:10.1007/s10666-010-9225-3, 2010.

Zhang, T., Distance-decay patterns of nutrient loading at watershed scale: Regression modeling with a special spatial aggregation strategy, *Journal of Hydrology*, *402*(3-4), 239–249, doi:10.1016/j.jhydrol.2011.03.017, 2011.

Zhou, W., A. Troy, and M. Grove, Modeling residential lawn fertilization practices: integrating high resolution remote sensing with socioeconomic data., *Environmental management*, *41*(5), 742–52, doi:10.1007/s00267-007-9032-z, 2008.